Using Fluorescence Derivatization and Analytical Separations to Investigate Biomarkers of Oxidative Stress

By

Michael Logan Dobson Hogard
B.S., Truman State University, 2011
Kirksville, MO

Submitted to the graduate degree program in Chemistry and the Graduate Faculty of the University of Kansas in partial fulfillment of the requirements for the degree of Doctor of Philosophy.

_____

Chairperson: Susan Lunte

_____

Robert Dunn

_____

Yong Zeng

_____

Cindy Berrie

_____

Brian Ackley

Date Defended: June 30th, 2017

The dissertation committee for Michael Logan Dobson Hogard certifies
that this is the approved version of the following dissertation:

Using Fluorescence Derivatization and Analytical Separations to Investigate Biomarkers of Oxidative Stress

_____

Chairperson: Susan Lunte

Date Approved: June 30th, 2017

Abstract

Oxidative stress occurs when there is an overproduction of reactive nitrogen and oxygen species in the body. This condition has been linked to many prominent diseases. This thesis details analytical methods that use fluorescence derivatization in order to detect small molecule biomarkers of oxidative stress as they relate to epilepsy, inflammation, and traumatic brain injury.

A liquid chromatography-fluorescence method was developed for the detection of reactive aldehyde biomarkers, which are by-products of oxidative stress following epileptic seizures. The method was applied to an animal model of epilepsy and used to monitor concentrations of the analytes over several days in urine samples. This study revealed a circadian cycling of these aldehydes, as well as elucidating which ones were present at increased levels after a seizure.

A microchip electrophoresis-fluorescence method was then developed for the detection of carnosine, an endogenous dipeptide that is involved in oxidative stress-induced inflammation following prolonged activation of macrophage cells. The method was used to measure the native presence of carnosine in these cells, as well as investigate its uptake under normal and pro-oxidative conditions. This study indicated that carnosine's antioxidant properties might lead to its increased uptake by macrophage cells under inflammatory conditions.

Another microchip electrophoresis-fluorescence method was developed to examine excitatory amino acid neurotransmitters involved in neuronal damage following traumatic brain injury. The microchip electrophoresis chip was coupled to microdialysis sampling with on-line derivatization for continuous monitoring of these analytes with a total lag time of twelve minutes and 90 second temporal resolution. Further work with this system will focus on improving the limits of detection so that it could be used by medical professionals to monitor the neurochemical health of a TBI patient.

Acknowledgments

It hardly seems fair that this, the shortest section of my thesis, was probably the most important when it came to earning my doctorate degree. I'll do my best to do it justice. I'll probably forget a name or two simply because there are so many people that I need to thank.

First, I want to acknowledge my late research advisor, Dr. Craig Lunte. When I first stepped into his lab as part of the Research Experience for Undergraduates program I didn't plan on going to graduate school. However, it was impossible to work with Craig without being swept along in his passion for chemistry. By the end of that summer he had inspired me to continue my education, and I joined his lab as a graduate researcher the next year. Here I am, seven years later and on the cusp of receiving my doctorate degree, and it's all thanks to Craig. He encouraged me to step outside my comfort zone, to always ask more questions, and to never forget the basics when confronted with a new problem. I miss his enthusiasm and guidance every day. I consider myself lucky for getting to experience his mentorship firsthand.

Most graduate students struggle to find a single research advisor that they connect with; I was fortunate enough to have two. Dr. Susan Lunte graciously accepted me into her research group after Craig passed away despite how difficult it must have been. She provided endless guidance over the last two years of my doctorate work. Words cannot express how grateful I am for her willingness to take me into her group and help me get my degree. Sue helped me publish two papers and a book chapter, as well as sending me to multiple conferences (including two in Sweden). She never runs out of ideas or new experiments to try and always believes in her students. Trying to live up to her expectations has made me a better scientist and person. Without Sue's support I'm not sure I could have made it. Hopefully one day she'll forgive me for being too tall for the hooding ceremony.

Research can never be completed in a vacuum. Every scientist needs peers to share ideas and learn new techniques. Some of the biggest breakthrough in my graduate career started with a casual conversation and some sketches or calculations jotted down on the back of a cocktail napkin. I'm very grateful to all the members of both the Craig and Susan Lunte research groups who've helped me out in innumerable ways. They are, in no particular order: Carl, Megan, Sara, Ryan, Nhan, Amanda, Hasitha, Mitchell, Kavisha, Tom, Dulan, Rachel, Joe, Nate, Shamal, Manjula, Abdullah, Giuseppe, Claudia, Kelci, and Galina.

I've had great friends support me throughout graduate school as well. You can't spend every minute in the lab, after all. Whether its board games, a barbeque, or just sharing a drink after a long day, all of these people have helped me wind down and recover from the stress of graduate school: Brad, Lee, Aaron, Joe, Nat, Rob and Rob (yes, both of you), Shelby, JW, Samantha, Pat, Mary, Mason, Jess, Tom, Ryan, Nhan, and Daniel. Thanks for everything, you guys.

I need to thank my family as well. My mom and dad have always believed in me and never questioned my decision to go for a Ph.D. They'll be the first to admit they don't understand what I do, but I know they're proud of me regardless. I'm sure the same goes for my brother, Ryan, although you probably will never hear him say it (he's quiet). I'm so grateful for all of your support.

Last but certainly not least is my wife, Ellen Duesterhaus. Her love and patience are the only thing that made all of this possible. She's my best friend, my confidante, my entire world. Mere thanks aren't sufficient to express how grateful I am for her. Graduate school has been a long haul, with plenty of ups and downs along the way, but we're finally crossing the finish line. I can't imagine spending the rest of my life with anyone else and I can't wait to see where life takes us next. It might be my name on this thesis, but you've been there holding me up every step of the way. Take all the credit you want, you earned it.

Table of Contents

Tables

Figures

Chapter 1:

Analytical Techniques for Monitoring Biomarkers of Oxidative Stress

1.1. Research Objectives

Oxidative stress is a state where the excessive production of reactive nitrogen and oxygen species (RNOS) overcomes the body's natural antioxidant defense system, resulting in damage to biomolecules and the alteration of biochemical pathways [1]. Oxidative stress has been linked to several prominent disease states such as Alzheimer's disease [2], Parkinson's disease [3], ischemia [4], diabetes [5], cancer [6], inflammation [7], traumatic brain injury [8], and epilepsy [9]. Oxidative stress has even been proposed as a key component of the free radical theory of aging, in which the decline of the antioxidant defense system is responsible for aging [10]. Due to the widespread prevalence and impact of oxidative stress, there is a huge interest in the development of analytical methods that can better monitor its biomarkers in living systems.

When it comes to the detection of RNOS and their biomarkers, fluorescence derivatization has proven to be an invaluable tool due to its high sensitivity, simplicity in data collection and manipulation, and its high spatial resolution when combined with microscopic imaging [11]. A wide range of fluorescent probes have been developed to directly detect RNOS and small molecule biomarkers produced via their activity [11-14]. This dissertation discusses the use of fluorescence derivatization to monitor the small molecule by-products of oxidative stress in three prominent conditions: epilepsy, inflammation, and traumatic brain injury. Reverse-phase liquid chromatography and microchip electrophoresis are used to separate the derivatized biomarkers from complex biological matrixes, such as urine, bulk cell lysates, and artificial cerebrospinal fluid.

1.2. Oxidative Stress

Under normal physiological conditions there exists a complex biochemical control network designed to modulate the amount of RNOS present in the body, which is known as the antioxidant defense system [15]. Many of the RNOS responsible for the deleterious effects of oxidative stress are free radicals. Radicals are compounds or molecules that possess an unpaired electron that makes them less stable and they are therefore usually highly reactive with biomolecules [16]. Free radical RNOS include the superoxide radical ($O_2^{\bullet-}$), hydroperoxyl radical ($HO_2^{\bullet}$), hydroxyl radical ($HO^{\bullet}$), peroxyl radical ($ROO^{\bullet}$), nitrogen dioxide radical ($^{\bullet}NO_2$), and nitric oxide ($^{\bullet}NO$). Some key RNOS are also non-radical species, such as hydrogen peroxide (H_2O_2), singlet oxygen ($^1O_2$), hypochlorous acid (HOCl), the peroxynitrite anion ($ONOO^-$), and peroxynitrous acid (ONOOH) [16-18].

Endogenously produced RNOS play a pivotal role in several important biochemical pathways, such as the production of $O_2^{\bullet-}$ by NADPH oxidase in phagocytes [19] and the synthesis of $^{\bullet}NO$ by inducible nitric oxide synthase in macrophage cells [20]. Normally these species are kept in check via the antioxidant defense system, which contains enzymatic and non-enzymatic pathways that prevent damage by scavenging excess RNOS [21]. When RNOS are produced in high concentrations due to disease or trauma, they overcome the ability of these defense systems to intercept them, leading to reactions with key biomolecules and the disturbance of natural pathways [1]. RNOS have been known to react with DNA [22], proteins [23], and lipids [24]. The damage caused by $O_2^{\bullet-}$ and $^{\bullet}NO$ is referred to as nitrosative and oxidative damage, respectively, and causes more damage in addition to the original pathophysiological pathway. A selection of the pathways of RNOS formation and subsequent damage is shown in Figure 1.1. The exact role of

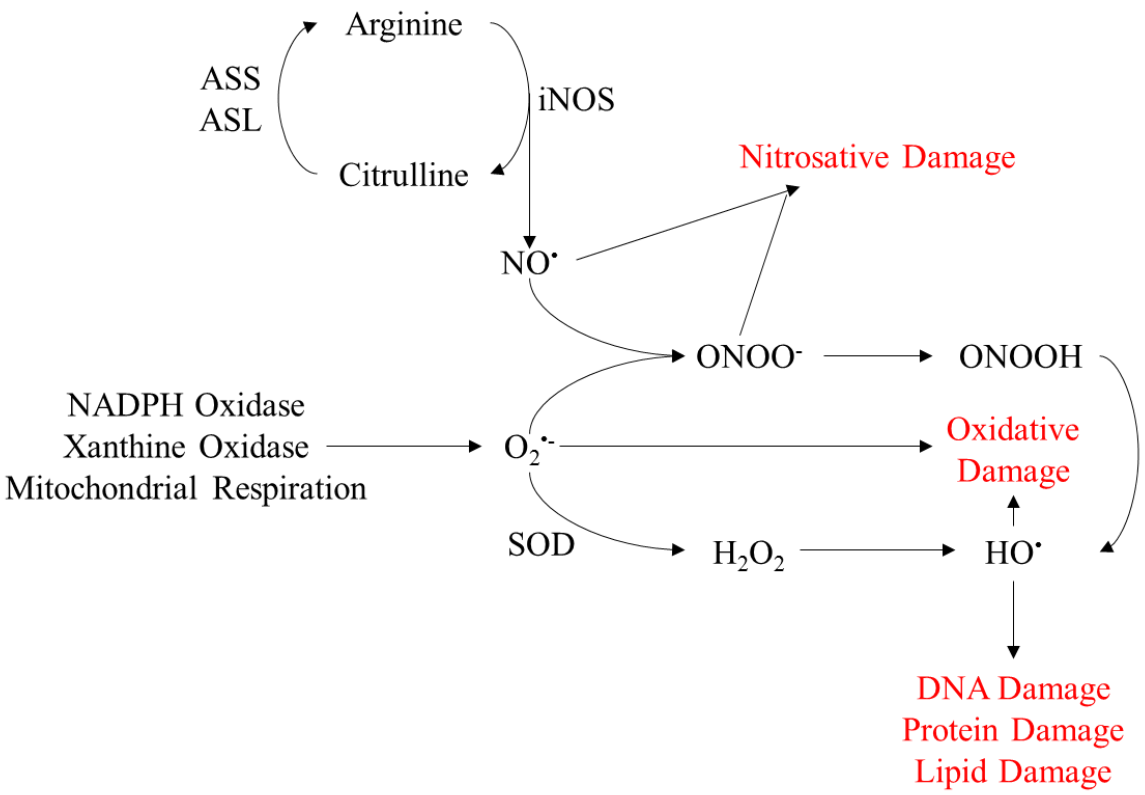

Figure 1.1: Biological pathways of RNOS formation

The formation of RNOS leads to deleterious damage to biomolecules and biochemical pathways. ASS = argininosuccinate synthase; ASL = argininosuccinate lyase; iNOS = inducible nitric oxide synthase; SOD = superoxide dismutase.

oxidative stress as it relates to epilepsy, inflammation, and traumatic brain injury will be discussed further in the relevant chapters.

1.3. Fluorescence

1.3.1. Theory of Fluorescence

The term fluorescence was first coined by Sir George Stokes, who used it to describe a phenomenon where the wavelength of dispersed light was longer than the wavelength of the original light used to illuminate a particular sample [25]. This change in wavelength is now referred to as the Stokes shift and is key to the basic theory of fluorescence.

In fluorescence, an electron is elevated to an excited orbital via absorption of the energy from an incoming photon. It can then return to the ground state by the rapid emission of another photon. This can be visually demonstrated by a Jablonski diagram, which shows a theoretical representation of the ground (s_0), first (s_1), and second (s_2) electronic states of the particular compound, as shown in Figure 1.2. When an incoming photon is abosorbed, an electron can be excited into the vibrational levels of a higher electronic state. This electron will usually return to the lowest vibrational level of the electronic state through a series of non-radiative interactions collectively referred to as internal conversion. The electron can then return to the vibrational levels of the ground state, emitting a photon of a different energy level, and consequently, a different wavelength [26]. This photon is then measured as the fluorescent signal.

As an excited electron usually goes from the ground state into higher vibrational level of the excited state, while fluorescence occurs from the lowest vibrational level of the excited state back to the ground state, the energy associated with emission is normally lower than that of excitation. This difference in energy is reflected by a longer wavelength in the emitted photon, causing the Stokes shift.

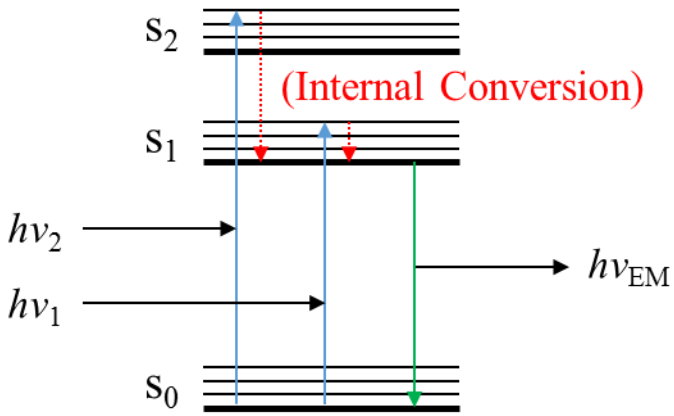

Figure 1.2: Jablonski diagram demonstrating mechanism of fluorescence

In fluorescence, electrons are excited from the ground state (s_0) into the vibrational levels of the first (s_1) or second (s_2) electronic state by the absorption of energy from an incoming photon (hv_1 or hv_2). They will then undergo internal conversion to transition to s_1 before returning to s_o via the rapid emission of a photon (hv_{EM}), which is measured as the fluorescent signal.

The fluorescence of a particular molecule is often dependent on its aromaticity. The π electrons associated with a highly-conjugated structure are more easily excited at energy levels correlating to the visible spectrum of light [27]. This makes them suitable for use with common excitation sources, such as arc lamps, light-emitting diodes (LEDs), and various laser designs [28].

Another important factor to consider when studying fluorescence is quantum yield (Φ). This is the relationship between the number of photons emitted and the number of photons absorbed, with a 1:1 ratio resulting in an Φ of 1.0. The experimental determination of this value is key to making quantitative fluorescent measurements [29].

1.3.2. Fluorescence in Biological Samples

Fluorescence detection is highly desirable when examining biological samples due to its high sensitivity and the specificity that comes from having a specific excitation and emission wavelength that is uniqure to the fluorophore of interest, which leads to a measurement that is considered background free. Endogenously present fluorescent molecules are known as intrinsic fluorophores [30]. Some of the most-studied intrinsic fluorophores are the aromatic amino acids tryptophan, tyrosine, and phenylalanine, which all display low fluorescent signals with ultraviolet excitation wavelengths [31, 32]. Another common intrinsic fluorophore is the reduced form of the coenzyme nicotinamide adenine dinucleotide (NADH) [33]. All four of these compounds display low Φ (as shown in Table 1.1) and have a correspondingly low fluorescent signal response. This highlights a key issue concerning intrinsic fluorophores: as they are endogenously present, their spectrometric properties cannot be easily altered to optimize the response. Also, since such a small fraction of biologically-relevant molecules possess are intrinsically fluorescent, they cannot be used to investigate many prominent diseases and conditions of interest.

Table 1.1: Examples of the three fluorescent amino acids and one fluorescent coenzyme, along with their quantum yield (Φ), excitation maximum (λ_{EX}), and emission maximum (λ_{EM}) [31-33].

Name	Structure	Φ	λ_{EX} (nm)	λ_{EM} (nm)
Tryptophan	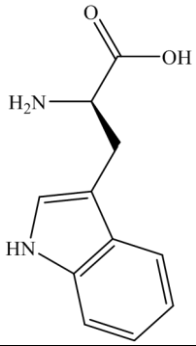	0.13	280	348
Tyrosine	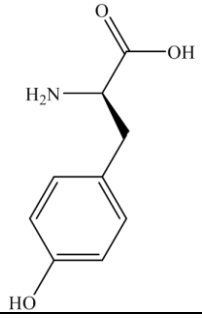	0.14	274	303
Phenylalanine	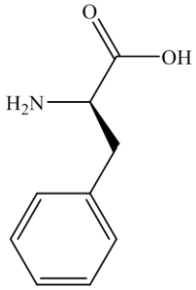	0.024	257	282
NADH	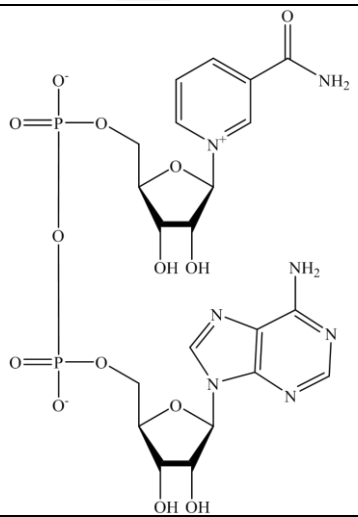	0.019	340	470

Extrinsic fluorophores are rationally designed in order to specifically bind to a molecule of interest and lend them the desired spectrometric property. These reagents are designed to possess a signaling moiety, a biomolecule-specific moiety, and a spacer to connect them [34]. The design of an extrinsic fluorophore usually begins with a compound that possesses a high Φ and large degree of aromaticity that is fine-tuned to achieve better spectral properties and specific binding to the analyte of interest. One such example is xanthene, which has been used as a scaffolding to create a wide range of rhodamine and fluorescein derivatives with high Φ values, as shown in Figure 1.3 [35, 36].

1.3.3. Extrinsic Fluorescent Probes for Biomarkers of Oxidative Stress

A variety of fluorescent probes have been developed specifically for the direct detection of RNOS [11, 13, 14]. However, the short lifetimes and high reactivity of these molecules has given rise to doubts about the specificity of these probes and their ability to actually measure RNOS concentrations [12, 37]. This has led to the development of probes that derivatize small molecule biomarkers of oxidative stress as opposed to the RNOS themselves.

When looking at carbonyl biomarkers, the most commonly used derivatization reagent is 2,4-dinitrophenylhydrazine [38]. This compound possesses high specificity for carbonyls, but has limited aromaticity and is therefore most commonly used for UV absorbance measurements and mass spectrometry [39]. Alterations of its structure gave rise to several fluorescent hydrazide species that maintained the high affinity for carbonyls while possessing better spectrometric properties [40]. One such derivative is dansylhydrazine (DNSH), which is shown in Figure 1.4. This derivatization reagent has the added advantage of binding more readily to aldehydes than ketones and has analytical reproducibility [41], fast reaction times (<15 minutes) [42], and good quantum yield [43].

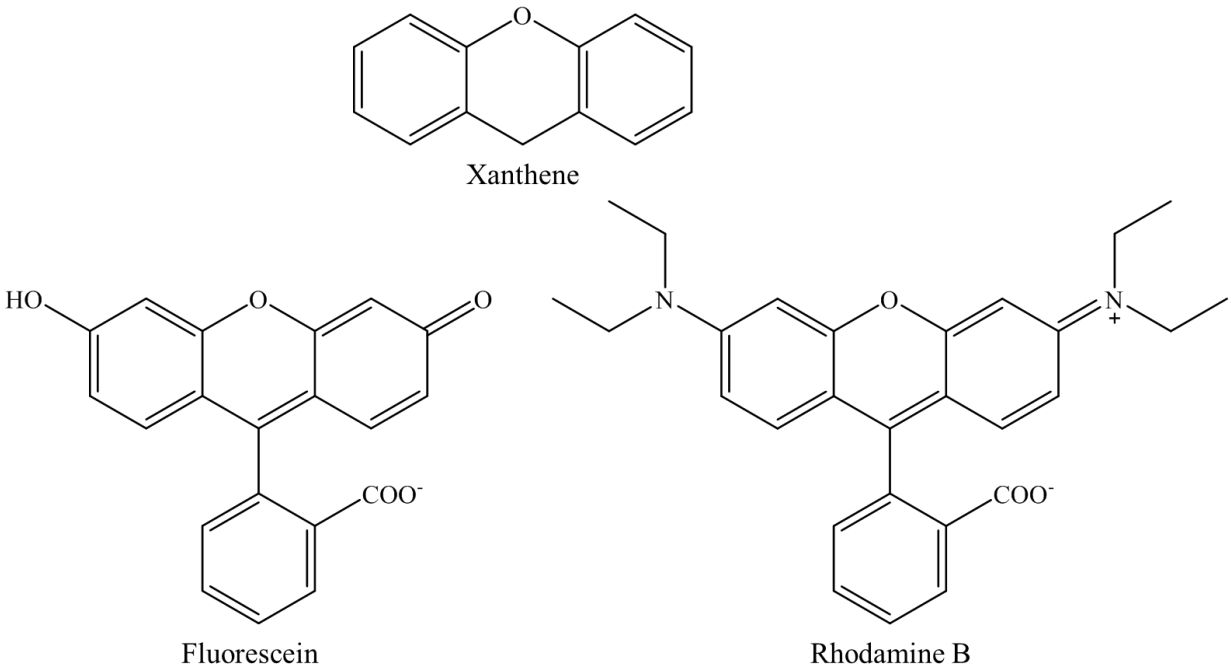

Figure 1.3: Examples of fluorescent reagents based on structure of xanthene

Although xanthene is not naturally fluorescent, its structure has been used as the scaffolding to create two highly efficient fluorescent reagents: fluorescein (Φ = 0.79) and rhodamine B (Φ = 1.0).

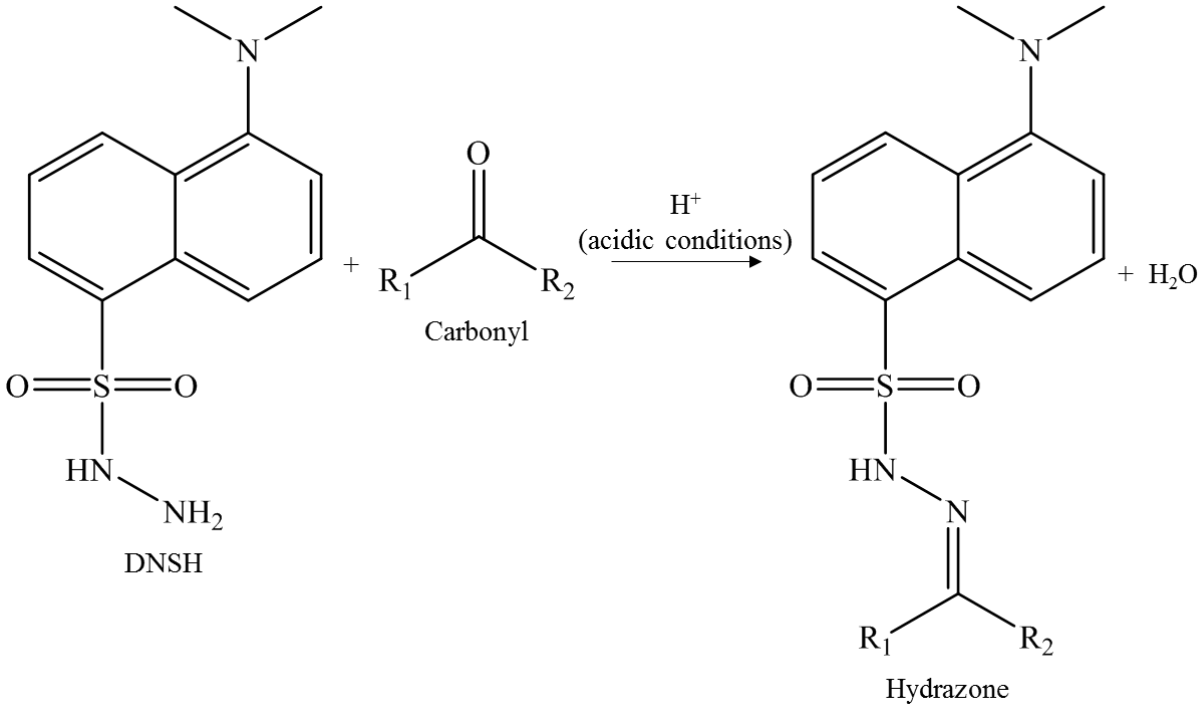

Figure 1.4: Reaction of DNSH with carbonyls to form a fluorescent hydrazone

Under acidic conditions, dansylhydrazine (DNSH) will react with carbonyls in order to form a fluorescent hydrazone derivative.

There exists a literature precedence that suggests oxidative stress can impact amino acid concentrations and functionality [16, 23]. A large number of extrinsic fluorescent probes have been developed specifically for the determination of amino acids via a reaction with either the primary amine or carboxylic acid moiety [44, 45]. A selection of these are shown in Table 1.2, along with some key spectrophotometric information and the relevant literature references [46-54]. Of particular interest is naphthalene-2,3-dicarboxaldehyde (NDA) [48], a probe designed to improve on the common derivatization agent *o*-phthaldialdehyde (OPA) [47]. This extrinsic probe has the added benefit of being a fluorogenic reagent; NDA is non-fluorescent until it reacts with a primary amine to form a highly-fluorescent cyanobenz[*f*]isoindole (CBI) derivative, as shown in Figure 1.5. This reaction requires the presence of a strong nucleophile to proceed and cyanide (CN) has been found to produce the most stable end product. Since NDA itself is not fluorescent it will not interfere with the fluorescent signal of the CBI derivatives, simplifying their separation and detection. NDA also possesses a high quantum yield (Φ = 0.54) and relatively fast reaction times (15-45 minutes). Additionally, the CBI derivatives are more stable than the end product of the OPA reaction ($t_{1/2}$ = 1.5 hours) and lose less than 10% of their overall fluorescence response after 10 hours [48].

1.3.4. Instrumental Considerations for Fluorescence Detection

One of the most important instrument considerations when using fluorescence detection is the excitation source used to provide the original photons. There is a direct relationship between the amount of photons absorbed and the amount emitted via fluorescence, meaning that more intense light sources will naturally provide a higher signal response [28]. Light sources with a continuous emission over a wide range of wavelengths can prove desirable in some cases, as they

Table 1.2: Examples of common fluorescent reagents used for the derivatization of amino acids based on a reaction with their amine (NH_2) or carboxylic acid (COOH) moieties.

Reagent Name (Abbreviation)	Target Group	Reaction Time	Φ	λ_{EX} (nm)	λ_{EM} (nm)	References
o-Phthaldialdehyde (OPA)	NH_2	10 minutes (with 2-mercaptoethanol)	0.33 - 0.47	340	455	[46, 47]
9-Fluorenylmethyl chloroformate (FOMC)	COOH	10 minutes	0.54	265	315	[49, 51]
Napthalene-2,3-dicarboxaldehyde (NDA)	NH_2	15 - 45 minutes (with cyanide)	0.54	420, 440	490	[48]
2-(9-Anthryl)ethyl chloroformate (AEOC)	COOH	5 minutes	0.23	258	418	[50]
Fluorescein isiothiocyanate (FITC)	NH_2	2 hours	0.37 - 0.93	490	525	[52, 53]

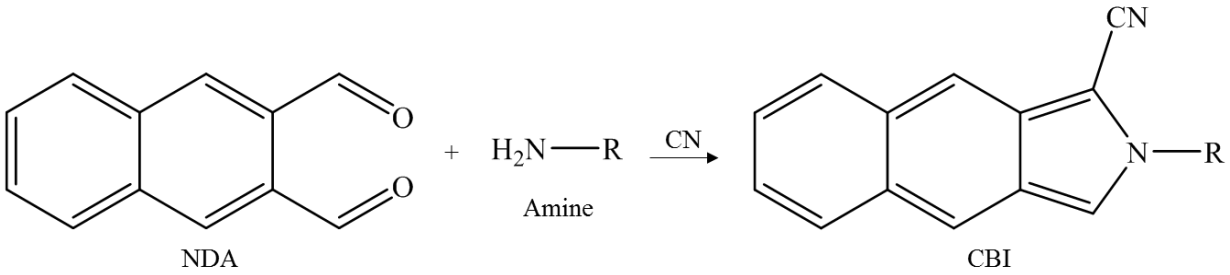

Figure 1.5: Reaction of NDA with primary amines to form a fluorescent CBI

In the presence of a strong nucleophile (such as cyanide), non-fluorescent naphthalene-2,3-dicarboxaldehyde (NDA) will react with primary to form a fluorescent cyanobenz[*f*]isoindole (CBI) derivative.

can be used for a variety of fluorescent probes. Some examples of this type of light source are Xenon arc lamps [55] and LEDs [56], which both provide a continuous light output over a wide range of wavelengths. However, these rarely provide the sensitivity required for biological measurements. Lasers can be used to provide monochromatic radiation at a much higher intensity and have the potential to be pulsed for different experimental setups [28]. Using a laser as an excitation source is commonly referred to as laser-induced fluorescence (LIF).

1.4. Analytical Separations

Although fluorescence can usually provide higher specificity than other spectroscopic techniques, the complexity of biological samples usually requires that it be coupled with a method of separating out and isolating the various components of the sample matrix. A brief discussion of three separation methods pivotal to this work follows.

1.4.1. Liquid Chromatography

The term chromatography (literally "color writing") was coined by Mikail Tswett, who used it to describe the separation of pigments from plant extracts [57]. Over the years various different chromatographic techniques have been developed for different purposes, such as gas chromatography, thin layer chromatography, micellar electrokinetic chromatography, supercritical fluid chromatography, and countercurrent chromatography.

Perhaps one of the best-known chromatographic techniques is liquid chromatography (LC). Like all chromatographic techniques, the separation of molecules in LC is dependent on their affinity for a stationary phase, which in modern instrumentation consists of micron-sized particles packed within a column. A solvent (the mobile phase) is flowed through this packed column at a specific flow rate. The length of time it takes for the analytes to elute from the column depends on their affinity for the stationary phase.

The exact nature of the stationary phase determines the basis of the separation. The most common LC separations are dependent on the polarity of the molecules. When the mobile phase is less polar than the stationary phase, it is referred to as normal-phase LC. Conversely, when the mobile phase is more polar than the stationary phase, it is referred to as reverse-phase LC (RP-LC). There are many other modes of separation for LC, such as ion affinity, size exclusion, and hydrophilic interactions. Examples of some common LC strategies are shown in Table 1.3 [58-63]. The experiments in this thesis utilize RP-LC, in which the most common stationary phases consist of long hydrocarbon chains bound to silica particles, such as octyl (C8) or octadecyl (C18) functional groups [63].

The efficiency of a chromatographic separation depends on three variables that are related using the Knox Equation, shown in Equation 1. Here *H* represents a theoretical value known as the height equivalent of a theoretical plate, which is a direct measure of a separation efficiency [64].

$$H = Au^{1/3} + \frac{B}{u} + Cu \qquad (1)$$

The efficiency of the separation is highly dependent on the mobile phase velocity (u). The multipath term (A) is a measure of the packed nature of a modern chromatographic column and accounts for the difference in migration time that arises from the different routes available for analytes to travel through the packing material. This is mostly dependent on the particle and column dimensions, but the number of paths that the analyte can take will diminish at higher u. The longitudinal diffusion term (B) is a measure of band broadening that occurs due to diffusion of the analyte within the column. At faster velocities there is less time for the analytes to diffuse within the column, so this is inversely proportional to u. The mass transfer term (C) is a measure

Table 1.3: Some examples of common separation techniques in LC, including some basic stationary and mobile phases.

Name	Separation Basis	Stationary Phase	Mobile Phase	References
Normal Phase (NP-LC)	Polarity	Polar: • Silica • Amino • Cyano • Diol	Nonpolar solvents: • Benzene • Chloroform	[63]
Reversed Phase (RP-LC)	Polarity	Nonpolar: • Octadecyl (C_{18}) • Octyl (C_8) • Phenyl	Polar solvents: • Aqueous solutions	[59, 63]
Size Exclusion (SEC)	Hydrodynamic Radius	• Porous materials with specific pore sizes	• Aqueous solutions	[60]
Ion Exchange (IEC)	Ionic Properties	Cation Exchange: • Sulfonic acid • Carboxylic acid Anion Exchange: • Ammonium • Amine	• Electrolyte solutions	[62]
Hydrophilic Interaction (HILIC)	Hydrophilicity	Polar: • Silica • Amino • Cyano • Diol	Polar solvents: • Aqueous solutions with >50% organic content	[58, 61]

of how well the analytes can diffuse between the mobile and stationary phase to reach an equilibrium. At faster velocities there is less opportunity for this equilibrium to be reached, so it is directly proportional to u. Since the A/B and C terms directly work against each other, there exists an optimal mobile phase velocity at which a chromatographic separation will be most efficient that must be experimentally optimized. A graphical representation of the Knox Equation is shown in Figure 1.6 that demonstrates this optimal value of u.

A wide range of detectors can be coupled with LC such as refractive index, evaporative light scattering, UV/Vis absorption, electrochemical, conductometric, mass spectrometry, and fluorescence detectors [65]. LC has been a dominant analytical tool for decades and has been heavily utilized for pharmaceutical and biomedical analyses [66].

1.4.2. Capillary Electrophoresis

Capillary electrophoresis (CE) is a separation method for charged species based on their electrophoretic mobility (μ_e). μ_e is influenced by the hydrodynamic radius (r) and charge (q) of the analyte in question, as well as the viscosity of the solution (η) as it relates to the frictional coefficient, as described by Equation 2 [67]:

$$\mu_e = \frac{q}{6\pi\eta r} \qquad (2)$$

A CE separation traditionally occurs in a fused silica capillary (with an inner diameter of 25-250 μm) containing a conductive solution, known as the background electrolyte (BGE). The velocity of a particular analyte (v) depends on its affinity towards either the anode or cathode depending on its inherent charge. This is a factor of the total electric field strength (E), which is established by applying a voltage (V) across the length of the capillary (L). This relationship is shown by Equation 3 [68]:

$$v = \mu_e E = \frac{\mu_e V}{L} \qquad (3)$$

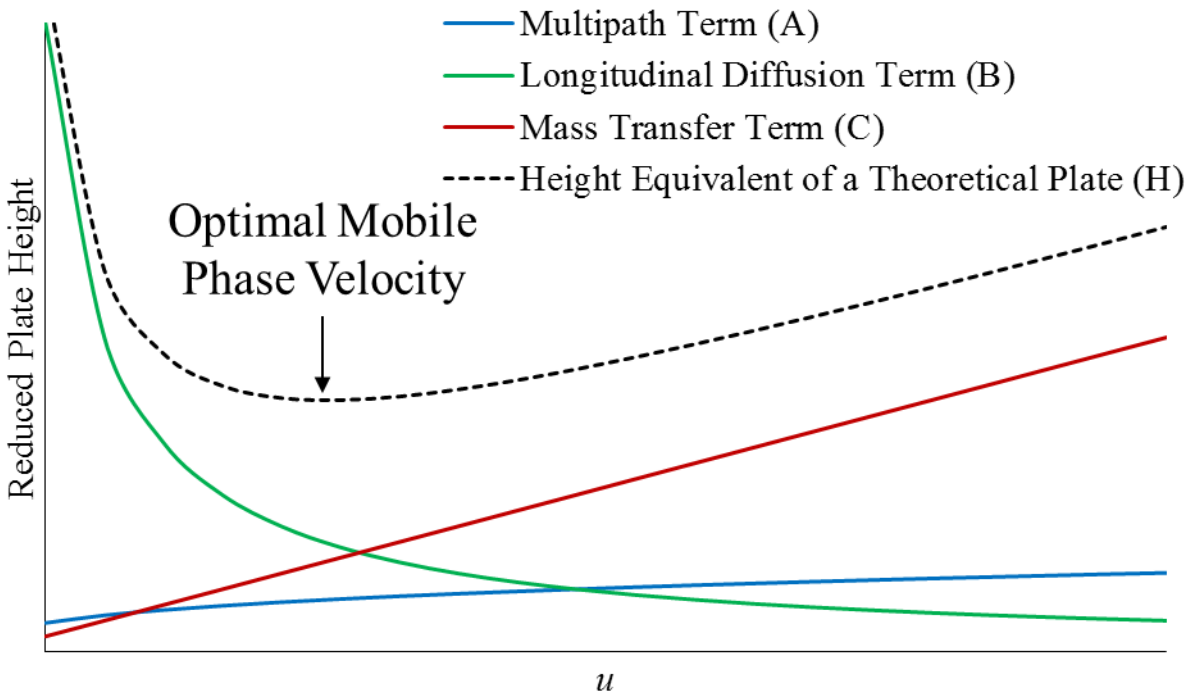

Figure 1.6: Visual representation of the parameters influencing the Knox Equation for LC

This demonstrates the overall impact of the mobile phase velocity (u) on the overall efficiency of the separation, as indicated by the height equivalent of a theoretical plate. There exists an optimal u at which the most efficient separation can be achieved.

The direction of an ion's velocity is dependent on its charge; cations will be drawn towards the cathode, while anions will be drawn towards the anode. However, in most cases all of the analytes are moved in the same direction thanks to a bulk flow known as the electroosmotic flow (EOF). The EOF is a result of the interaction between the surface walls of the capillary with the BGE. Above a pH of 3, the silica groups on the surface of the capillary walls will become ionized, forming a net negative surface charge. A layer of hydrated cations from the BGE will form along the walls in response to the negative charge, forming an adsorbed and a diffuse layer of charge. These two layers are referred to as the electrical double layer and exist between the bulk BGE solution and silica walls. When the voltage is applied across the capillary, the diffuse layer will move towards the cathode, producing a bulk flow that will drag the BGE as a whole towards the cathode. This bulk flow is usually stronger than the electrophoretic mobility of ions that would normally migrate in the opposite direction, carrying all of the ions present in the capillary in the same direction to allow for detection [67, 69]. Therefore the overall apparent electrophoretic mobility depends not only of that belonging to the ion, but also the electrophoretic mobility of the EOF, as shown in Figure 1.7.

When considering the Knox Equation, CE separations are intrinsically more efficient than chromatography. This is because two of the primary terms in that equations (the multipath term and mass transfer term) do not apply to CE, given its open columns and lack of stationary phase. This means that only the longitudinal diffusion term will influence the efficiency of the separation. However, the main weakness of CE is that it fails to separate neutral compounds, since their lack of charge means they do not possess a natural μ_e and will therefore move at the same flow rate at μ_{EOF}. Many different buffer additives have been studied that will allow for the separation of neutral

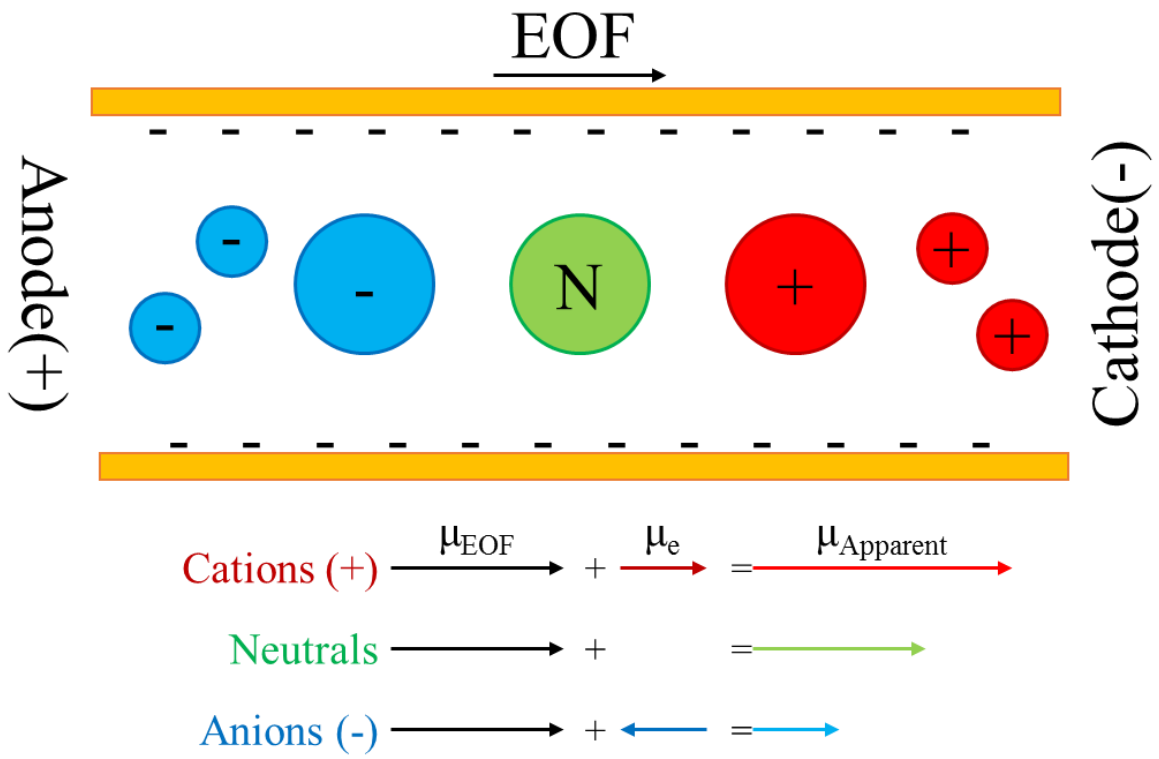

Figure 1.7: Basic schematic of a CE separation

The apparent electrophoretic mobility of the analytes ($\mu_{Apparent}$) depends not only on their electrophoretic mobility (μ_e), but also the mobility of the electroosmotic flow (μ_{EOF}). This results in all of the analytes being carried in the same direction (pictured here is normal polarity, where the EOF flows towards the cathode).

species, usually by using surfactants to create micelles [70]. The neutral species can partition in and out of the micelles, which in turn migrate at a different rate than the EOF based on their own electrophoretic mobility. The time spent within the micelles will separate the neutral species from the EOF, allowing them to be detected separately. Due to the fact that this results in a transition between two phases, as is the basis of chromatography, this technique is referred to as micellar electrokinetic chromatography.

1.4.3. Microchip Electrophoresis

Microchip electrophoresis (ME) was developed in an effort to miniaturize the footprint of CE separations. Whereas CE usually occurs in a silica capillary that is 50 – 100 cm in length, ME separations occur within microfabricated channels that are typically 5 – 15 cm long. This has the obvious benefit of requiring smaller volumes of BGE, as well as using a fraction of the voltage to produce the same electric field strength. Additionally, due once again to the smaller separation length and channel dimensions (15 μm deep by 50 μm wide), ME separations occur on a much faster time scale with less sample diffusion, allowing for better temporal resolution than traditional CE systems [71]. Modern microfabrication techniques also allow for the creation of complicated features that be directly integrated on the microchip, such as gating, tapered channels, on-chip electrodes, and micromixers [72]. Due to these advantages, ME has been extensively employed as a separation technique since its introduction in the 1990s [73, 74].

A typical ME setup uses two electrodes connected to a high voltage power supply in order to generate the electric field. A high voltage is applied to the buffer reservoir, while the reservoir at the end of the separation channel is held at ground. This creates an electric field along the microfabricated separation channel, which separates the analytes based on their electrophoretic mobility [67]. These microfluidic channels are typically fabricated in a glass or polymer (e.g.

polydimethylsiloxane or cyclic olefin copolymer) substrate [75]. The exact methods for fabricating an all-glass and a polymer-glass hybrid microchip are discussed in Chapters 3 and 4, respectively.

The two most basic microchip designs are a simple-t and serpentine, as shown in Figure 1.8. Three of the four reservoirs in the design are filled with BGE, while the last reservoir contains the sample to be analyzed. Two separate electric fields are maintained via the use of two high voltage power supplies. One *E* runs from the BGE reservoir down the length of the separation channel, while the second *E* goes from the sample reservoir to the waste. This results in the formation of electrokinetic gate at the junction of these two electric fields that keeps the separate flows from mixing. In order to inject a sample plug into the separation channel, the voltage applied to the BGE reservoir is temporarily floated, which allows the sample to free flow into the gate area. When the voltage is then reestablished a small analyte plug is formed and isolated within the separation electric field, at which point the electrophoretic separation can occur. The exact volume of the sample plug can be calculated depending on the two field strengths and the length of the injection and is highly reproducible [76]. The process of an electrokinetically gated injection is shown in Figure 1.9. The length of the sample plug can be calculated using Equation 4 [77]:

$$l_i = t_{inj} E \mu_e \qquad (4)$$

Here, l_i is the length of the sample plug, while t_{inj} is the injection time. Note that l_i is dependent on the electrophoretic mobility of the analyte, which means that the charge of the ion must be taken into consideration when using this injections scheme.

The most commonly used detection methods for ME are electrochemistry and fluorescence. Electrochemistry (usually amperometry) has the advantage of being highly specific, but suffers from higher noise due to the electric fields necessary for the electrophoretic separation

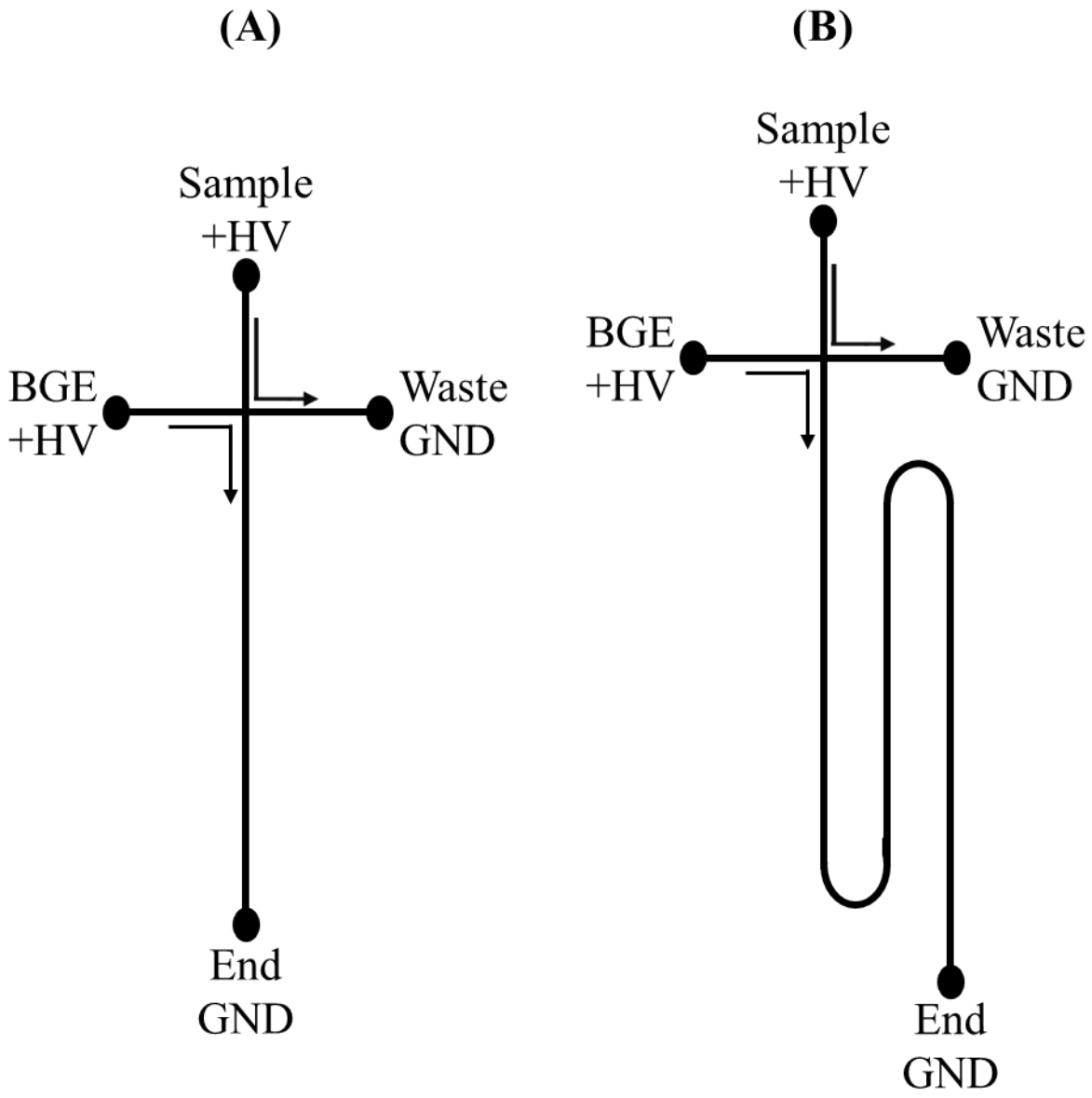

Figure 1.8: Two basic ME channel designs

Two basic microchip electrophoresis (ME) designs: (A) simple-t; (B) serpentine.

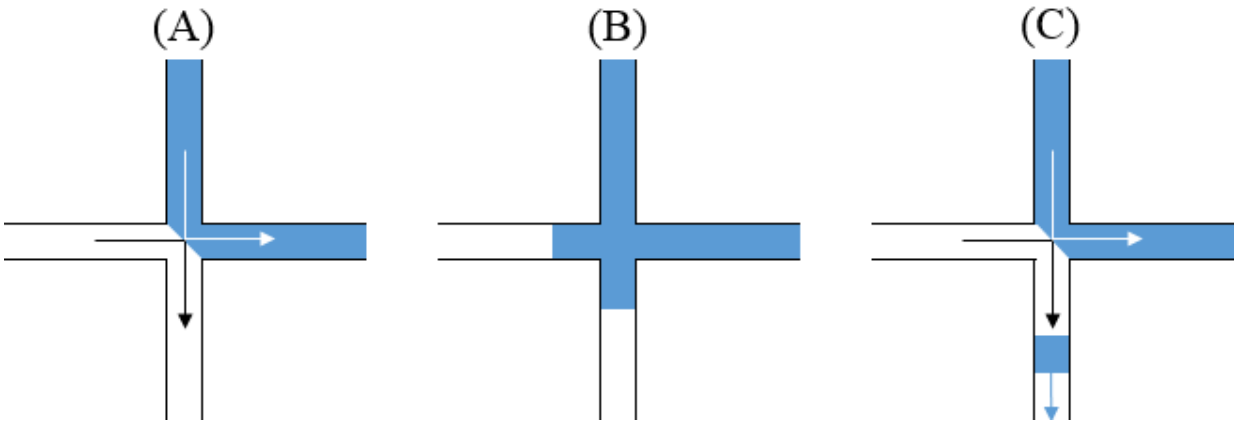

Figure 1.9: Schematic of electrokinetically gated injections in ME

The following process applies to electrokinetic injections for the basic ME device designs shown in Figure 1.8: (A) An electrokinetic gate is formed at the junction by the application of two separate high voltages; (B) The separation voltage is temporarily floated, allowing the sample solution (blue) to fill the junction; (C) The separation voltage is reestablished, isolating a sample plug that is carried down the separation channel and electrophoretically separated.

[78]. Solving this usually requires the use of an isolated potentiostat [79], dual separation channels [80], or the inclusion of a metal decoupler [81]. Fluorescence, by comparison, couples relatively easily with ME due to the optical transparency of most common substrates [82]. Monochromatic excitation sources (such as diode lasers) are especially convenient due to the fact that the light can be focused at any point within the separation channel with a simple optics setup, allowing the detection location to be freely moved for highly sensitive measurements. An example schematic of a ME-LIF experimental setup is shown in Figure 1.10.

1.5. Chapter Summaries

The following is a summary of the chapters of this thesis, which employs liquid chromatography, microchip electrophoresis, and fluorescence derivatization to monitor by-products of RNOS overproduction and oxidative stress.

1.5.1. Chapter 2

Epilepsy is a condition well-known for causing unprompted seizures in patients. One effect of seizures is the overproduction of RNOS, leading to oxidative stress and secondary damage. Free radical RNOS will readily react with lipids, leading to lipid peroxidation, a chain reaction in which lipids are radicalized and produce more radicals. The byproducts of this process (such as reactive aldehyde species) can be used as biomarkers for the extent of lipid peroxidation and oxidative stress. In this chapter, reactive aldehydes are derivatized with DNSH to produce hydrazone derivatives, which are subsequently separated using RP-LC and detected via their fluorescence.

1.5.2. Chapter 3

Inflammation plays a role in a host of different disease states. This is partially due to the immune system, in which activated macrophage cells will produce $^{\bullet}$NO via inducible nitric oxide

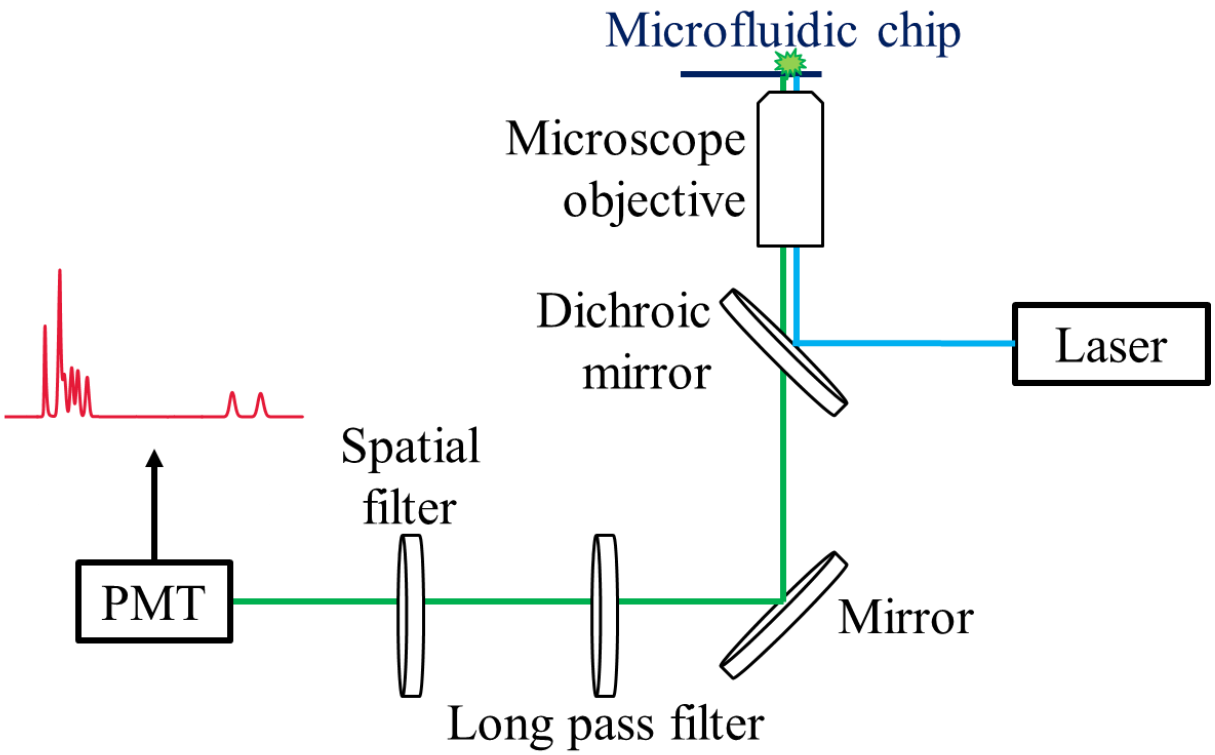

Figure 1.10: Optical set-up for ME-LIF experiments

The wavelengths of the diode laser and filters can be modified for the fluorescent probe of interest.

synthase (iNOS). Over-activation of these cells will result in an excess of •NO, which will lead to oxidative stress. Carnosine is an endogenous dipeptide that is known to show antioxidant properties. In this chapter, the uptake of carnosine into macrophage cells under pro-inflammatory conditions is investigated. Carnosine is monitored in cell lysates following NDA/CN derivatization and separation from other amino acids by use of ME-LIF.

1.5.3. Chapter 4

Traumatic brain injury (TBI) is the most common type of neurotrauma in the world and is caused by blunt-force trauma to the brain. Patients with severe TBIs require their skulls to be opened to relieve pressure, which also allows medical professionals to use microdialysis sampling (MD) to gauge their neurochemical health and evaluate treatment. Excitatory amino acids (EAAs) are a key factor in post-injury health for TBI patients that can lead to neurotoxicity, so being able to monitor their concentration will help with therapeutic treatment. In this chapter, an overall MD-ME-LIF system was optimized with on-line derivatization of EAAs using the NDA/CN reaction.

1.5.4. Chapter 5

This chapter summarizes the progress on these three research projects to date. It also provides immediate and long-term future directions. These include probing different brain regions with epileptic seizures, further studies of iNOS activity in macrophage cells, and improvements in the design of a therapeutic monitoring device for TBI patients.

1.6. References

1. H. Sies. Oxidative stress: oxidants and antioxidants. *Exp. Physiol.,* **1997,** *82* (2), 291-295.

2. C. Cervellati, P. L. Wood, A. Romani, G. Valacchi, M. Squerzanti, J. M. Sanz, B. Ortolani and G. Zuliani. Oxidative challenge in Alzheimer's disease: state of knowledge and future needs. *J. Investig. Med.,* **2016,** *64* (1), 21-32.

3. A. H. Tsang and K. K. Chung. Oxidative and nitrosative stress in Parkinson's disease. *Biochim. Biophys. Acta,* **2009,** *1792* (7), 643-650.

4. C. Li and R. M. Jackson. Reactive species mechanisms of cellular hypoxia-reoxygenation injury. *Am. J. Physiol. Cell Physiol.,* **2002,** *282* (2), C227-241.

5. A. C. Maritim, R. A. Sanders and J. B. Watkins, 3rd. Diabetes, oxidative stress, and antioxidants: a review. *J. Biochem. Mol. Toxicol.,* **2003,** *17* (1), 24-38.

6. S. Reuter, S. C. Gupta, M. M. Chaturvedi and B. B. Aggarwal. Oxidative stress, inflammation, and cancer: how are they linked? *Free Radic. Biol. Med.,* **2010,** *49* (11), 1603-1616.

7. F. Di Virgilio. New pathways for reactive oxygen species generation in inflammation and potential novel pharmacological targets. *Curr. Pharm. Des.,* **2004,** *10* (14), 1647-1652.

8. A. Lewen, P. Matz and P. H. Chan. Free radical pathways in CNS injury. *J. Neurotrauma,* **2000,** *17* (10), 871-890.

9. E. J. Shin, J. H. Jeong, Y. H. Chung, W. K. Kim, K. H. Ko, J. H. Bach, J. S. Hong, Y. Yoneda and H. C. Kim. Role of oxidative stress in epileptic seizures. *Neurochem. Int.,* **2011,** *59* (2), 122-137.

10. F. L. Muller, M. S. Lustgarten, Y. Jang, A. Richardson and H. Van Remmen. Trends in oxidative aging theories. *Free Radic. Biol. Med.,* **2007,** *43* (4), 477-503.

11. A. Gomes, E. Fernandes and J. L. F. C. Lima. Fluorescence probes used for detection of reactive oxygen species. *J. Biochem. Bioph. Meth.,* **2005,** *65* (2-3), 45-80.

12. B. Halliwell and M. Whiteman. Measuring reactive species and oxidative damage in vivo and in cell culture: how should you do it and what do the results mean? *Brit. J. Pharmacol.,* **2004,** *142* (2), 231-255.

13. X. Q. Chen, X. Z. Tian, I. Shin and J. Yoon. Fluorescent and luminescent probes for detection of reactive oxygen and nitrogen species. *Chem. Soc. Rev.,* **2011,** *40* (9), 4783-4804.

14. A. Gomes, E. Fernandes and J. L. F. C. Lima. Use of fluorescence probes for detection of reactive nitrogen species: A review. *J. Fluoresc.,* **2006,** *16* (1), 119-139.

15. S. Vertuani, A. Angusti and S. Manfredini. The antioxidants and pro-antioxidants network: an overview. *Curr. Pharm. Des.,* **2004,** *10* (14), 1677-1694.

16. J. M. McCord. The evolution of free radicals and oxidative stress. *Am. J. Med.,* **2000,** *108* (8), 652-659.

17. R. S. Pardini. Toxicity of Oxygen from Naturally-Occurring Redox-Active Pro-Oxidants. *Arch. Insect Biochem.,* **1995,** *29* (2), 101-118.

18. C. L. Murrant and M. B. Reid. Detection of reactive oxygen and reactive nitrogen species in skeletal muscle. *Microsc. Res. Techniq.,* **2001,** *55* (4), 236-248.

19. B. M. Babior. Phagocytes and oxidative stress. *Am. J. Med.,* **2000,** *109* (1), 33-44.

20. S. Moncada, R. M. J. Palmer and E. A. Higgs. Nitric-Oxide - Physiology, Pathophysiology, and Pharmacology. *Pharmacol. Rev.,* **1991,** *43* (2), 109-142.

21. A. M. Pisoschi and A. Pop. The role of antioxidants in the chemistry of oxidative stress: A review. *Eur. J. Med. Chem.,* **2015,** *97*, 55-74.

22. M. S. Cooke, M. D. Evans, M. Dizdaroglu and J. Lunec. Oxidative DNA damage: mechanisms, mutation, and disease. *FASEB J.,* **2003,** *17* (10), 1195-1214.

23. Y. Wang, J. Yang and J. Yi. Redox Sensing by Proteins: Oxidative Modifications on Cysteines and the Consequent Events. *Antioxid. Redox. Sign.,* **2012,** *16* (7), 649-657.

24. J. M. C. Gutteridge. Lipid-Peroxidation and Antioxidants as Biomarkers of Tissue-Damage. *Clin. Chem.,* **1995,** *41* (12B), 1819-1828.

25. B. Valeur and M. N. Berberan-Santos. A Brief History of Fluorescence and Phosphorescence before the Emergence of Quantum Theory. *J. Chem. Educ.,* **2011,** *88* (6), 731-738.

26. J. R. Lacowicz. Introduction to Fluorescence. In *Principles of Fluorescence Spectroscopy*, 3rd ed.; Springer Science & Business Media, 2006; 1-26.

27. I. B. Berlman. *Handbook of Fluorescence Spectra of Aromatic Molecules*. 2nd ed.; Academic Press 1971.

28. J. R. Lacowicz. Instrumentation for Fluorescence Spectroscopy. In *Principles of Fluorescence Spectroscopy*, 3rd ed.; Springer Science & Business Media, 2006; 27-61.

29. D. F. Eaton. International Union of Pure and Applied Chemistry Organic Chemistry Division Commission on Photochemistry. Reference materials for fluorescence measurement. *J. Photochem. Photobiol. B,* **1988,** *2* (4), 523-531.

30. J. R. Lacowicz. Fluorophores. In *Principles of Fluorescence Spectroscopy*, 3rd ed.; Springer Science & Business Media, 2006; 63-95.

31. F. W. J. Teale and G. Weber. Ultraviolet Fluorescence of the Aromatic Amino Acids. *Biochem. J.,* **1957,** *65* (3), 476-482.

32. R. F. Chen. Fluorescence Quantum Yields of Tryptophan and Tyrosine. *Anal. Lett.,* **1967,** *1* (1), 35-42.

33. T. G. Scott, R. D. Spencer, N. J. Leonard and G. Weber. Emission Properties of Nadh . Studies of Fluorescence Lifetimes and Quantum Efficiencies of Nadh, Acpyadh, and Simplified Synthetic Models. *J. Am. Chem. Soc.,* **1970,** *92* (3), 687-&.

34. X. Li, X. Gao, W. Shi and H. Ma. Design strategies for water-soluble small molecular chromogenic and fluorogenic probes. *Chem. Rev.,* **2014,** *114* (1), 590-659.

35. H. Zheng, X. Q. Zhan, Q. N. Bian and X. J. Zhang. Advances in modifying fluorescein and rhodamine fluorophores as fluorescent chemosensors. *Chem. Commun.,* **2013,** *49* (5), 429-447.

36. R. E. Kellogg and R. G. Bennett. Radiationless Intermolecular Energy Transfer .3. Determination of Phosphorescence Efficiencies. *J. Chem. Phys.,* **1964,** *41* (10), 3042-&.

37. J. Zielonka and B. Kalyanaraman. Hydroethidine- and MitoSOX-derived red fluorescence is not a reliable indicator of intracellular superoxide formation: Another inconvenient truth. *Free Radic. Biol. Med.,* **2010,** *48* (8), 983-1001.

38. O. L. Brady. The use of 2 4-dinitrophenylhydrazine as a reagent for carbonyl compounds. *J. Chem. Soc.,* **1931**, 756-759.

39. S. Uchiyama, Y. Inaba and N. Kunugita. Derivatization of carbonyl compounds with 2,4-dinitrophenylhydrazine and their subsequent determination by high-performance liquid chromatography. *J. Chromatogr. B,* **2011,** *879* (17-18), 1282-1289.

40. J. M. Anderson. Fluorescent Hydrazides for the High-Performance Liquid-Chromatographic Determination of Biological Carbonyls. *Anal. Biochem.,* **1986,** *152* (1), 146-153.

41. N. Binding, H. Klaning, U. Karst, W. Potter, P. A. Czeschinski and U. Witting. Analytical reliability of carbonyl compound determination using 1,5-dansylhydrazine-derivatization. *Fresen J. Anal. Chem.,* **1998,** *362* (3), 270-273.

42. S. A. Perez and L. A. Colon. Determination of carbohydrates as their dansylhydrazine derivatives by capillary electrophoresis with laser-induced fluorescence detection. *Electrophoresis,* **1996,** *17* (2), 352-358.

43. E. A. Pereira, E. Carrilho and M. F. M. Tavares. Laser-induced fluorescence and UV detection of derivatized aldehydes in air samples using capillary electrophoresis. *J. Chromatogr. A,* **2002,** *979* (1-2), 409-416.

44. H. Kaspar, K. Dettmer, W. Gronwald and P. J. Oefner. Advances in amino acid analysis. *Anal. Bioanal. Chem.,* **2009,** *393* (2), 445-452.

45. D. Fekkes. State-of-the-art of high-performance liquid chromatographic analysis of amino acids in physiological samples. *J. Chromatogr. B,* **1996,** *682* (1), 3-22.

46. J. R. Benson and P. E. Hare. O-phthalaldehyde: fluorogenic detection of primary amines in the picomole range. Comparison with fluorescamine and ninhydrin. *Proc. Natl. Acad. Sci. USA,* **1975,** *72* (2), 619-622.

47. R. F. Chen, C. Scott and E. Trepman. Fluorescence properties of o-phthaldialdehyde derivatives of amino acids. *Biochim. Biophys. Acta,* **1979,** *576* (2), 440-455.

48. P. Demontigny, J. F. Stobaugh, R. S. Givens, R. G. Carlson, K. Srinivasachar, L. A. Sternson and T. Higuchi. Naphthalene-2,3-Dicarboxaldehyde Cyanide Ion - a Rationally Designed Fluorogenic Reagent for Primary Amines. *Anal. Chem.,* **1987,** *59* (8), 1096-1101.

49. S. Einarsson, B. Josefsson and S. Lagerkvist. Determination of Amino-Acids with 9-Fluorenylmethyl Chloroformate and Reversed-Phase High-Performance Liquid-Chromatography. *J. Chromatogr.,* **1983,** *282* (Dec), 609-618.

50. A. J. Faulkner, H. Veening and H. D. Becker. 2-(9-Anthryl)Ethyl Chloroformate - a Precolumn Derivatizing Reagent for Polyamines Determined by Liquid-Chromatography and Fluorescence Detection. *Anal. Chem.,* **1991,** *63* (3), 292-296.

51. B. Mohammadi, M. B. Majnooni, P. M. Khatabi, R. Jalili and G. Bahrami. 9-fluorenylmethyl chloroformate as a fluorescence-labeling reagent for derivatization of carboxylic acid moiety of sodium valproate using liquid chromatography/tandem mass spectrometry for binding characterization: a human pharmacokinetic study. *J. Chromatogr. B,* **2012,** *880* (1), 12-18.

52. G. Nouadje, H. Rubie, E. Chatelut, P. Canal, M. Nertz, P. Puig and F. Couderc. Child cerebrospinal fluid analysis by capillary electrophoresis and laser-induced fluorescence detection. *J. Chromatogr. A,* **1995,** *717* (1-2), 293-298.

53. R. Sjoback, J. Nygren and M. Kubista. Absorption and Fluorescence Properties of Fluorescein. *Spectrochim. Acta A,* **1995,** *51* (6), L7-L21.

54. W. W. You, R. P. Haugland, D. K. Ryan and R. P. Haugland. 3-(4-Carboxybenzoyl)quinoline-2-carboxaldehyde, a reagent with broad dynamic range for the assay of proteins and lipoproteins in solution. *Anal. Biochem.,* **1997,** *244* (2), 277-282.

55. B. L. Diffey. Sources and measurement of ultraviolet radiation. *Methods,* **2002,** *28* (1), 4-13.

56. S. J. Hart and R. D. JiJi. Light emitting diode excitation emission matrix fluorescence spectroscopy. *Analyst,* **2002,** *127* (12), 1693-1699.

57. J. C. Touchstone. History of Chromatography. *J. Liq. Chromatogr.,* **1993,** *16* (8), 1647-1665.

58. A. J. Alpert. Hydrophilic-interaction chromatography for the separation of peptides, nucleic acids and other polar compounds. *J. Chromatogr.,* **1990,** *499*, 177-196.

59. J. G. Dorsey and K. A. Dill. The Molecular Mechanism of Retention in Reversed-Phase Liquid-Chromatography. *Chem. Rev.,* **1989,** *89* (2), 331-346.

60. S. Fekete, A. Beck, J. L. Veuthey and D. Guillarme. Theory and practice of size exclusion chromatography for the analysis of protein aggregates. *J. Pharm. Biomed. Anal.,* **2014,** *101,* 161-173.

61. P. Jandera. Stationary and mobile phases in hydrophilic interaction chromatography: a review. *Anal. Chim. Acta*, **2011,** *692* (1-2), 1-25.

62. A. I. Liapis and B. A. Grimes. The coupling of the electrostatic potential with the transport and adsorption mechanisms in ion-exchange chromatography systems: Theory and experiments. *J. Sep. Sci.,* **2005,** *28* (15), 1909-1926.

63. J. W. Robinson, E. M. Skelly Frame and G. M. Frame II. High-Performance Liquid Chromatography (HPLC). In *Undergraduate Instrumental Analysis*, 6th ed.; Marcel Decker, 2005; 797-834.

64. J. W. Robinson, E. M. Skelly Frame and G. M. Frame II. How do Column Variables Affect Efficiency (Plate Height)? In *Undergraduate Instrumental Analysis*, 6th ed.; Marcel Decker, 2005; 797-834.

65. J. W. Robinson, E. M. Skelly Frame and G. M. Frame II. HPLC Detector Design and Operation. In *Undergraduate Instrumental Analysis*, 6th ed.; Marcel Decker, 2005; 809-821.

66. C. M. Riley. *Pharmaceutical and Biomedical Applications of Liquid Chromatography*. 1st ed.; Newnes: 1994.

67. S. F. Y. Li. *Capillary Electrophoresis: Principles, Practice, and Applications*. 1st ed.; Elsevier Science: 1992; Vol. 52.

68. J. W. Jorgenson and K. D. Lukacs. Zone Electrophoresis in Open-Tubular Glass-Capillaries. *Anal. Chem.,* **1981,** *53* (8), 1298-1302.

69. J. W. Robinson, E. M. Skelly Frame and G. M. Frame II. Electrophoresis. In *Undergraduate Instrumental Analysis*, 6th ed.; Marcel Decker, 2005; 850-865.

70. J. P. Quirino and S. Terabe. Exceeding 5000-fold concentration of dilute analytes in micellar electrokinetic chromatography. *Science,* **1998,** *282* (5388), 465-468.

71. C. S. Henry. Microchip capillary electrophoresis: an introduction. *Methods Mol. Biol.,* **2006,** *339*, 1-10.

72. J. P. Landers. *Handbook of Capillary and Microchip Electrophoresis and Associated Microtechniques*. 3rd ed.; CRC Press: 2007.

73. A. Manz, N. Graber and H. M. Widmer. Miniaturized Total Chemical-Analysis Systems - a Novel Concept for Chemical Sensing. *Sensor Actuat B-Chem,* **1990,** *1* (1-6), 244-248.

74. S. C. Jacobson, R. Hergenroder, L. B. Koutny and J. M. Ramsey. High-Speed Separations on a Microchip. *Anal. Chem.,* **1994,** *66* (7), 1114-1118.

75. P. N. Nge, C. I. Rogers and A. T. Woolley. Advances in microfluidic materials, functions, integration, and applications. *Chem. Rev.,* **2013,** *113* (4), 2550-2583.

76. S. V. Ermakov, S. C. Jacobson and J. M. Ramsey. Computer simulations of electrokinetic injection techniques in microfluidic devices. *Anal. Chem.,* **2000,** *72* (15), 3512-3517.

77. K. Seiler, D. J. Harrison and A. Manz. Planar Glass Chips for Capillary Electrophoresis - Repetitive Sample Injection, Quantitation, and Separation Efficiency. *Anal. Chem.,* **1993,** *65* (10), 1481-1488.

78. N. M. Contento and P. W. Bohn. Electric field effects on current-voltage relationships in microfluidic channels presenting multiple working electrodes in the weak-coupling limit. *Microfluid. Nanofluid.,* **2015,** *18* (1), 131-140.

79. D. B. Gunasekara, M. K. Hulvey and S. M. Lunte. In-channel amperometric detection for microchip electrophoresis using a wireless isolated potentiostat. *Electrophoresis,* **2011,** *32* (8), 832-837.

80. C. Chen and J. H. Hahn. Dual-channel method for interference-free in-channel amperometric detection in microchip capillary electrophoresis. *Anal. Chem.,* **2007,** *79* (18), 7182-7186.

81. N. A. Lacher, S. M. Lunte and R. S. Martin. Development of a microfabricated palladium decoupler/electrochemical detector for microchip capillary electrophoresis using a hybrid glass/poly(dimethylsiloxane) device. *Anal. Chem.,* **2004,** *76* (9), 2482-2491.

82. J. M. Ng, I. Gitlin, A. D. Stroock and G. M. Whitesides. Components for integrated poly(dimethylsiloxane) microfluidic systems. *Electrophoresis,* **2002,** *23* (20), 3461-3473.

Chapter 2:

Detection of Reactive Aldehyde Biomarkers as a Measure of Lipid Peroxidation Following Epileptic-like Seizures

2.1. Epilepsy

A patient is officially diagnosed with epilepsy after experiencing two or more unprovoked seizure events over the course of their lifetime. This neurodegenerative disease is extremely prevalent, with an estimated 45 million people affected worldwide. The exact cause of new-onset epilepsy is unknown in a majority of patients (62%), while others develop the condition after strokes, head trauma, tumors, and other conditions [1]. Up to a third of all patients diagnosed with epilepsy are non-responsive to currently available antiepileptic drug therapies [2]. Furthering our understanding of epilepsy and its underlying mechanisms is the first step in developing new therapeutics to help combat this disease.

Recent research has shown that epileptic seizures result in the overproduction of RNOS, leading to oxidative stress and damage. The subsequent neurotoxicity can in turn make a patient more susceptible to seizure initiation in the future [3]. It is therefore of pivotal importance to examine and limit oxidative stress in relation to this neurodegenerative disease.

2.1.1. Neuronal Activity and Signaling

Neurons are the primary cells in the central nervous system responsible for transmitting nerve impulses from one cell to the next. This occurs in a space between the synaptic knob of one neuron and the dendrite of an adjacent neuron known as the synaptic cleft. Impulses are carried along the neuron due to differences in potential generated by ion gradients. A neuron has a resting cell membrane potential of approximately -60 mV. This is because the cytoplasm of a neuron is

naturally low in Na^+ and Cl^-, while high in K^+, compared to the surrounding extracellular fluid (ECF) [4].

Specific proteins known as ion channels exist that allow ions such as Na^+, Cl^-, K^+, and Ca^{2+} to cross the cell membrane in response to a physiological stimulus (such as a potential change or neurotransmitter response). This process is referred as opening the gates of the ion channel [5]. When the cell membrane is depolarized (to around -40 mV) it opens up the gate of Na^+ channels, which results in an increase of Na^+ permeability and an influx of Na^+ into the neuron from the ECF. When the depolarization reaches a membrane potential of approximately +30 mV, the Na^+ channels will close and K^+ channels will open, which will return the membrane back to its resting potential via the release of K^+ into the ECF, a process known as repolarization [6]. This overall rise and fall of the membrane potential is known as the action potential and is responsible for the propagation of nerve impulses along the axon of a neuron, as shown in Figure 2.1. When action potentials reach the synaptic knob, they cause the secretion of neurotransmitters into the synaptic cleft. Some common neurotransmitter families include cholinergic agents, catecholamines, amino acids, and peptides, among others [4].

2.1.2. Excitatory and Inhibitory Mechanism of Seizures

Several amino acids (and derivatives) function as neurotransmitters. This includes alanine, aspartate, cystathione, glycine, glutamate, histamine, proline, serotonin, taurine, tyrosine, and γ-aminobutyric acid (GABA) [4, 7]. Dysfunctions in these amino acid neurotransmitters has been linked to several diseases impacting the central nervous system [8]. This is especially true of epilepsy because glutamate and GABA are the most abundant excitatory and inhibitory neurotransmitters in the brain, respectively. An imbalance of these two neurotransmitters is one of the primary causes of seizures [9].

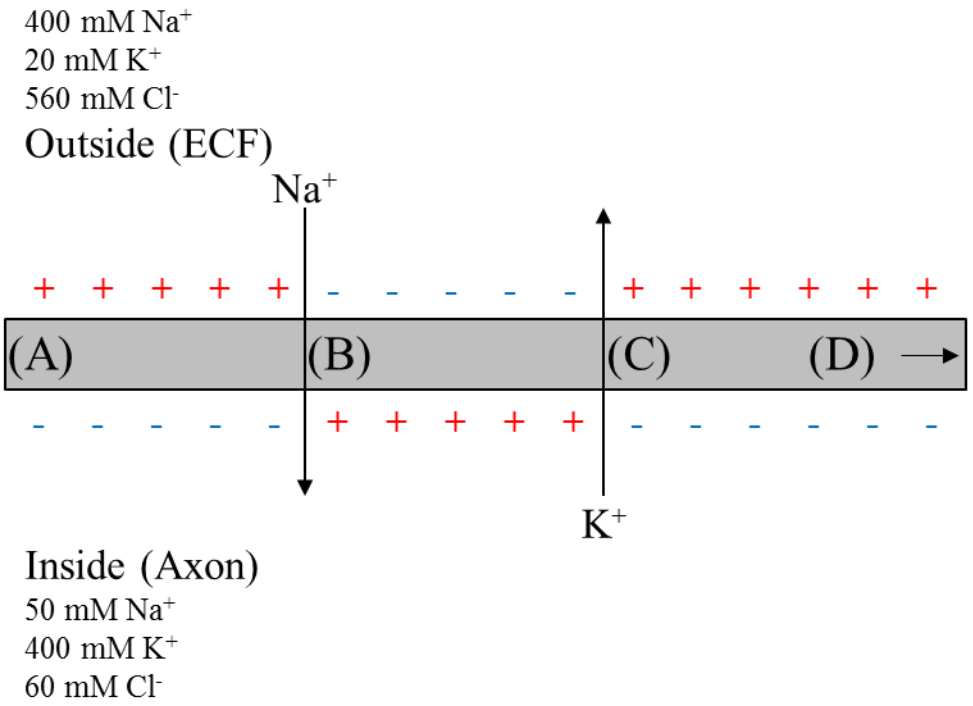

Figure 2.1: Propogation of the action potential along an axon

(A) The resting potential of the cell membrane is due to the differences in ion concentration between the inside and outside of the axon; (B) Gates on the Na^+ ion channels open up, causing depolarization via an influx of Na^+ into the cell; (C) When the influx of Na^+ stops, the gates on K^+ ion channels will open, causing repolarization via the expulsion of K^+ into the ECF; (D) The resting potential is re-established, allowing for the continuation of the action potential down the length of the axon.

The prolonged release and overproduction of glutamate lead to excitation of the ionotropic receptors responsible for its regulation, such as the N-methyl-D-aspartate (NMDA), α-amino-3-hydroxy-5-methyl-4-isoxasole-propionic acid (AMPA), and kainite receptors. This will open the gate of Ca^{2+} and Na^{+} ion channels, leading to an influx of these ions. These signals are normally inhibited via the opening of K^{+} or Cl^{-} channels by GABA to repolarize the neuron. However, when glutamate is overproduced, these inhibitory mechanisms are unable to maintain this balance. This results in constant neuronal transmission that leads to excitotoxicity, forcing cells to undergo apoptosis and releasing more glutamate into the synaptic cleft [10]. The continuous firing of the affected neurons will produce a wave of synchronous neuronal activity; in other words, a seizure.

2.1.3. Chemically Induced Seizure Models

When examining epilepsy in a laboratory setting, it becomes necessary to find a method to consistently and reproducibly induce similar seizures in an animal model. There are two primary approaches to this, depending on the type of seizure desired: a focal or general seizure. Focal seizures are defined as those that both originate and remain within one hemisphere of the brain, and are thus achieved through local dosing at the desired location. Conversely, a general seizure results in neuronal activity that spreads across the distributed networks of both brain hemispheres, and are achieved through the bolus dosing or constant infusion of a convulsant [11].

Our group has previously developed a steady-state chemical seizure model in rodents using 3-mercaptopropionic acid (3-MPA). This compound inhibits the functionality of glutamic acid decarboxylase (GAD), the enzyme responsible for converting glutamate to GABA, as shown in Figure 2.2. The subsequent imbalance between the excitatory and inhibitory neurotransmitters in the brain can lead to generalized or focal seizures, depending on the method of dosing. The

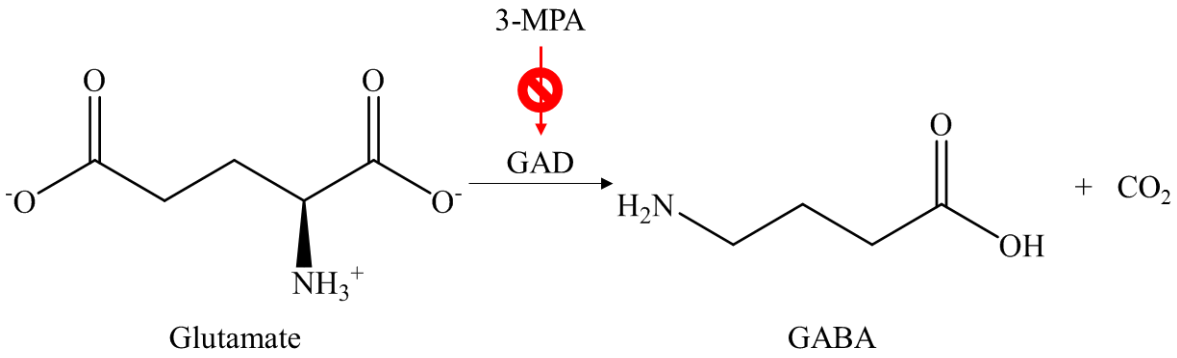

Figure 2.2: Mechanism of seizures induced by 3-MPA

Under normal physiological conditions, the balance between the excitatory (glutamate) and inhibitory (GABA) amino acid neurotransmitters is maintained by the glutamic acid decarboxylase enzyme (GAD). 3-mercaptopropionic acid (3-MPA) competeitively reacts with GAD, leading to an overproduction of glutamate and chemically induced seizures.

pharmacokinetics [12] and correlating concentration of amino acid neurotransmitters [13] in the 3-MPA seizure model have previously been explored in detail using microdialysis sampling.

2.1.4. Epileptic Seizures and Oxidative Stress

Although several studies have correlated an increase RNOS concentrations with epileptic seizures, the exact mechanism linking them is not fully understood. Several different hypotheses have been suggested for the overproduction of RNOS related to this condition [3]. This includes the production of RNOS through mitochondrial dysfunction [14] and the alteration of cyclooxygenase and lipoxygenase functionality [15]. This is compounded by the fact that the brain is heavily susceptible to oxidative stress and damage due to the high demand for oxygen, low concentration of endogenous antioxidants in the ECF, and abundance of polyunsaturated fatty acids (PUFAs) [16, 17]. The secondary damage caused by oxidative stress can sometimes prove more harmful than the initial seizure event itself and make patients more susceptible to the onset of additional seizures [3].

Free radical RNOS are primarily responsible for this damage, especially in the case of PUFAs, where they will readily react with the biomolecule to alter their structure and functionality [18]. This can result in a self-propagating chain reaction in which RNOS create radical species, which in turn beget the formation of new radicals; this process is referred to as lipid peroxidation.

2.2. Lipid Peroxidation

2.2.1. Onset and Mechanism of Lipid Peroxidation

PUFAs are a subgroup of lipids that consist of long-chain carboxylic acids with more than one carbon-carbon double bond in their backbone. PUFAs can be separated into categories depending on the distance between the methyl-end of the backbone and the final double bond, indicated by (ω-X), where X is the position of the final bond. The length of the C-C chain (Y) and

the number of double bonds (Z) are also indicated by Y:Z. For example, arachidonic acid is labeled as a 22:4 (ω-6) PUFA; this means that its carbon backbone is twenty-two carbon molecules long, has four double bonds, with the final double bond at the sixth carbon from the methyl end. Some further examples of PUFA naming conventions are shown in in Table 2.1.

PUFAs are highly susceptible to attack by RNOS. The process by which lipid peroxidation occurs can be divided into three steps: initiation, propagation, and termination, as shown in Figure 2.3. In the initiation step, a RNOS (usually $OH^{\bullet}$) will abstract hydrogen from a PUFA, resulting in the formation of water and a lipid radical ($L^{\bullet}$). Propagation will then occur when the lipid radical rapidly reacts with molecular oxygen to form a lipid peroxy-radical ($LOO^{\bullet}$). This will in turn scavenge protons off of other lipids, forming a lipid hydroperoxide and another lipid radical. This lipid radical will react with molecular oxygen to restart this process, leading to a cascade of radical formation. In the termination step, various antioxidants (such as vitamin C or glutathione) [19, 20] detoxify these lipid hydroperoxides to form stable lipid alcohols and other small molecules.

2.2.2. Reactive Aldehyde Species as Biomarkers

The breakdown of lipid hydroperoxides in the termination stage of lipid peroxidation will produce a large number of aldehyde species. There is a great deal of literature using these reactive aldehyde species as small molecule biomarkers of lipid peroxidation and, consequently, oxidative stress and damage. Three of the most commonly examined are 4-hydroxynonenal, malondialdehyde, and acrolein [21]. The structures of these compounds are shown in Figure 2.4.

4-Hydroxynonenal (4-HNE) is formed during lipid peroxidation due to the beta-cleavage of ω-6 PUFAs, such as linoleic acid (18:2) and arachidonic acid (22:4) [22]. Various studies have

Table 2.1: Naming conventions and corresponding structures of the PUFAs primarily responsible for the formation of reactive aldehyde species.

Name	Designation	Structure
Docosahexaenoic Acid	22:6 (ω-3)	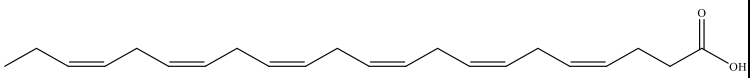
Linoleic Acid	18:2 (ω-6)	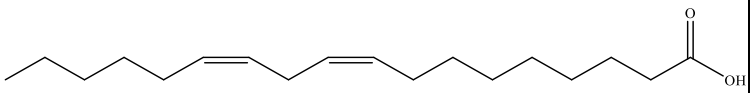
Arachidonic Acid	20:4 (ω-6)	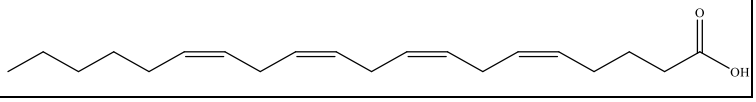

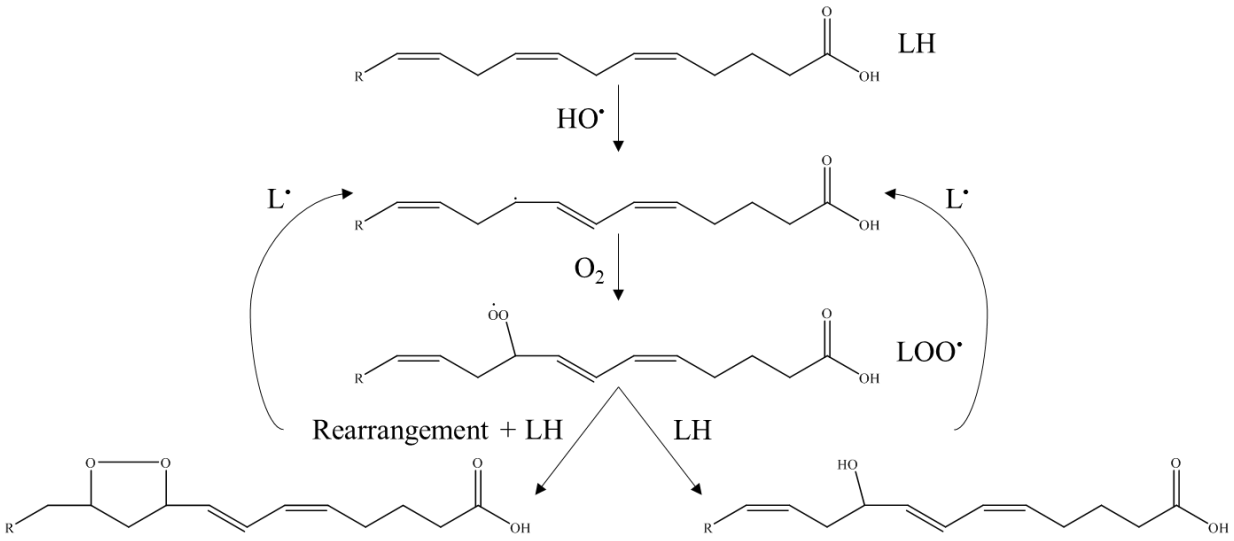

Figure 2.3: Mechanism of lipid peroxidation

Lipid peroxidation is a self-propagating chain reaction that ends in the formation lipid bicycloendoperoxides and lipid alcohols. The propagation occurs via the removal of protons from nearby lipids by radical species. LH = normal lipid; L• = lipid radical; LOO• = lipid peroxyl radical.

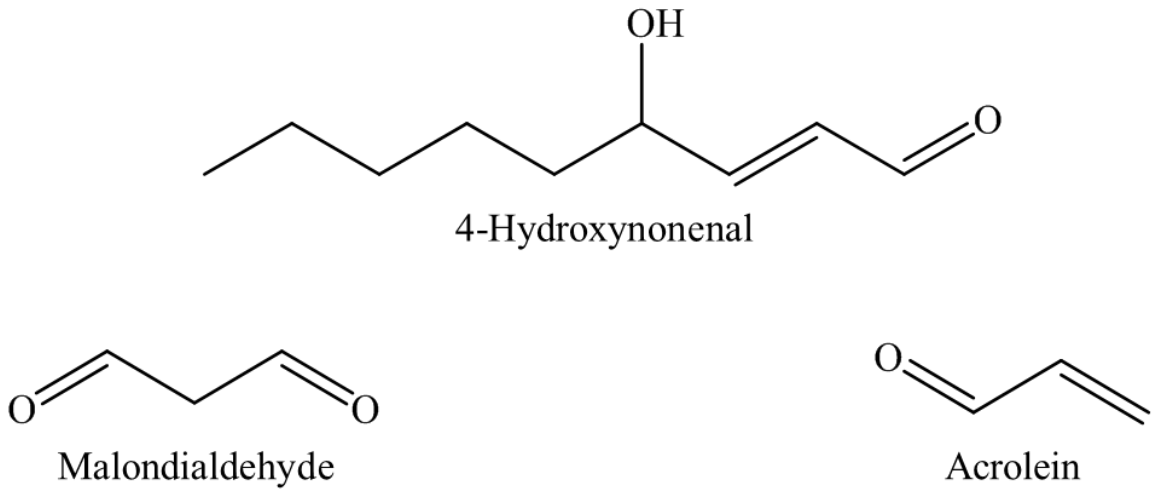

Figure 2.4: Chemical structures of the reactive aldehyde biomarkers of interest

shown that 4-HNE disturbs mitochondrial functionality, resulting in cytotoxicity, as well as reacting with proteins, phospholipids, and DNA *in vivo* due to its high reactivity with thiol and amino groups [21, 23]. 4-HNE is one of the most heavily studied biomarkers of lipid peroxidation due to its toxicity and the fact that it acts as a specific marker of oxidative stress.

Malondialdehyde (MDA) primarily forms from PUFAs that will degrade into bicycloendoperoxides during the propagation steps of lipid peroxidation, such as ω-6 arachidonic acid (20:4) and ω-3 docosahexaenoic acid (22:6). These unstable bicylcoendoperoxides will then thermally degrade to form MDA [24]. MDA has a pair of aldehyde moieties will undergo reactions with nucleophilic centers on biomolecules, giving it a high potential to cause toxicity and mutagenicity [25]. This reactivity has also been exploited to detect MDA via the use of 2-thiobarbituric acid (TBA) to form a fluorescent product. However, TBA will also react with other endogenous dialdehydes and pyrimidine, making the assay non-specific [26].

Several 2-alkenal species can be produced via the oxidation of PUFAs by molecular oxygen, including 2-pentenal, 2-heptenal, 2-octenal, and 2-nonenal. By far the most toxic of these is acrolein, a component of cigarette smoke and byproduct of overheating oils [21]. Acrolein is an incredibly strong electrophile and shows higher reactivity than 4-HNE or MDA with biomolecules containing thiol or amine moieties. Due to its high reactivity, acrolein is most often detected in biological samples after binding to the cysteine residues of proteins [27].

Despite the importance of these three reactive aldehyde species, there are few studies in the literature examining them simultaneously in a biological system. By taking advantage of their shared aldehyde moieties, a fluorescent derivatization assay can be used to simultaneously detect 4-HNE, MDA, and acrolein.

2.3. Methods

2.3.1. Materials and Reagents

HPLC-grade acetonitrile (ACN) and glacial acetic acid were purchased from Fisher (Waltham, MA). Potassium dihydrogen phosphate (KH_2PO_4), MDA (malondialdehyde tetrabutylammonium salt), DNSH (bioreagent, suitable for fluorescence, ≥ 95%), and acrolein (analytical standard) were obtained from Sigma-Aldrich (St. Louis, MO, USA). 4-HNE was purchased from Cayman Chemical (Ann Arbor, MI, USA). All solutions were prepared using nanopure water from a Labconco Water Pro Plus purification system (Kansas City, KS, USA).

2.3.2. Fluorescent Derivatization of Aldehydes

Dansylhydrazine (DNSH) is a derivatization reagent that was originally developed for the detection of carboxylic acids [28]. This compound will react with any target containing a carbonyl moiety under acidic conditions [29], although past work has shown it will bind more readily to aldehydes than ketones [30]. It has been used for this purpose in tissue [31] and air samples [32, 33]. In acidic conditions, DNSH will react with aldehydes to form a fluorescent hydrazone derivative, as was shown in Figure 1.4.

The method used to derivatize the aldehydes was adapted from the literature [34, 35]. DNSH was dissolved in a solution of ACN containing 0.1% glacial acetic acid at a concentration of 100 mM and stored at 4 °C. This derivatization solution was reacted with the sample in a 1:10 ratio by volume and allowed to proceed for 20 minutes at 50 °C before injection into the chromatographic system.

2.3.3. Liquid Chromatography System

Sample analysis was performed using an LC-fluorescence system that consisted of a Shimadzu LC-20AD Solvent Delivery Unit and Jasco FP-2020 Plus Intelligent Fluorescence

Detector. A Phenomenex Gemini C_{18} column (100 × 2.00 mm, 3 µm particle) with matching guard column (4 × 2.0 mm) was used for the separation. An underfill injection of 10 µL was used in a 20 µL Rheodyne® stainless steel injection loop. An isocratic mobile phase containing 12 mM KH_2PO_4 (pH = 7.7) buffer and acetonitrile was employed for the separation. The acetonitrile (ACN) percentage in the mobile phase was determined experimentally and is discussed in more detail in the Discussion section.

2.3.4. Solid Phase Extraction

Solid phase extraction (SPE) was performed using a Sep-Pak C_{18} obtained from Waters Corporation (Milford, MA) and a vacuum manifold from Supelco Analytical (St. Louis, MO). SPE was use to preconcentrate the hydrazone derivatives following the DNSH reaction. The Sep-Pak cartridges were conditioned with 3 mL of ACN and 3 mL of H_2O before being loaded with 1 mL of derivatized sample. This was washed with 5 mL of H_2O and an experimentally determined ACN:H_2O solution, the composition of which is mentioned in the Discussion section. The hydrazone derivatives were eluted in 2 mL ACN, which was evaporated under a steady stream of argon gas while being held at 25 °C with a heating block. The solid residue was reconstituted in 50 µL of 50:50 ACN:H_2O before being injected on the LC system.

2.3.5. Animal Seizure Model

Animal experiments were performed using Wistar rats from Charles Rivers Laboratories, Inc. (Wilmington, MA) that were in the weight range of 300-400 g. The rats were housed in temperature- and humidity-controlled rooms with a 24-h light/dark cycle and free access to food and water. Forty-eight hours prior to dosing, the animals were transferred to a metabolic cage on a rodent workstation, both from Bioanalytical Systems, Inc. (West Lafayette, IN). Urine was collected for 12 h in sync with the light/dark cycle. All urine samples were filtered with a

0.22 µm polyethersulfone syringe filter. The first 0.5 mL of urine was used to wet the filter and discarded. The remaining urine was filtered into a 20 mL scintillation vial and stored at -80 °C until they could be derivatized and analyzed.

Seizure model animals received a 5 mL bolus interperitoneal (i.p.) dose of 50 mg 3-MPA/kg body weight, and were observed to confirm seizure activity. The 3-MPA solution was prepared by diluting the proper volume of reagent per rat body weight with sterile 0.9% saline to a total volume of 5 mL. Control animals received a 5 mL bolus i.p. dose of 0.9% saline. Rats were housed in the metabolism cage for a total of 120 hours. The animal experiments described here follows the principles and regulations stated in the Guide for the Care and Use of Laboratory Animals and was approved by the University of Kansas Lawrence Institutional Animal Care and Use Committee.

2.4. Discussion

2.4.1. Dansylhydrazine Derivatization Optimization

Previous methods have used DNSH to measure acrolein, and the derivatization procedure used here was based on those findings [34]. The reaction solution contained 100 mM of DNSH and 0.1% glacial acetic acid to promote the formation of the hydrazone derivatives.

Although hydrazone derivatives have previously been detected on an LC system an excitation (EX) wavelength of 240 nm and an emission (EM) wavelength of 470 nm, this was using a mobile phase with a different organic composition (32% ACN) and samples fully dissolved in ACN [35]. Using a different mobile phase composition (50% ACN with 12 nM KH_2PO_4) resulted in a much lower fluorescence intensity, which required the EX and EM wavelength maxima to be determined experimentally. This is due to the influence of the sample matrix on the fluorescence. Additionally, since there was excess DNSH in the reaction sample to avoid limiting

the reaction with the aldehyde species, a fluorometer could not be used for this analysis. This is because the large molar concentration of DNSH obscured the signal from the derivatized products.

Instead the optimal wavelengths were determined using the chromatographic separation with a variable wavelength fluorescence detector. The maximum EM wavelength was determined first by exciting at 240 nm and changing the EM wavelength, zeroing in on the maximum fluorescence response, which was found to be 550 nm. A similar experiment was conducted to identify the maximum EX wavelength, where the emission was kept at 550 nm, in order to find the optimal EX wavelength of 250 nm.

2.4.2. Chromatographic Separation

The excess DNSH present in the reaction sample also complicated the chromatographic separation, as the polar reagent was present early in the separation as a large peak. The mobile phase composition was optimized to obtain sufficient resolution between the excess DNSH and the most polar of the aldehydes of interest, acrolein.

Starting with an ACN composition of 60%, the organic percentage of the mobile phase was varied by 10% until adequate resolution was obtained between the acrolein and residual DNSH peaks as shown in Figure 2.5. This was determined to be at a mobile phase consisting of 50% ACN with 12 mM KH_2PO_4 (pH = 7.7). These experiments were performed using standards prepared in mobile phase to avoid peak broadening due to a mismatch in organic content between the sample matrix and mobile phase.

Under these conditions, all three dansyl derivatives displayed high linearity over a biologically-relevant concentration range. Acrolein and MDA had limits of detection in the low

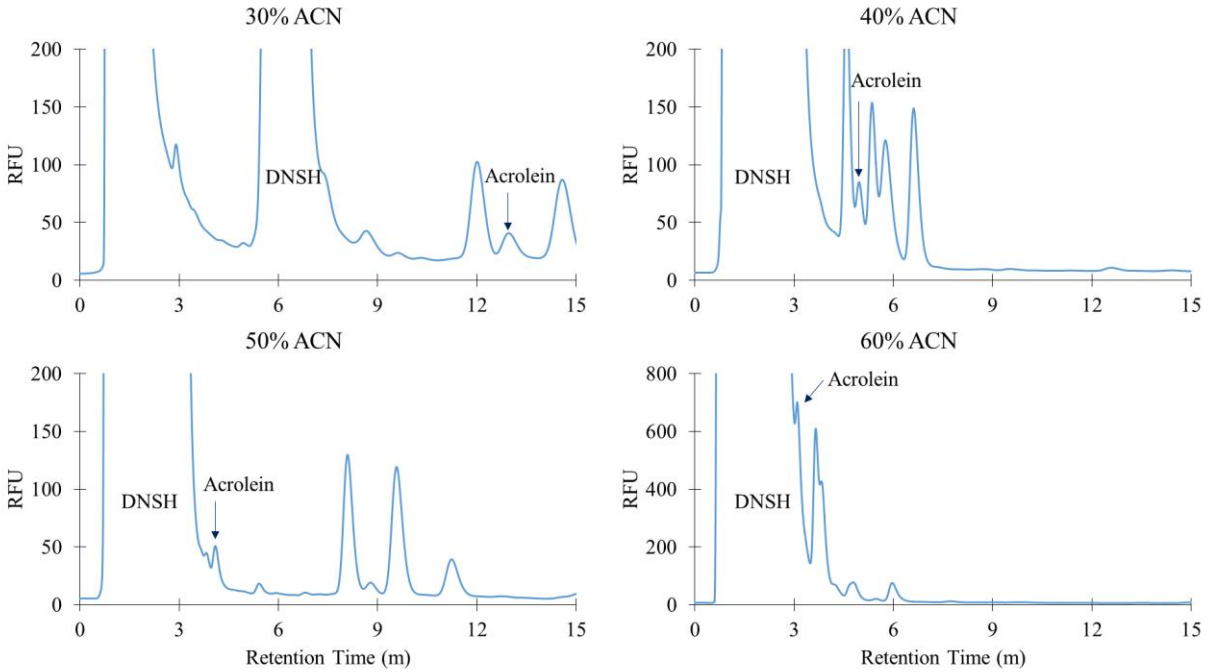

Figure 2.5: Optimization of LC mobile phase to achieve adequate resolution

The resolution between the acrolein and excess DNSH peaks was highly dependent on the organic composition of the mobile phase. The final mobile phase consisted of 50% ACN with 12 mM KH_2PO_4 (pH = 7.7).

micromolar range (2.6 and 3.8 µM, respectively), while HNE had LOD in the nanomolar range (122 nM). The final separation is shown in Figure 2.6, with the corresponding figures of merit in Table 2.2.

2.4.3. Solid Phase Extraction Pre-Concentration

Since initial results indicated the LOD of this method was insufficient for use in urine samples (where concentrations were estimated to be near 1 µM), SPE was used as a pre-concentration method. In order to properly elute the hydrazone derivatizes off of the SPE cartridge, the proper organic composition needed to be optimized to minimize the loss of analyte and minimize interferences. The optimal elution solvent was found to be a 70:30 ACN:H_2O solution.

The pre-concentration procedure was optimized by running a series of standards near the expected biological concentration range through the SPE procedure and comparing the signal response to non-treated standards at twenty times the concentration. Following the SPE procedure mentioned in the Methods section, this should result in a 20-fold concentration of the derivatized analytes. This process showed a 96% agreement between the pre-concentrated and untreated standards.

The reproducibility of the SPE procedure was also evaluated using standards. 4-HNE and MDA exhibited a recovery of 109 ± 5% and 110 ± 25%, respectively. The % RSDs for the recovery of these analytes from urine samples were 17.6% and 8.0%, which is considered an acceptable margin of error for biological samples, as variations in specific analyte concentrations can be expected between different animals and samples. The twenty-fold enrichment due to the sample treatment led an improvement in the LOD for final values of 6.1 nM for 4-HNE and 192 nM for MDA, allowing them to be separated and detected in control and dosed rat urine, as shown in

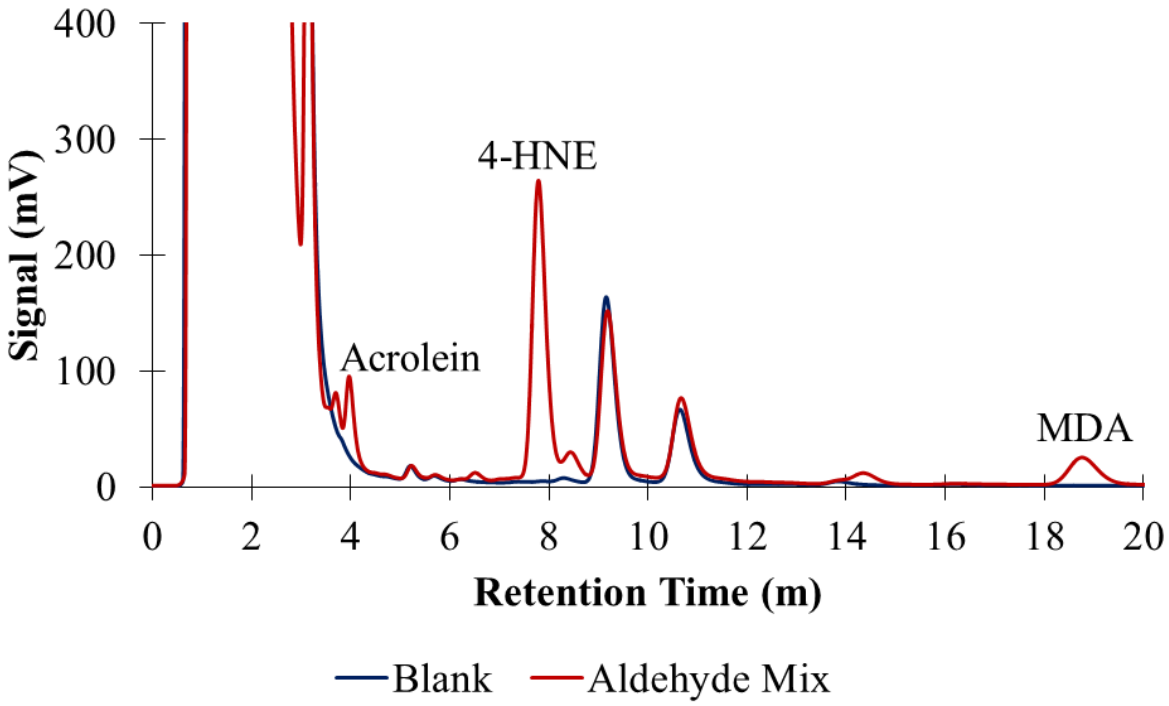

Figure 2.6: Final LC-FL separation of derivatized aldehydes

Table 2.2: Figures of merit for the separation of the reactive aldehyde hydrazone derivatives.

	Acrolein	4-HNE	MDA
LOD (µM) (S/N = 3)	2.6	0.122	3.8
Resolution (R)	0.94	6.4	2.1
Theoretical Plates (N)	2125	1344	1104
Linearity (R^2)	0.976	0.991	0.961
Linear Range (µM)	10-150	0.5-100	5-100

Figure 2.7. Although there was a peak that eluted close to that of 4-HNE, it was decided that the resolution between them (R = 0.71) was sufficient for quantitation.

2.4.4. Animal Seizure Model

This method was used to monitor the concentration of the three reactive aldehydes of interest in urine samples before and after an oxidative stress event. An epileptic-like seizure was chemically induced using 3-MPA, with urine collected in 12 hour intervals. Unfortunately, MDA could not be detected in enough of the urine samples to make any conclusive statements. Past studies in our group have studied this compound in the brain following an epileptic seizure, but there was no information regarding its systemic response [36].

When analyzing urine samples, there was a reproducible trend of shifting retention times in subsequent separations. This was due to the gradual adsorption of biological compounds to the guard column cartridge. This irreproducibility in retention times was addressed by running fresh standards between each derivatized urine sample to validate the peak identities, as well as replacing the guard cartridge between each individual animal study.

The overall procedure of the animal experiments is shown in Figure 2.8 that includes the sample preparation and chromatographic system.

2.4.5. Importance of Seizure Timing on Aldehyde Concentrations

Seizures induced during the transition from the dark to light period were referred to as the morning dose. As seen in Figure 2.9, there was a noticeable circadian rhythm in the concentration of aldehydes in urine samples, with acrolein possessing higher concentrations during the light period and 4-HNE possessing higher concentrations during the dark period. These results have not been previously reported in the literature. Acrolein levels also exhibited a 400% increase compared

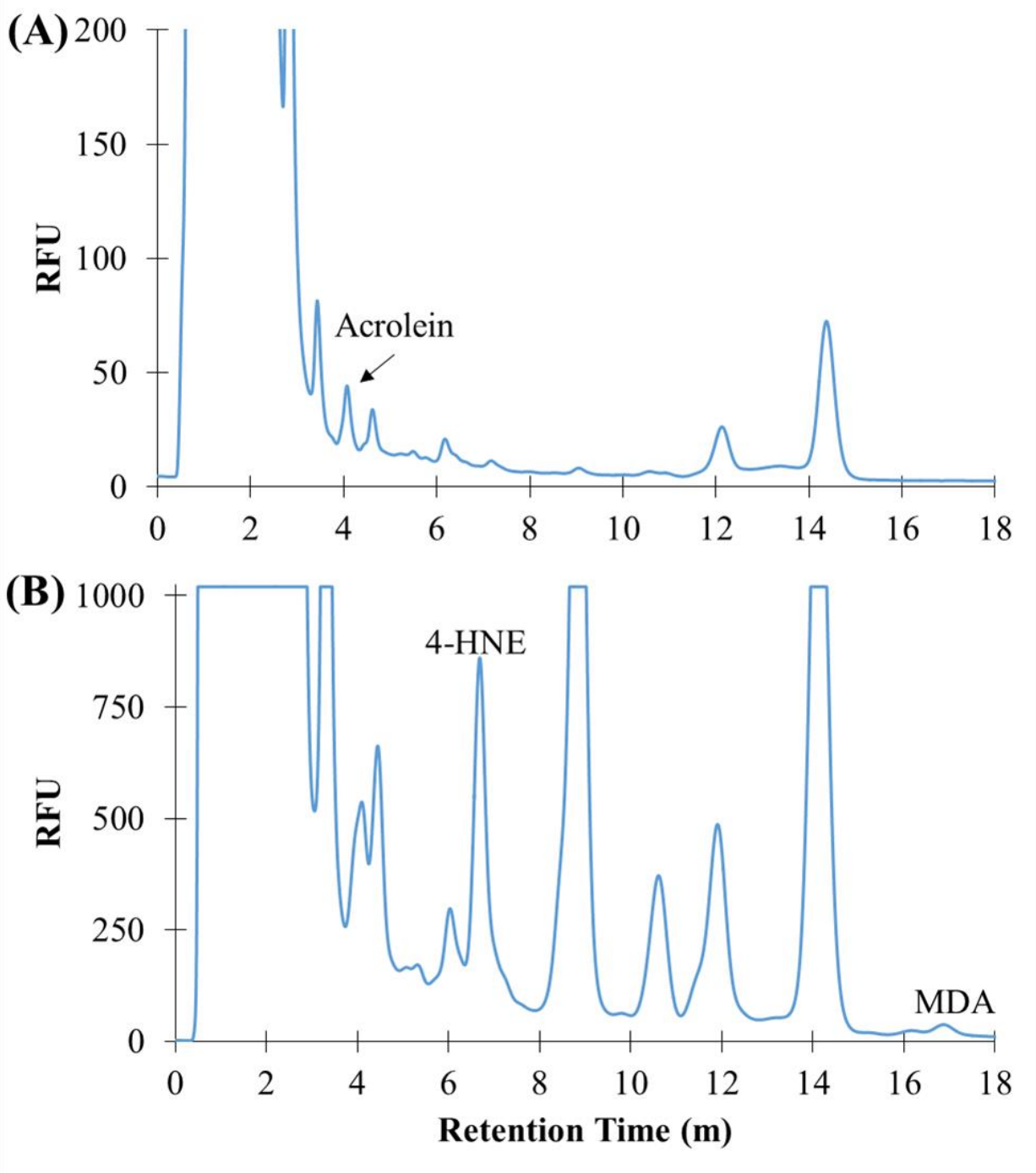

Figure 2.7: Comparison of urine analysis pre- and post-SPE treatment

Although only an acrolein peak is present in the plain urine samples (A), 4-HNE and MDA peaks are easily visible following the SPE pre-concentration procedure (B).

Figure 2.8: Flow chart of animal experiment procedure

to basal levels in the 12-h period immediately following the event ($p = 0.024$), correlating with previous findings for MDA. Conversely, 4-HNE levels were not significantly impacted ($p = 0.26$). This suggests there is an unexplored difference in the metabolism of these reactive aldehydes *in vivo.*

A second set of experiments was conducted to guarantee that the rise in acrolein concentration was not due to artificial inflation from the circadian cycle. In these studies, the seizure was induced during the transition from the light to dark period (referred to as the evening dose). Similar results were observed regarding the circadian nature of aldehyde concentration, the elevation in acrolein levels ($p = 0.069$), and the lack of response from 4-HNE ($p = 0.15$), as shown in Figure 2.10. Although the rise in acrolein was not significantly different at the 95% confidence interval, there is still a clear trend present from these experiments.

2.5. Conclusion

A LC-fluorescence method was developed for the detection of reactive aldehyde biomarkers of lipid peroxidation using SPE pre-concentration to prepare bulk biological samples, such as urine. The LOD obtained were sufficient to detect two important biomarkers, 4-HNE and acrolein, in 12-h urine samples in a rodent model of epilepsy. These compounds follow a previously unreported circadian cycle that corresponds to the light/dark cycle of the animal. Furthermore, acrolein displayed a significant increase in concentration following a chemically induced epileptic seizure, which has previously been confirmed with MDA using microdialysis sampling.

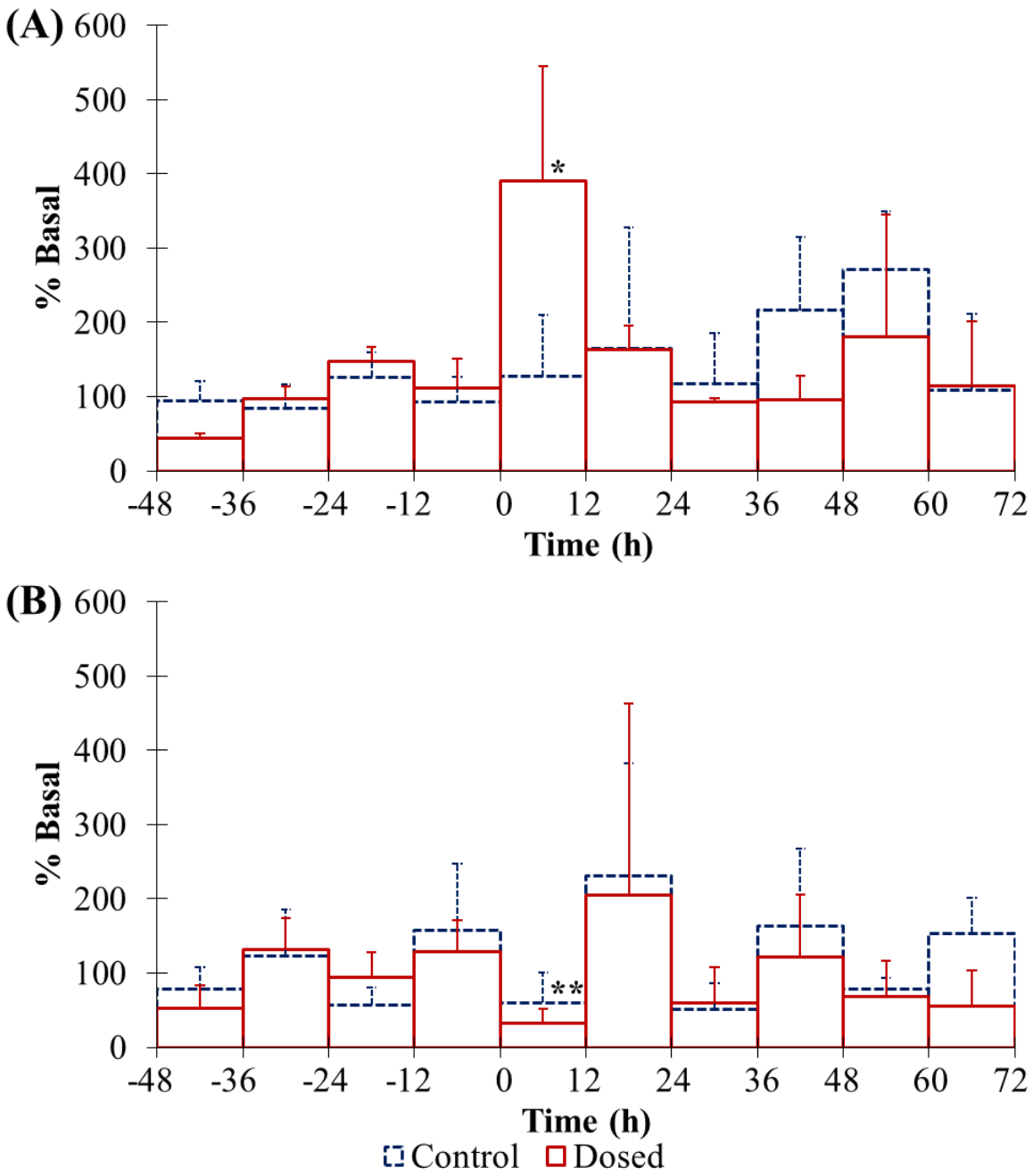

Figure 2.9: Aldehyde concentrations in urine following morning 3-MPA dosage

Although both aldehyde species demonstrate a circadean cycle, only acrolein (A) shows an increase in basal concentration following the induced seizure (t = 0 h), while 4-HNE (B) levels do not show any significant change. *p = 0.024 **p = 0.26

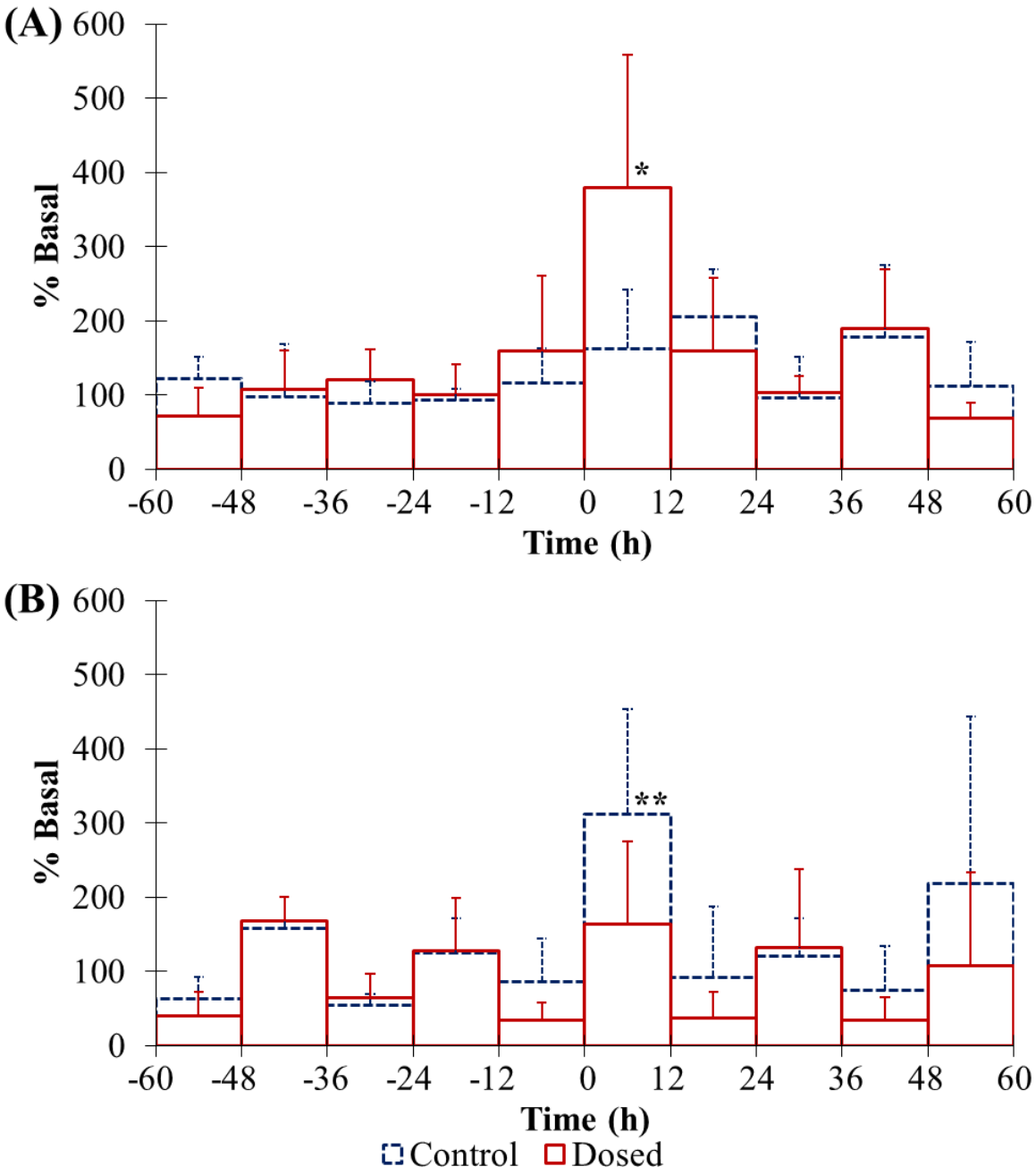

Figure 2.10: Aldehyde concentrations in urine following evening 3-MPA dosage

Acrolein (A) still shows a rise in response while 4-HNE (B) does not. *p = 0.069 **p = 0.15

2.6. References

1. J. A. French and T. A. Pedley. Clinical practice. Initial management of epilepsy. *N. Engl. J. Med.,* **2008,** *359* (2), 166-176.

2. M. J. Brodie. Diagnosing and predicting refractory epilepsy. *Acta Neurol. Scand. Suppl.,* **2005,** *181*, 36-39.

3. E. J. Shin, J. H. Jeong, Y. H. Chung, W. K. Kim, K. H. Ko, J. H. Bach, J. S. Hong, Y. Yoneda and H. C. Kim. Role of oxidative stress in epileptic seizures. *Neurochem. Int.,* **2011,** *59* (2), 122-137.

4. R. H. Garrett and C. M. Grisham. *Biochemistry*. 4th ed.; Mary Finch: 2010.

5. B. Hille. Ionic Channels in Excitable Membranes - Current Problems and Biophysical Approaches. *Biophys. J.,* **1978,** *22* (2), 283-294.

6. A. L. Hodgkin and A. F. Huxley. A Quantitative Description of Membrane Current and Its Application to Conduction and Excitation in Nerve. *J. Physiol.,* **1952,** *117* (4), 500-544.

7. W. Timmerman and B. H. C. Westerink. Brain microdialysis of GABA and glutamate: What does it signify? *Synapse,* **1997,** *27* (3), 242-261.

8. N. J. Allen, R. Karadottir and D. Attwell. Reversal or reduction of glutamate and GABA transport in CNS pathology and therapy. *Eur. J. Physiol.,* **2004,** *449* (2), 132-142.

9. H. F. Bradford. Glutamate, GABA and epilepsy. *Prog. Neurobiol.,* **1995,** *47* (6), 477-511.

10. J. T. Coyle and P. Puttfarcken. Oxidative stress, glutamate, and neurodegenerative disorders. *Science,* **1993,** *262* (5134), 689-695.

11. A. T. Berg and I. E. Scheffer. New concepts in classification of the epilepsies: entering the 21st century. *Epilepsia,* **2011,** *52* (6), 1058-1062.

12. E. W. Crick, I. Osorio, N. C. Bhavaraju, T. H. Linz and C. E. Lunte. An investigation into the pharmacokinetics of 3-mercaptopropionic acid and development of a steady-state chemical seizure model using in vivo microdialysis and electrophysiological monitoring. *Epilepsy Res.,* **2007,** *74* (2-3), 116-125.

13. E. W. Crick, I. Osorio, M. Frei, A. P. Mayer and C. E. Lunte. Correlation of 3-mercaptopropionic acid induced seizures and changes in striatal neurotransmitters monitored by microdialysis. *Eur. J. Pharm. Sci.,* **2014,** *57*, 25-33.

14. M. Patel. Mitochondrial dysfunction and oxidative stress: Cause and consequence of epileptic seizures. *Free Radic. Biol. Med.,* **2004,** *37* (12), 1951-1962.

15. J. W. Phillis, L. A. Horrocks and A. A. Farooqui. Cyclooxygenases, lipoxygenases, and epoxygenases in CNS: Their role and involvement in neurological disorders. *Brain Res. Rev.,* **2006,** *52* (2), 201-243.

16. B. Halliwell. Reactive Oxygen Species and the Central-Nervous-System. *J. Neurochem.,* **1992,** *59* (5), 1609-1623.

17. L. M. Sayre, G. Perry and M. A. Smith. Oxidative stress and neurotoxicity. *Chem. Res. Toxicol.,* **2008,** *21* (1), 172-188.

18. A. M. Pisoschi and A. Pop. The role of antioxidants in the chemistry of oxidative stress: A review. *Eur. J. Med. Chem.,* **2015,** *97*, 55-74.

19. E. A. Lutsenko, J. M. Carcamo and D. W. Golde. Vitamin C prevents DNA mutation induced by oxidative stress. *J. Biol. Chem.,* **2002,** *277* (19), 16895-16899.

20. G. E. Arteel and H. Sies. The biochemistry of selenium and the glutathione system. *Environ. Toxicol. Pharmacol.,* **2001,** *10* (4), 153-158.

21. H. Esterbauer, R. J. Schaur and H. Zollner. Chemistry and biochemistry of 4-hydroxynonenal, malonaldehyde and related aldehydes. *Free Radic. Biol. Med.,* **1991,** *11* (1), 81-128.

22. C. Schneider, K. A. Tallman, N. A. Porter and A. R. Brash. Two distinct pathways of formation of 4-hydroxynonenal. Mechanisms of nonenzymatic transformation of the 9- and 13-hydroperoxides of linoleic acid to 4-hydroxyalkenals. *J. Biol. Chem.,* **2001,** *276* (24), 20831-20838.

23. G. Poli and R. J. Schaur. 4-Hydroxynonenal in the pathomechanisms of oxidative stress. *IUBMB Life,* **2000,** *50* (4-5), 315-321.

24. W. A. Pryor and J. P. Stanley. Letter: A suggested mechanism for the production of malonaldehyde during the autoxidation of polyunsaturated fatty acids. Nonenzymatic production of prostaglandin endoperoxides during autoxidation. *J. Org. Chem.,* **1975,** *40* (24), 3615-3617.

25. D. Tsikas. Assessment of lipid peroxidation by measuring malondialdehyde (MDA) and relatives in biological samples: Analytical and biological challenges. *Anal. Biochem.,* **2017,** *524*, 13-30.

26. D. R. Janero. Malondialdehyde and thiobarbituric acid-reactivity as diagnostic indices of lipid peroxidation and peroxidative tissue injury. *Free Radic. Biol. Med.,* **1990,** *9* (6), 515-540.

27. K. Igarashi and K. Kashiwagi. Protein-conjugated acrolein as a biochemical marker of brain infarction. *Mol. Nutr. Food Res.,* **2011,** *55* (9), 1332-1341.

28. P. Weber, F. W. Harrison and L. Hof. Histochemical Application of Dansylhydrazine as a Fluorescent Labeling Reagent for Sialic-Acid in Cellular Glycoconjugates. *Histochem.,* **1975,** *45* (4), 271-277.

29. P. Demontigny, J. F. Stobaugh, R. S. Givens, R. G. Carlson, K. Srinivasachar, L. A. Sternson and T. Higuchi. Naphthalene-2,3-Dicarboxaldehyde Cyanide Ion - a Rationally Designed Fluorogenic Reagent for Primary Amines. *Anal. Chem.,* **1987,** *59* (8), 1096-1101.

30. N. Binding, H. Klaning, U. Karst, W. Potter, P. A. Czeschinski and U. Witting. Analytical reliability of carbonyl compound determination using 1,5-dansylhydrazine-derivatization. *Fresenius J. Anal. Chem.,* **1998,** *362* (3), 270-273.

31. F. W. Harrison, P. Weber and L. Hof. Fluorescent Demonstration of Tissue Aldehydes with Dansylhydrazine. *Histochem.,* **1976,** *49* (4), 349-351.

32. L. Nondek, D. R. Rodler and J. W. Birks. Measurement of Sub-Ppbv Concentrations of Aldehydes in a Forest Atmosphere Using a New HPLC Technique. *Environ. Sci. Technol.,* **1992,** *26* (6), 1174-1178.

33. D. R. Rodler, L. Nondek and J. W. Birks. Evaluation of Ozone and Water Vapor Interfaces in the Derivatization of Atmospheric Aldehydes with Dansylhydrazine. *Environ. Sci. Technol.,* **1993,** *27*, 2814-2820.

34. J. Herrington, L. Zhang, D. Whitaker, L. Sheldon and J. J. Zhang. Optimizing a dansylhydrazine (DNSH) based method for measuring airborne acrolein and other unsaturated carbonyls. *J. Environ. Monit.,* **2005,** *7* (10), 969-976.

35. I. Zhang, L. Zhang, Z. Fan and V. Ilacqua. Development of the personal aldehydes and ketones sampler based upon DNSH derivatization on solid sorbent. *Environ. Sci. Technol.,* **2000,** *34* (12), 2601-2607.

36. J. C. Cooley and C. E. Lunte. Detection of malondialdehyde in vivo using microdialysis sampling with CE-fluorescence. *Electrophoresis,* **2011,** *32* (21), 2994-2999.

Chapter 3:

Measuring Carnosine Uptake in Macrophage Cells under Pro-Inflammatory Conditions as a Measure of its Antioxidant Properties

3.1. Inflammation and the Immune Response

Inflammation is a complex biological process that occurs after exposure to a wide variety of harmful environmental stimuli such as infections, allergens, chemicals, radiation, obesity, alcohol, tobacco, and chronic diseases [1]. Acute (or therapeutic) inflammation is actually caused via the endogenous immune response and is used to help ward off infections over a short period of time [2]. Chronic inflammation, on the other hand, can prove extremely deleterious and harmful to the body and has been linked to a wide number of diseases, including tumor formation in prominent types of cancer, such as pancreatic [3] and breast [4] cancer. Acute inflammation is caused by the production of nitric oxide ($NO^{\bullet}$) in order to eliminate pathogens; in cases of chronic inflammation, this also leads to oxidative stress [5]. A better understanding of how endogenous antioxidants help mitigate the concentration of RNOS produced by inflammatory pathways could provide new therapeutic pathways for the treatment of chronic inflammation.

3.1.1. The Immune Response and Acute Inflammation

Macrophages are immune cells that are responsible for the primary response to pathogens, as well as serving several other roles related to the immune response [6]. The phagocytic activity of macrophages is promoted by lymphocytes such as T helper (Th) cells and natural killer (NK) cells that respond to specific antigens [7]. Macrophages can be activated via different pathways for different functionalities. Classically activated macrophages (or M1) are in response to the production of the cytokine interferon gamma (INF-γ) from Th1 cells and NK cells or the presence of tumor-necrosis factor (TNF). Alternatively activated macrophages (or M2) are produced in

response to the production of interleukin-4 (IL-4) by Th2 cells and granulocytes [8, 9]. Macrophages can also be directly activated by bacterial endotoxins such as lipopolysaccharide (LPS) [10]. M1 macrophages protect against microbial activity and bacterial pathogens, while M2 macrophages deal with tissue repair, parasitic infections, and tumors [8, 9]. A third population of macrophages can be activated by interleukin 10 (IL-10) and serve regulatory and anti-inflammatory functions [11]. These various modes of macrophage activation are shown in Figure 3.1.

M1 activated macrophages are pivotal in host defense against microbial pathogens. This is accomplished by the activation of the protein inducible nitric oxide synthase (iNOS), which converts arginine to citrulline in order to produce $NO^{\bullet}$ [5]. The production of $NO^{\bullet}$ is meant to result in cytotoxic effects on bacteria and protozoa. However, $NO^{\bullet}$ is highly reactive and will just as readily result in the nitrosation and nitration of important biomolecules. The non-specificity of $NO^{\bullet}$ directly causes acute inflammation via these reactions, and long-term overproduction by M1 activated macrophages will also result in chronic inflammation and oxidative stress [12].

Previous studies have shown that macrophages can be activated in an *in vitro* environment that mimics the natural progression of the immune response. Specifically, stimulating RAW 264.7 murine macrophages with a combination of INF- γ and LPS have been shown to increase iNOS activity by increasing RNOS production [13].

3.1.2. Oxidative Stress from the Immune Response

One of the primary sources of oxidative stress following the immune response is the reaction of $NO^{\bullet}$ with superoxide ($O_2^{\bullet-}$) to produce peroxynitrite ($ONOO^-$). Cellular $O_2^{\bullet-}$ is mainly produced via breakdowns in the electron transport chain of mitochondria, in which an estimated

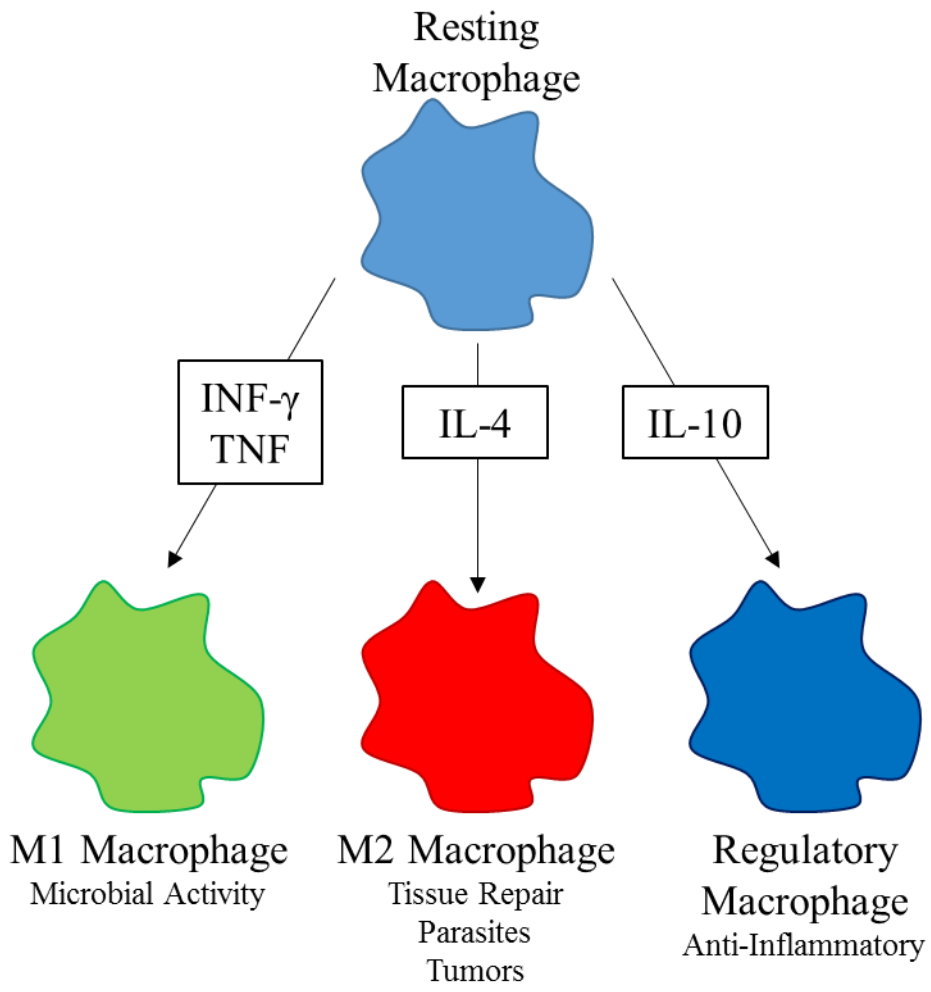

Figure 3.1: Activation of macrophages dependent on cytokine signaling

1-4 % of molecular oxygen is incompletely reduced to $O_2^{\bullet-}$ [14]. $ONOO^-$ is cytotoxic and leads to further damage to biomolecules [15]. $ONOO^-$ can also be protonated to form peroxynitrous acid, which in turn leads to the formation of another highly reactive RNOS: the hydroxyl radical [16]. This overall process was previously shown in Figure 1.1.

$NO^{\bullet}$ can act as a further precursor of oxidative stress due to its reactivity with endogenous antioxidant enzymes. For example, superoxide dismutases (SOD) are a family of enzyme that responsible for scavenging excess $O_2^{\bullet-}$ intracellularly and reducing it to hydrogen peroxide and water, a process that is normally highly efficient due to the intracellular abundance of SOD [17]. However, $NO^{\bullet}$ will competitively react with SOD, restricting this activity and directly leading to hgher intracellular concentrations of $O_2^{\bullet-}$ and $ONOO^-$ [18].

One therapeutic strategy for conditions such as chronic inflammation is using antioxidants in order to bolster the body's natural defense systems [19]. This has led to a high demand for studies investigating molecules that exhibit antioxidant properties that could possibly scavenge RNOS before they result in deleterious effects.

3.2. Carnosine

One endogenous biomolecule that has demonstrated antioxidant properties and is believed to be a part of the antioxidant defense system is carnosine, a dipeptide composed of β-alanine and L-histidine. Carnosine was first discovered in 1900 in meat extract and has since been heavily studied due to its natural presence in several mammalian tissues, including the central nervous system, skeletal muscles, and the lens of the eye in humans [20]. Carnosine is produced via the enzyme carnosine synthase, an ATP-dependent ligase that combines its constituent peptides [21]. It can also be degraded by the enzyme carnosinase, re-forming these two pepetides [22]. The metabolic pathway of carnosine is shown in Figure 3.2.

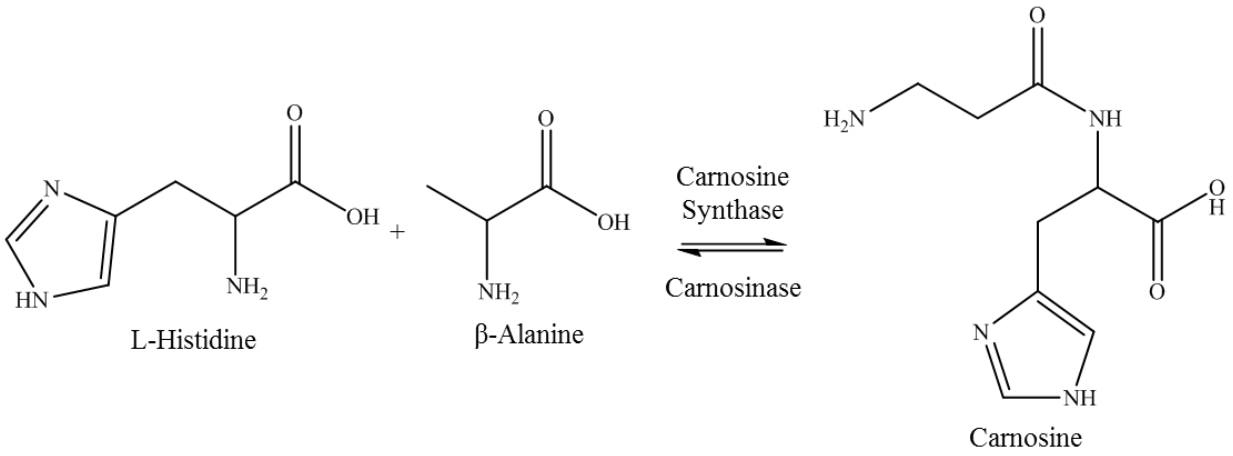

Figure 3.2: Formation and degradation pathway of carnosine

3.2.1. Biochemistry of Carnosine

Carnosine serves a wide host of functions in the body [23]. At physiological pH (7.4) it is zwitterionic, allowing it to function as an endogenous buffering species. It will also readily form complexes with transition metal ions, the most biologically relevant of which are copper [24] and zinc [25]. Carnosine has also been shown to regulate macrophage functionality, although the exact mechanism of this is not yet fully understood [26].

3.2.2. Antioxidant Properties of Carnosine

Carnosine and its structurally related compounds have demonstrated antioxidant properties [26, 27]. Its specific role as a neuroprotective antioxidant have also been investigated and found that it will readily scavenge free radical RNOS that could otherwise cause oxidative stress [28]. The dipeptide has been shown to scavenge both $O_2^{\bullet-}$ [29] and $HO^{\bullet}$ [30], two free radical RNOS whose role in oxidative stress was discussed earlier. It has also been shown to scavenge peroxyl radicals, one of the byproducts of lipid peroxidation that leads to the propagation of the radical chain reaction [31].

In vitro and *in vivo* experiments have been conducted to determine the effects of carnosine on pathologies known to cause oxidative stress and damage. This includes Alzheimer's disease [32], Parkinson's disease [33], diabetes [34], atherosclerosis [35], and ischemic stroke [36]. The exact mechanism by which carnosine influences these pathologies is not completely understood, but is thought to be primarily due to its antioxidant, chelating, and anti-glycation functions [20]. A better understanding of its antioxidant properties could allow progress to be made towards therapeutics for these diseases.

Investigating the inherent uptake of carnosine by unstimulated macrophage cells will provide information regarding its normal concentration in the body. If the M1 activation of these macrophages alters their ability to uptake carnosine, it will also indicate whether or not its antioxidant properties are being exploited in order to reduce chronic inflammation.

3.3. Methods

3.3.1. Rational for Separation Selection

Microchip electrophoresis (ME) provides many benefits that make it a desirable technique for bulk cell lysate analysis that has led to its use for related studies [13, 37, 38]. The short length of microfluidic channels and the high field strengths applied lead to rapid separations, high throughput, and minimal sample dilution. Additionally, electokinetic injections allows for reproducible and small-volume sample injections, which is desirable when studying biological samples such as cell lysates. This also allows for more separations to be conducted using the same patch of cells to guarantee the reproducibility of the results. The inherently high conductivity of the sample matrix also pairs well with ME, where the background electrolyte (BGE) can be modified to match, making it unnecessary to desalt the lysate [39]. Finally, the compatibility between ME and laser excitation sources for fluorescence allows for the detection of molecules in cell lysate at physiologically relevant concentrations.

3.3.2. Materials and Reagents

Murine RAW 264.7 cells (ATCC® TIB71™), Dulbecco's Modified Eagle's Medium (DMEM), phenol red-free DMEM, fetal bovine serum (FBS), and penicillin/streptomycin antibiotic solution were purchased from American Type Culture Collection (ATCC, Manassas, VA, USA). AZ1518 precoated glass substrates were purchased from AZ Electronic Materials Corp (Somerville, NJ), while MIF 300 AZ1518 developer was obtained from Emd Performance

Materials (Somerville, NJ). Chrome etchant was supplied by Cyantek (Fremont, CA). L-carnosine, sodium cyanide (NaCN), anhydrous dimethyl sulfoxide (DMSO), phosphate-buffered saline (PBS), Trypan blue solution, lipopolysaccharides (LPS), Triton X-100, and bovine serum albumin (BSA) were all supplied by Sigma-Aldrich (St. Louis, MO, USA). Sodium hydroxide (NaOH), hydrochloric acid (HCl), hydrofluoric acid (HF), Alconox^{TM} powdered detergent, 25 mL polystyrene culture flasks, boric acid, and ethanol (95%) were obtained from Fisher Scientific (Pittsburgh, PA, USA). Interferon-γ (IFN-γ) was supplied by Calbiochem (Gibbstown, NJ, USA). Naphthalene-2,3-dicarboxaldehyde (NDA) was obtained from Invitrogen (Carlsbad, CA, USA). Polyethersulfone (PES) membrane (3K) was purchased from VWR International (West Chester, PA, USA). C-Chip disposable hemocytometer was purchased from Bulldog Bio, Inc. (Portsmouth, NH, USA). All water used was Ultrapure (18.3 MΩ cm) (Milli-Q Synthesis A10, Millipore, Burlington, MA, USA).

3.3.3. Preparation of Carnosine Standards and Background Electrolyte

The sodium borate background electrolyte (BGE) was prepared from 20 mM boric acid titrated to pH 9.2 via the addition of 0.1 M NaOH. Carnosine standards were prepared at 0.5 M in water before further dilution in BGE to the desired concentration (such as the 100 µM solution used in the standard addition experiments). The carnosine standards were prepared weekly and stored at -20 °C to avoid degradation.

3.3.4. Fluorescent Derivatization of Carnosine and Intracellular Amines

Naphthalene-2,3-dicarboxaldehyde (NDA) is a fluorogenic reagent designed for the derivatization of primary amines such as carnosine [40] that was previously discussed in Chapter 1. NDA will react with primary amines in the presence of a strong electrophile, such as cyanide, to produce a highly-fluorescent 1-cyanobenz[*f*]isoindole (CBI) derivative, as shown in Figure 1.5.

For this study, NDA was prepared at a concentration of 5 mM in ACN. NaCN was prepared at a concentration of 10 mM in H_2O. Both of these derivatization solutions were prepared weekly, stored at 4 °C, and protected from light exposure to prevent photobleaching.

Standards were derivatized by diluting the appropriate volume of 0.5 M carnosine with BGE to a final volume of 1540 µL to achieve the desired final concentration. Thirty microliters of the NDA and NaCN solutions were sequentially added with mixing, after which the reaction was allowed to proceed for at least 30 minutes at room temperature while being protected from light. For cell samples, 40 µL of filtered cell lysate was diluted with 100 µL of BGE before the addition of 30 µL of the NDA and NaCN solutions, followed by mixing and a thirty minute reaction time in the dark.

For the standard addition experiments, 20 µL of native cell lysate was divided into four portions. The appropriate volume of a 100 µM carnosine standard (diluted in BGE) was added to the lysate to produce final concentrations of 1, 2.5, and 5 µM in the samples. They were then diluted with BGE to a final volume of 70 µL before the addition of 15 µL of the NDA and NaCN solutions. This reaction was also allowed to proceed for at least thirty minutes while protected from light exposure.

3.3.5. Cell Culture and Treatment Protocol

RAW 264.7 macrophage cells were cultured in DMEM containing 10% (v/v) FBS, L-glutamine (2 mM), penicillin (50 IU mL^{-1}), and streptomycin (0.3 mg mL^{-1}). The cells were maintained in a humidified environment at 37°C and 5% CO_2 and cultured in 25 mL polystyrene culture flasks. Cells were passaged every 2–3 days at approximately 90% confluence to avoid overgrowth. On the day of the experiment, cells were harvested, counted, and plated at the density of 1.5×10^7 cells/flask. They were then placed in an incubator under a humidified environment at

37 °C and 5% CO_2. Once the cells adhered to the flask surface they were immediately stimulated with LPS (100 ng/mL) and INF-γ (600 U/mL). After 4 h of stimulation, carnosine (at a final concentration of 20 mM) was added to the cell medium, and the cells were left to incubate for an additional 20 h. For the control experiments, RAW 264.7 cells from the same population were incubated with only 20 mM carnosine (no preincubaton with stimulation agents). Additionally, untreated (native) RAW 264.7 cells were analyzed to estimate the basal carnosine concentration. At the end of incubation the cells were harvested using a cell scraper, and the cell suspension was transferred to a centrifuge tube (15 mL). A 100 µL aliquot of the solution containing macrophage cells was taken out and cells counted. The cells were then centrifuged at 1137 × *g* for 4 min at 4°C. After centrifugation, the supernatant was removed and the cell pellet was washed twice using cold 0.01 M PBS at pH 7.4. Next, cell pellets were lysed using 300 µL of 10 mM boric acid and 0.5 % Triton X-100 at pH 9.2. The lysate solution was filtered by centrifugation at 18690 × *g* for 10 min in centrifuge tubes equipped with 3 kDa cut-off filters. The filtered lysates were then ready for the NDA/CN derivatization procedure. Prior to ME-LIF analysis, each sample lysate (except the native one) was diluted by a factor of 20 in BGE. A schematic of this process is shown in Figure 3.3.

Cell viability was measured using a Tryphan blue exclusion assay and cell count using a C-chip disposable hemocytometer (Bulldog Bio, Inc., Portsmouth, NH, USA). The RAW264.7 cell suspension was diluted at a 1:1 and 1:3 ratio with 0.4% Trypan blue solution. The number of viable cells and cell density were determined using a 4 mm^2 total area hemocytometer. Native cells typically had densities of about 6 million cells in a 25 cm^2 flask. Cell images were obtained using an Accu-Scope microscope (Mel Sobel Microscopes Ltd, Hicksville, NY, USA) with MicoPublisher 3.3 RTV camera with QCapture Pro 6 software (Qimaging, Surrey, BC, Canada).

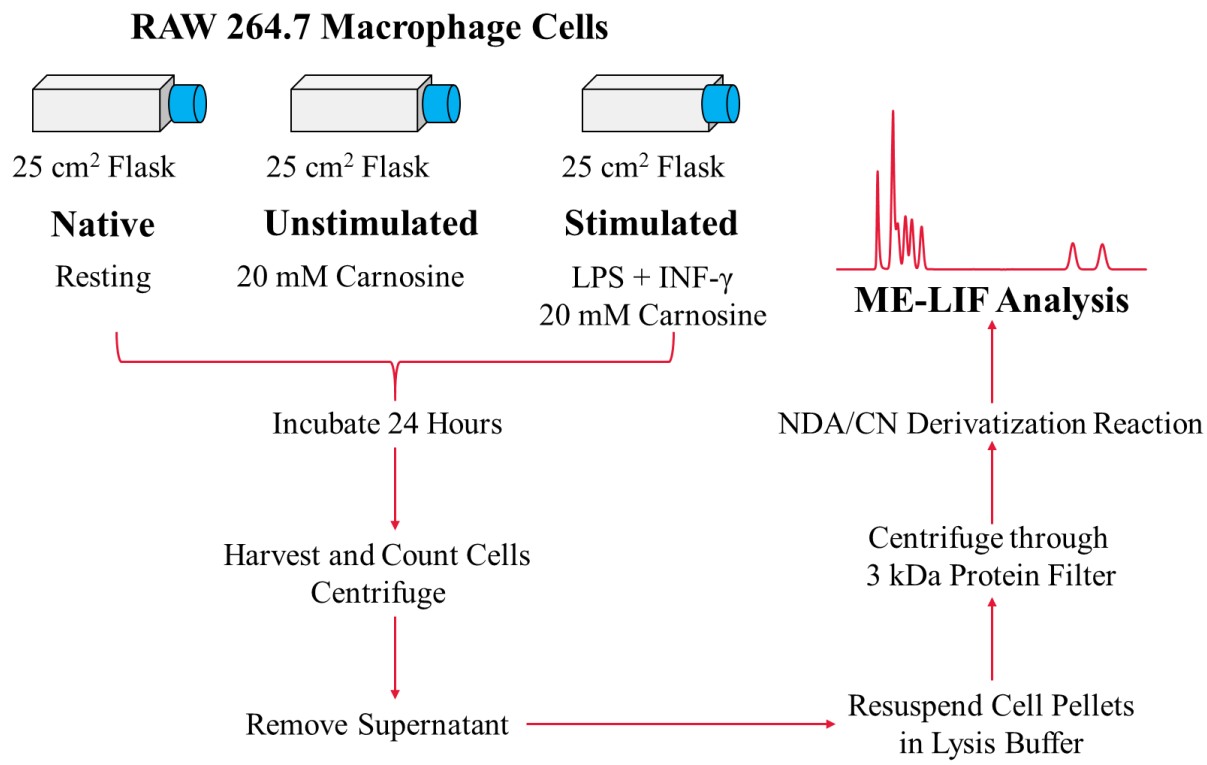

Figure 3.3: Stimulation procedure for RAW264.7 macrophages in this study

3.3.6. Fabrication of Glass-Glass Microfluidic Devices

Glass has many ideal properties as a microfluidic substrate, such as its optical clarity, its surface chemistry, its ability to withstand high voltages, and its similarity to fused-silica capillaries used for traditional electrophoresis [41]. The fabrication of these devices requires access to a clean room facility and a variety of specialized equipment. This includes an UV Flood Source and Mask Alignment System (ABM, Scotts Valley, CA), a PDC-32G Plasma Cleaner (Harrick Plasma, Ithaca, NY), a BD-20AC Laboratory Corona Treater (Electro-Technic Products, Chicago, IL), an Alpha-Step 200 Profilometer (KLA Tencor, Milpitas, CA), and a Scientific Muffle Furnace (Fisher, Wlatham, MA).

A schematic of the glass-glass microfluidic device construction process is shown in Figure 3.4. The microchannels are fabricated on a glass substrate spin-coated with a layer of chrome and positive photoresist (obtained from Telic, Valencia, CA). Briefly, a mask with the desired channel geometry is printed using drafting software to create a photomask, which is aligned on the substrate and exposed to UV light. This will cause the degradation of the exposed photoresist, which will allow it to be removed with developer. The exposed chrome can then be removed via chrome etchant, leaving the desired channel design on the glass substrate. Buffer reservoirs are then drilled into the substrate using a diamond drill bit (Ukam Industrial Superhard Tools, Valencia, CA). Placing the substrate in a bath of hydrofluoric acid will etch the channels to the appropriate depth, which should then be confirmed via a profilometer. The remaining photoresist and chrome can then be removed with acetone and chrome etchant, respectively. The etched substrate was then activated by exposure to oxygen plasma and thermally bonded to a piece of unmodified glass in order to create the complete microfluidic device [42, 43]. This fabrication process is explained in further detail in Appendix 1.

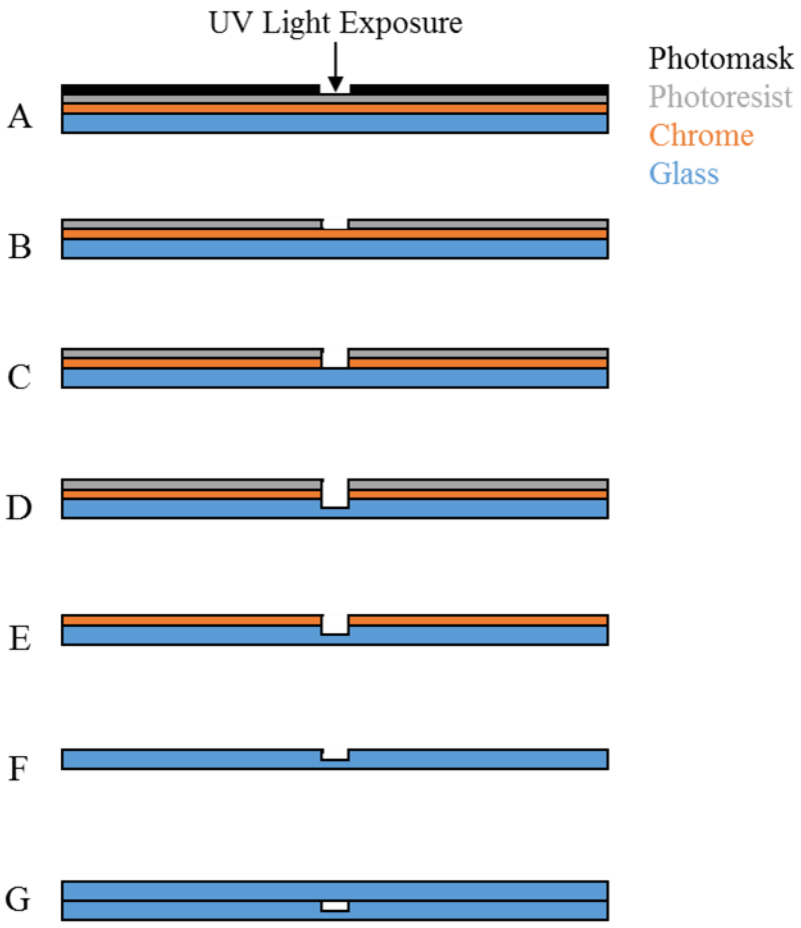

Figure 3.4: Schematic of glass-glass microchip fabrication

(A) Align photomask on positive photoresist coated glass substrate and expose to UV light; (B) Remove photomask and soak in developer to remove exposed photoresist; (C) Remove exposed chrome using chrome etchant; (D) Etch exposed glass with hydrofluoric acid, then confirm channel depth with profilometer and drill reservoirs; (E) Remove remaining photoresist with acetone (F) Remove remaining chrome with chrome etchant (G) Activate surface via plasma exposure and thermally bond to unmodified glass to form complete device.

3.3.7. Microchip Electrophoresis with Laser Excitation Source

For these experiments, a 15-cm serpentine separation channel was used, with 3-cm side channels and a 1.5-cm injection channel. A profilometer was used to confirm the microchannels were approximately 17 µm deep and 70 µm wide. Prior to use the microchip was sequentially conditioned with 0.1 M HCl, deionized H_2O, 0.1 M NaOH, and deionized H_2O again via the application of a negative pressure using a vacuum system. The channels were then completely filled with BGE in the same manner.

Separations were performed in normal polarity with a high voltage power supply (Ultravolt, Ronkonkoma, NY, USA) controlled by software written in Labview (National Instruments, Austin, TX, USA). To separate the derivatized amines, 10 kV was applied to the buffer reservoir and 7 kV to the sample reservoir, resulting in a field strength of 420 V/cm. Under these conditions the separation took 150 s to complete. Electrokinetic injections were employed by floating the buffer reservoir voltage for 0.5 seconds to produce the sample plug, as previously shown in Figure 1.9.

The benchtop laser system used for excitation consisted of a 445-nm PhoxX diode laser (Market Tech, Scotts Valley, CA, USA) coupled to an Eclipse Ti-U inverted microscope (Nikon Instruments Inc., Melville, NY, USA) with a fiber optics cable. The emission light was filtered through a long-pass edge filter with a 480 nm cutoff before being focused onto a photomultiplier tube (Hammatsu Corporation, Bridgewater, NJ, USA). The data was amplified and filtered before acquisition on the Labview software.

3.4. Discussion

3.4.1. Microchip Electrophoresis Separation

NDA/CN derivatization is non-specific and will react with any primary amines present in the cell lysate samples. A ME separation was optimized to guarantee that the carnosine peak did not co-migrate with any of the most abundant amino acids present in macrophages, as reported in the literature [44]. Using a 15-cm separation channel, 20 mM sodium borate BGE (pH 9.2), and field strength of 420 V/cm led to a separation that achieved this, as shown in Figure 3.5. The system displayed good linearity for carnosine from 65 nM to 50 µM, with a correlation coefficient (R^2) of 0.994 and an experimental LOD of 65 nM for carnosine (S/N = 3). The migration time of the CBI-carnosine peak exhibited an intraday relative standard deviation of 3.55%.

3.4.2. Quantification of Carnosine in Native Cell Lysate

When running cell lysate samples on the ME system, it was noticed that there was a shift in the migration time of all species compared to the standards prepared in BGE. This was determined to be due to the difference in the sample matrix conductivity, as the cell lysate was prepared in PBS and had a much higher conductivity. Previous findings in the literature have found that sample plugs with higher conductivity (compared to the BGE) will result in longer electrophoretic migration times [45]. The separation in cell lysate samples is shown in Figure 3.6, demonstrating the shift in migration time in a real sample.

In order to confirm the identity of the carnosine peak, a standard addition calibration curve was performed in the cell lysate samples, as described in the Methods section. The standard addition of response vs. the carnosine concentration yielded a R^2 value of 0.997, as shown in Figure 3.7. Using the cell counts obtained for each set of cells, the concentration of carnosine contained

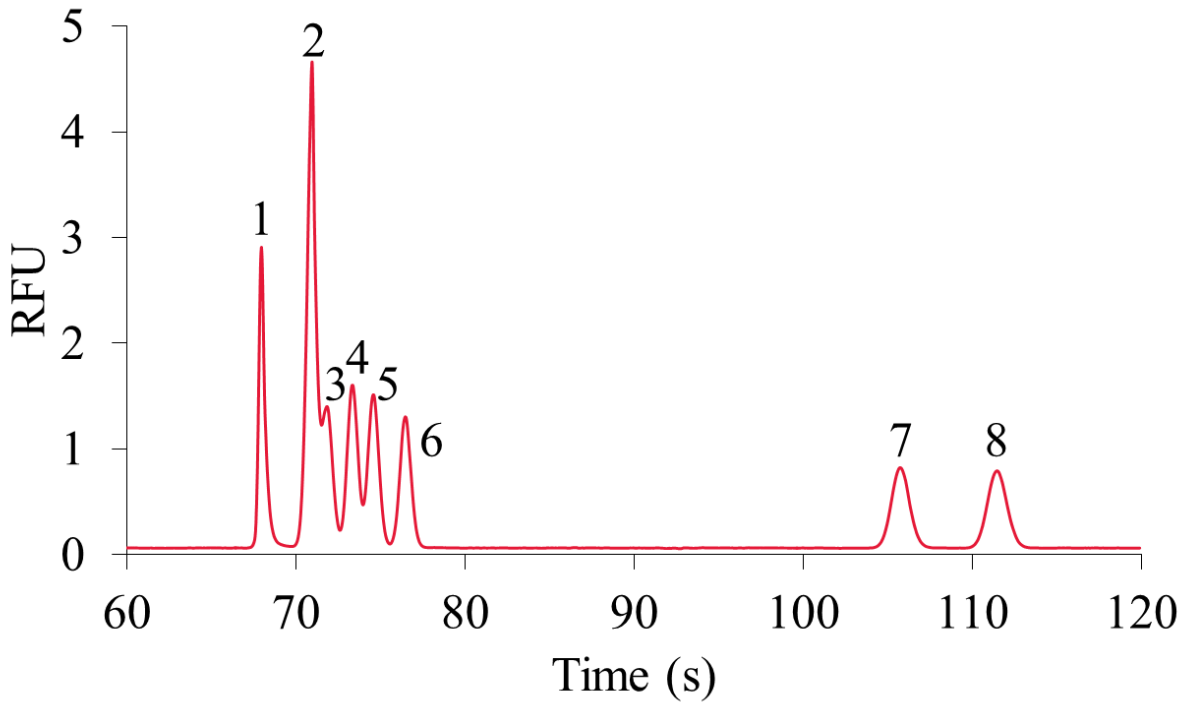

Figure 3.5: ME separation of carnosine from abundant intracellular primary amines

As the NDA/CN reaction will react with any primary amine, the microchip electrophoresis (ME) separation needed to resolve carnosine from other present species. (1) carnosine; (2) glutamine, isoleucine, leucine, histidine; (3) valine; (4) serine; (5) alanine; (6) glycine; (7) glutamate; (8) aspartate.

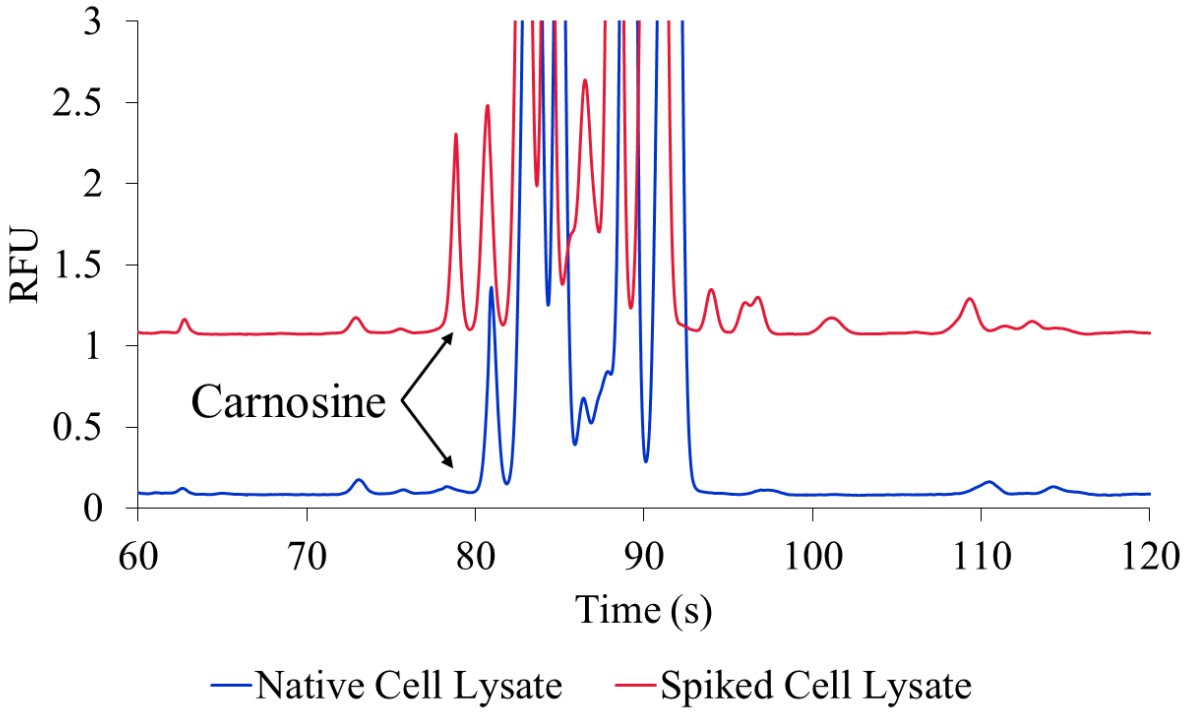

Figure 3.6: ME separation of carnosine in cell lysate

Electrophoretic separation of untreated RAW 264.7 macrophage cells, with the carnosine peak indicated. Spiking studies were done to confirm its identity due to a shift in migration times resulting from differences in the sample matrix. The other peaks that change in the spiked cell lysate are believed to be degradation products and did not respond linearly to the carnosine spikes.

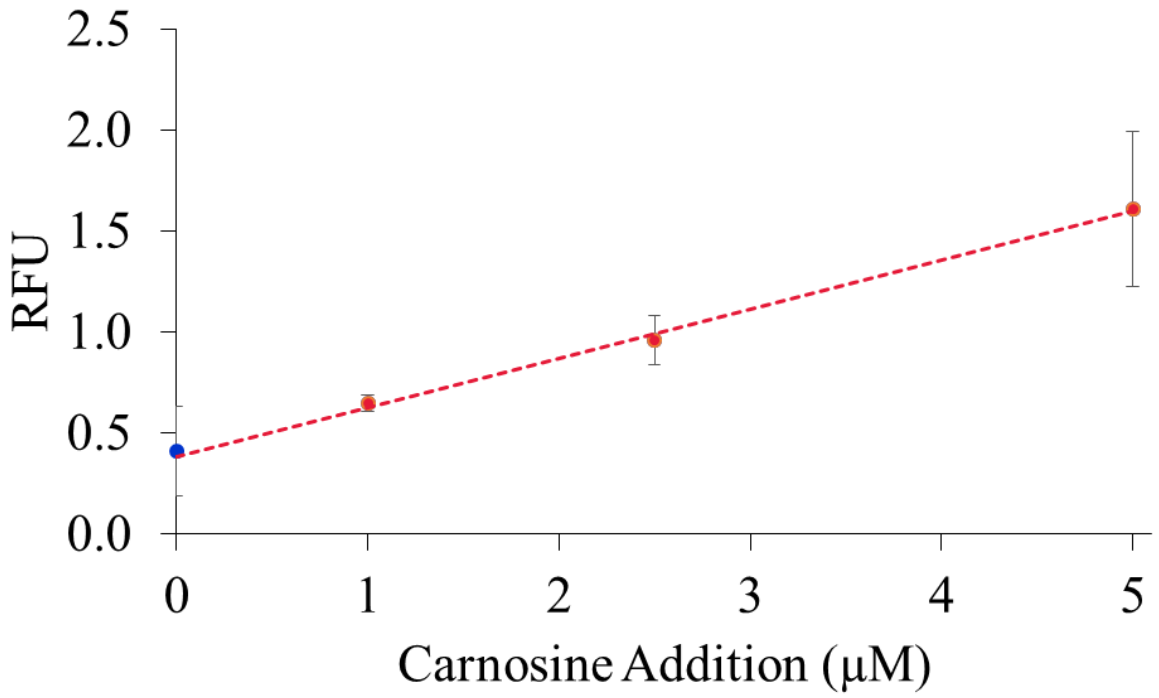

Figure 3.7: Standard addition calibration curve for carnosine in cell lysate

$y = 0.2429x + 0.3861$; $R^2 = 0.9972$.

per million native cells could be determined at a concentration of 0.08 (± 0.02) nmol per 10^6 cells. As macrophage cells are the first ones to respond to inflammation processes such as oxidative stress, the endogenous presence of carnosine could relate to its antioxidant properties and ability to scavenge RNOS.

3.4.3. Carnosine Uptake in Stimulated Macrophages

The variation in carnosine uptake between physiological and pro-inflammatory conditions could provide a better understanding of its role as an antioxidant during macrophage activation. In order to simulate pro-oxidative conditions *in vitro,* RAW 264.7 macrophage cells were incubated in LPS and INF-γ four hours prior to incubation with carnosine. When placed in cell medium, carnosine is naturally taken up. The control group consisted of cells that were incubated with only carnosine (at 20 mM), while the experimental group was first perturbed with LPS and INF-γ prior to incubation with carnosine (at the same concentration). Morphological changes were observed in the macrophage cells exposed to LPS that are consistent with inflammatory conditions, as shown in Figure 3.8.

There was a large difference in the degree of carnosine uptake between the two groups, which was calculated by dividing the measured carnosine concentration by the number of cells in each bulk cell sample. The unstimulated cells had a final intracellular carnosine concentration of 46.67 (± 8.61) nmol per 10^6 cells, while the stimulated cells had a drastically higher amount at 132.41 (± 12.22) nmol per 10^6 cells, a statistically significant difference ($p < 0.001$). This is a 2.83 (± 0.29) factor increase in carnosine uptake between the two experimental conditions.

The exact mechanism and reason behind the increased uptake of carnosine in stimulated macrophages is not yet understood, but could be due to a variety of reasons. One explanation is

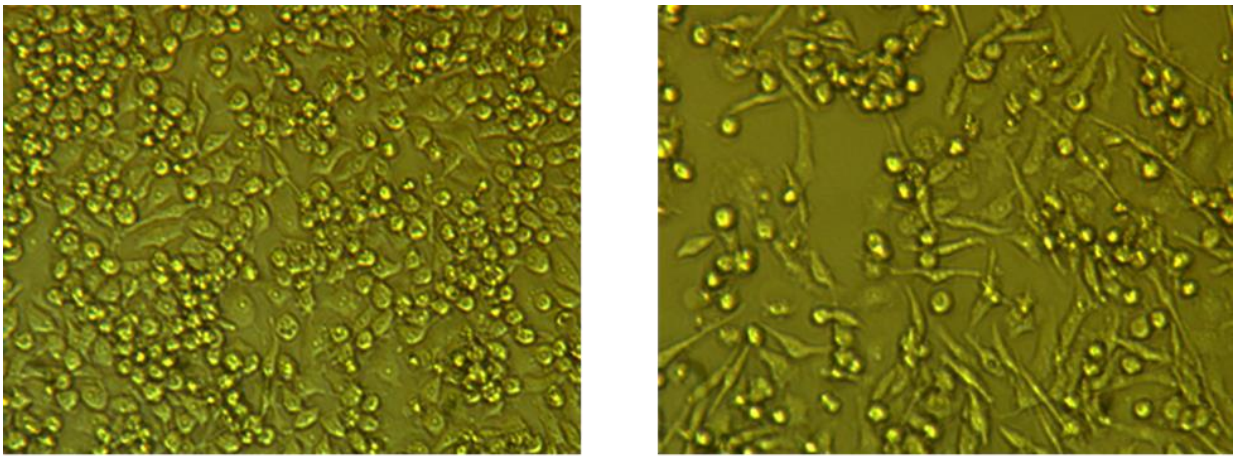

Figure 3.8: Morphological changes in activated macrophage cells

Native cells were incubated with carnosine alone and exhibited no morphological changes. Stimulated cells were treated with LPS and INF-γ prior to incubation with carnosine and demonstrated observable changes in cell morphology.

that these cells, which are integral to the immune response, actively take up antioxidant molecules in response to inflammatory stimuli. It is also possible that the use of LPS and INF-γ impact membrane permeability, leading to a passive increase in carnosine uptake. Further studies need to be conducted to study these macrophage cells following M1 activation to investigate whether this is the case via the use of dyes that can detect damage to the cell membrane.

3.5. Conclusion

A ME-fluorescence method was developed for the separation and detection of carnosine in bulk cell lysate using the NDA/CN derivatization. Standard addition was used to confirm that macrophages contain a low basal intracellular concentration of carnosine. Not only do these cells readily take up carnosine present in cell medium, there is also an approximately 3-fold increase in uptake under pro-oxidative and pro-inflammatory conditions.

3.6. References

1. S. Reuter, S. C. Gupta, M. M. Chaturvedi and B. B. Aggarwal. Oxidative stress, inflammation, and cancer How are they linked? *Free Radic. Biol. Med.,* **2010,** *49* (11), 1603-1616.

2. B. B. Aggarwal, R. V. Vijayalekshmi and B. Sung. Targeting Inflammatory Pathways for Prevention and Therapy of Cancer: Short-Term Friend, Long-Term Foe. *Clin. Cancer. Res.,* **2009,** *15* (2), 425-430.

3. B. Farrow and B. M. Evers. Inflammation and the development of pancreatic cancer. *Surg. Oncol.,* **2002,** *10* (4), 153-169.

4. L. R. Howe. Inflammation and breast cancer. Cyclooxygenase/prostaglandin signaling and breast cancer. *Breast Cancer Res.,* **2007,** *9* (4), 210.

5. D. S. Chi, M. Qui, G. Krishnaswamy, C. Li and W. Stone. Regulation of nitric oxide production from macrophages by lipopolysaccharide and catecholamines. *Nitric Oxide,* **2003,** *8* (2), 127-132.

6. F. O. Martinez, L. Helming and S. Gordon. Alternative activation of macrophages: an immunologic functional perspective. *Annu. Rev. Immunol.,* **2009,** *27*, 451-483.

7. J. R. David, E. Henshaw and C. Hirsch. Lymphocyte Mediators and Cellular Hypersensitivity. *New Engl. J. Med.,* **1973,** *288* (3), 143-149.

8. D. A. Hume. The Many Alternative Faces of Macrophage Activation. *Front. Immunol.,* **2015,** *6*, 370.

9. D. M. Mosser and J. P. Edwards. Exploring the full spectrum of macrophage activation. *Nat. Rev. Immunol.,* **2008,** *8* (12), 958-969.

10. E. T. Rietschel, H. Brade, O. Holst, L. Brade, S. Muller-Loennies, U. Mamat, U. Zahringer, F. Beckmann, U. Seydel, K. Brandenburg, A. J. Ulmer, T. Mattern, H. Heine, J. Schletter, H.

Loppnow, U. Schonbeck, H. D. Flad, S. Hauschildt, U. F. Schade, F. Di Padova, S. Kusumoto and R. R. Schumann. Bacterial endotoxin: Chemical constitution, biological recognition, host response, and immunological detoxification. *Curr. Top. Microbiol. Immunol.,* **1996,** *216*, 39-81.

11. J. P. Edwards, X. Zhang, K. A. Frauwirth and D. M. Mosser. Biochemical and functional characterization of three activated macrophage populations. *J. Leukoc. Biol.,* **2006,** *80* (6), 1298-1307.

12. S. Moncada, R. M. Palmer and E. A. Higgs. Nitric oxide: physiology, pathophysiology, and pharmacology. *Pharmacol. Rev.,* **1991,** *43* (2), 109-142.

13. D. B. Gunasekara, J. M. Siegel, G. Caruso, M. K. Hulvey and S. M. Lunte. Microchip electrophoresis with amperometric detection method for profiling cellular nitrosative stress markers. *Analyst*, **2014,** *139* (13), 3265-3273.

14. G. Lenaz, C. Bovina, M. D'Aurelio, R. Fato, G. Formiggini, M. L. Genova, G. Giuliano, M. Merlo Pich, U. Paolucci, G. Parenti Castelli and B. Ventura. Role of mitochondria in oxidative stress and aging. *Ann. N. Y. Acad. Sci.,* **2002,** *959*, 199-213.

15. G. Ferrer-Sueta and R. Radi. Chemical Biology of Peroxynitrite: Kinetics, Diffusion, and Radicals. *ACS Chem. Biol.,* **2009,** *4* (3), 161-177.

16. J. S. Beckman, H. Ischiropoulos, L. Zhu, M. Vanderwoerd, C. Smith, J. Chen, J. Harrison, J. C. Martin and M. Tsai. Kinetics of Superoxide Dismutase-Catalyzed and Iron-Catalyzed Nitration of Phenolics by Peroxynitrite. *Arch. Biochem. Biophys.,* **1992,** *298* (2), 438-445.

17. I. Fridovich. Superoxide Radical and Superoxide Dismutases. *Annu. Rev. Biochem.,* **1995,** *64*, 97-112.

18. M. Lechner, P. Lirk and J. Rieder. Inducible nitric oxide synthase (iNOS) in tumor biology: the two sides of the same coin. *Semin. Cancer Biol.,* **2005,** *15* (4), 277-289.

19. S. Cuzzocrea, D. P. Riley, A. P. Caputi and D. Salvemini. Antioxidant therapy: A new pharmacological approach in shock, inflammation, and ischemia/reperfusion injury. *Pharmacol. Rev.*, **2001,** *53* (1), 135-159.

20. S. Budzen and J. Rymaszewska. The biological role of carnosine and its possible applications in medicine. *Adv. Clin. Exp. Med.*, **2013,** *22* (5), 739-744.

21. M. Veiga-da-Cunha, N. Chevalier, V. Stroobant, D. Vertommen and E. Van Schaftingen. Metabolite proofreading in carnosine and homocarnosine synthesis: molecular identification of PM20D2 as beta-alanyl-lysine dipeptidase. *J. Biol. Chem.*, **2014,** *289* (28), 19726-19736.

22. A. A. Boldyrev, G. Aldini and W. Derave. Physiology and pathophysiology of carnosine. *Physiol. Rev.*, **2013,** *93* (4), 1803-1845.

23. A. Torreggiani, M. Tamba and G. Fini. Binding of copper(II) to carnosine: Raman and IR spectroscopic study. *Biopolymers*, **2000,** *57* (3), 149-159.

24. A. Torreggiani, S. Bonora and G. Fini. Raman and IR spectroscopic investigation of zinc(II)-carnosine complexes. *Biopolymers*, **2000,** *57* (6), 352-364.

25. A. Guiotto, A. Calderan, P. Ruzza and G. Borin. Carnosine and carnosine-related antioxidants: a review. *Curr. Med. Chem.*, **2005,** *12* (20), 2293-2315.

26. A. A. Boldyrev, A. M. Dupin, A. Bunin, M. A. Babizhaev and S. E. Severin. The antioxidative properties of carnosine, a natural histidine containing dipeptide. *Biochem. Int.*, **1987,** *15* (6), 1105-1113.

27. A. A. Boldyrev, S. L. Stvolinsky, O. V. Tyulina, V. B. Koshelev, N. Hori and D. O. Carpenter. Biochemical and physiological evidence that carnosine is an endogenous neuroprotector against free radicals. *Cell. Mol. Neurobiol.*, **1997,** *17* (2), 259-271.

28. G. I. Klebanov, O. Teselkin Yu, I. V. Babenkova, I. N. Popov, G. Levin, O. V. Tyulina, A. A. Boldyrev and A. Vladimirov Yu. Evidence for a direct interaction of superoxide anion radical with carnosine. *Biochem. Mol. Biol. Int.,* **1997,** *43* (1), 99-106.

29. M. Tamba and A. Torreggiani. Hydroxyl radical scavenging by carnosine and Cu(II)-carnosine complexes: a pulse-radiolysis and spectroscopic study. *Int. J. Radiat. Biol.,* **1999,** *75* (9), 1177-1188.

30. R. Kohen, Y. Yamamoto, K. C. Cundy and B. N. Ames. Antioxidant activity of carnosine, homocarnosine, and anserine present in muscle and brain. *Proc. Natl. Acad. Sci. U. S. A.*, **1988,** *85* (9), 3175-3179.

31. J. E. Preston, A. R. Hipkiss, D. T. Himsworth, I. A. Romero and J. N. Abbott. Toxic effects of beta-amyloid(25-35) on immortalised rat brain endothelial cell: protection by carnosine, homocarnosine and beta-alanine. *Neurosci. Lett.,* **1998,** *242* (2), 105-108.

32. S. J. Tsai, W. W. Kuo, W. H. Liu and M. C. Yin. Antioxidative and anti-inflammatory protection from carnosine in the striatum of MPTP-treated mice. *J. Agric. Food Chem.,* **2010,** *58* (21), 11510-11516.

33. F. Pfister, E. Riedl, Q. Wang, F. vom Hagen, M. Deinzer, M. C. Harmsen, G. Molema, B. Yard, Y. Feng and H. P. Hammes. Oral carnosine supplementation prevents vascular damage in experimental diabetic retinopathy. *Cell. Physiol. Biochem.,* **2011,** *28* (1), 125-136.

34. A. R. Hipkiss. Carnosine, a protective, anti-ageing peptide? *Int. J. Biochem. Cell Biol.,* **1998,** *30* (8), 863-868.

35. D. Dobrota, T. Fedorova, S. Stvolinsky, E. Babusikova, K. Likavcanova, A. Drgova, A. Strapkova and A. Boldyrev. Carnosine protects the brain of rats and Mongolian gerbils against ischemic injury: after-stroke-effect. *Neurochem. Res.,* **2005,** *30* (10), 1283-1288.

36. R. P. de Campos, J. M. Siegel, C. G. Fresta, G. Caruso, J. A. da Silva and S. M. Lunte. Indirect detection of superoxide in RAW 264.7 macrophage cells using microchip electrophoresis coupled to laser-induced fluorescence. *Anal. Bioanal. Chem.,* **2015,** *407* (23), 7003-7012.

37. G. Caruso, C. G. Fresta, F. Martinez-Becerra, L. Antonio, R. T. Johnson, R. P. de Campos, J. M. Siegel, M. B. Wijesinghe, G. Lazzarino and S. M. Lunte. Carnosine modulates nitric oxide in stimulated murine RAW 264.7 macrophages. *Mol. Cell. Biochem.,* **2017**.

38. C. Bylda, R. Thiele, U. Kobold and D. A. Volmer. Recent advances in sample preparation techniques to overcome difficulties encountered during quantitative analysis of small molecules from biofluids using LC-MS/MS. *Analyst,* **2014,** *139* (10), 2265-2276.

39. P. S. De Montigny, John F.; Givens, Richard S.; Carlson, Robert G.; Srinivasachar, Kasturi; Sternson, Larry A.; Higuchi, Takeru. Naphthalene-2,3-dicarboxyaldehyde/cyanide ion: a rationally designed fluorogenic reagent for primary amines. *Anal. Chem.,* **1987,** *59* (8), 1096-1101.

40. S. C. Jacobson, A. W. Moore and J. M. Ramsey. Fused Quartz Substrates for Microchip Electrophoresis. *Anal. Chem.,* **1995,** *67* (13), 2059-2063.

41. W. K. T. Coltro, S. M. Lunte and E. Carrilho. Comparison of the analytical performance of electrophoresis microchannels fabricated in PDMS, glass, and polyester-toner. *Electrophoresis,* **2008,** *29* (24), 4928-4937.

42. T. H. Linz, C. M. Snyder and S. M. Lunte. Optimization of the separation of NDA-derivatized methylarginines by capillary and microchip electrophoresis. *J. Lab. Autom.,* **2012,** *17* (1), 24-31.

43. H. Sato, H. Watanabe, T. Ishii and S. Bannai. Neutral amino acid transport in mouse peritoneal macrophages. *J. Biol. Chem.,* **1987,** *262* (27), 13015-13019.

44. Z. K. Shihabi. Effects of sample matrix on analysis by capillary electrophoresis. In *Handbook of Capillary Electrophoresis*, 2nd ed.; CRC Press, 1997; 457-477.

Chapter 4:

Advances in the Development of an On-line Microdialysis-Microchip System for Monitoring Glutamate after Severe Traumatic Brain Injuries

4.1. Traumatic Brain Injury

Traumatic brain injury (TBI) is the most common type of neurotrauma worldwide. In the United States alone there are over a million patients admitted to emergency departments with TBIs annually [1]. Additionally, it's estimated that 1% of the country's population lives with long-term disabilities following a TBI [2]. The initial injury can be the result of direct blunt-force trauma, acceleration, deceleration, or rotational forces, and is most often caused by falling injuries or automobile accidents [3]. This condition has also received a large amount of media attention due to its prevalence amongst sports players and veterans returning from active combat zones.

A mild TBI, commonly referred to as a concussion, is much more common than severe injuries. However, many patients who suffer from concussions do not receive immediate medical treatment, making it difficult to estimate the exact number of cases annually [4]. The clinical severity of a TBI is determined by medical personnel by using the Glasgow coma scale (GCS), a practical method of determining the level of consciousness following head injuries, as shown in Table 4.1 [5]. Although there is some evidence that suggests the GCS can predict long-term outcome after suffering a TBI, it does not examine any neurochemical indicators of short- or long-term damage [6].

If a patient has a score of less than 8 on the GCS, they are considered comatose and have suffered from a severe TBI. This usually necessitates a surgical procedure to reduce intracranial pressure, known as a decompressive craniectomy [7]. This involves removing a portion of the

Table 4.1: The Glasgow Come Scale, a clinical method of measuring the severity of TBI patients, with a best possible score of 15. Patients are considered comatose with a score of less than 8 and totally unresponsive with a minimum score of 3 [5].

Behavior	Response	Score
Eye opening response	• Spontaneously • To speech • To pain • No Response	4 3 2 1
Best verbal response	• Oriented and self-aware • Confused • Inappropriate words • Incomprehensible sounds • No response	5 4 3 2 1
Best motor response	• Obeys commands • Moves in response to localized pain • Flexion withdrawal from pain • Abnormal flexion • Abnormal extension • No response	6 5 4 3 2 1

skull, which also gives medical professionals access to the brain in order to monitor neurochemical indicators of short-or long-term damage. There has been a growing interest in using microdialysis sampling to monitor the neurotransmitters levels (and other indicators of brain health) following a severe TBI [8].

4.1.1. Severe Traumatic Brain Injury: Primary vs. Secondary Damage

When examining a TBI, the damage done to the brain can be broadly split into two categories. Primary damage is the result of the direct mechanical damage caused by an external force. This results in skull fractures, white-matter shearing, hematomas, blood vessel tears, focal contusions, and diffuse swelling. TBI patients can be separated into three categories depending on the degree of primary damage suffered: acute subdural hematoma (SDH) TBIs, diffuse axonal injury (DAI) TBIs, and contusion TBIs [9]. There is very little that can be done by medical professionals to limit primary damage, as it has already occurred before the patient receives emergency care.

However, the initial trauma can also initiate pathophysiological pathways that lead to additional brain damage, which is referred to as secondary damage. Some of the mechanisms that link primary and secondary damage are shown in Figure 4.1 [10]. The secondary damage itself is the result of inflammation [11], receptor-mediated damage [12], calcium-mediated damage [3], and oxidative stress [13]. The category of TBI determines which of these pathophysiological pathways results in the most secondary damage, as shown in Figure 4.2.

As secondary damage develop in the hours and days after the initial trauma event, medical professionals usually have the opportunity to monitor and treat these pathophysiological pathways. However, they require methods that will allow them to monitor the levels of biomolecules related to TBI damage with enough temporal resolution to administer the proper treatments.

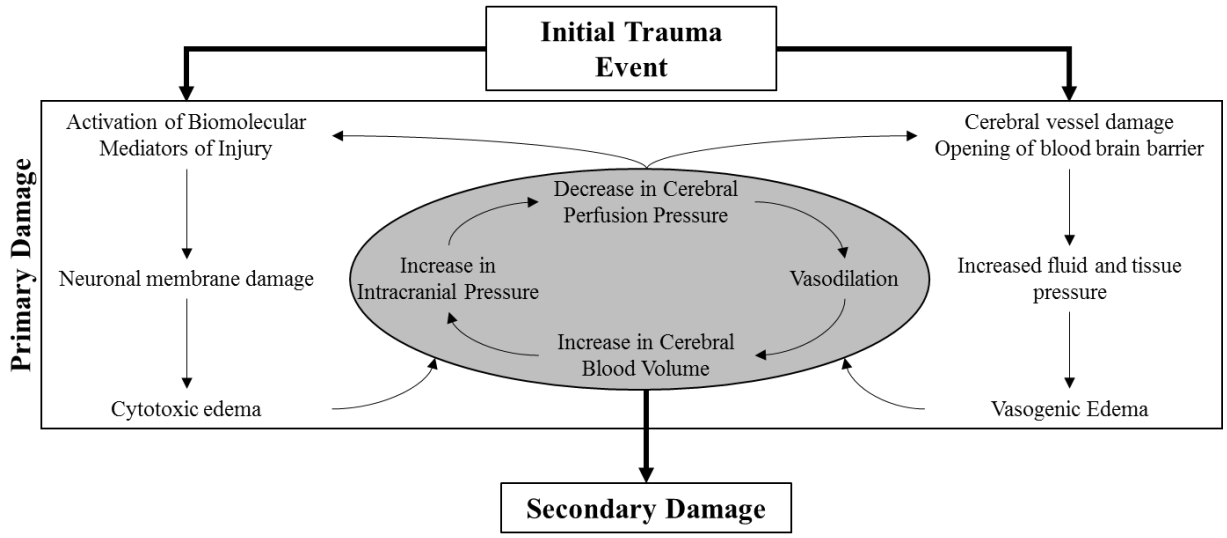

Figure 4.1: Relationship between primary and secondary damage following TBI

The initial trauma event directly causes primary damage, which in turn leads to secondary damage. The central gray loop is known as the vasodilatory cascade [10].

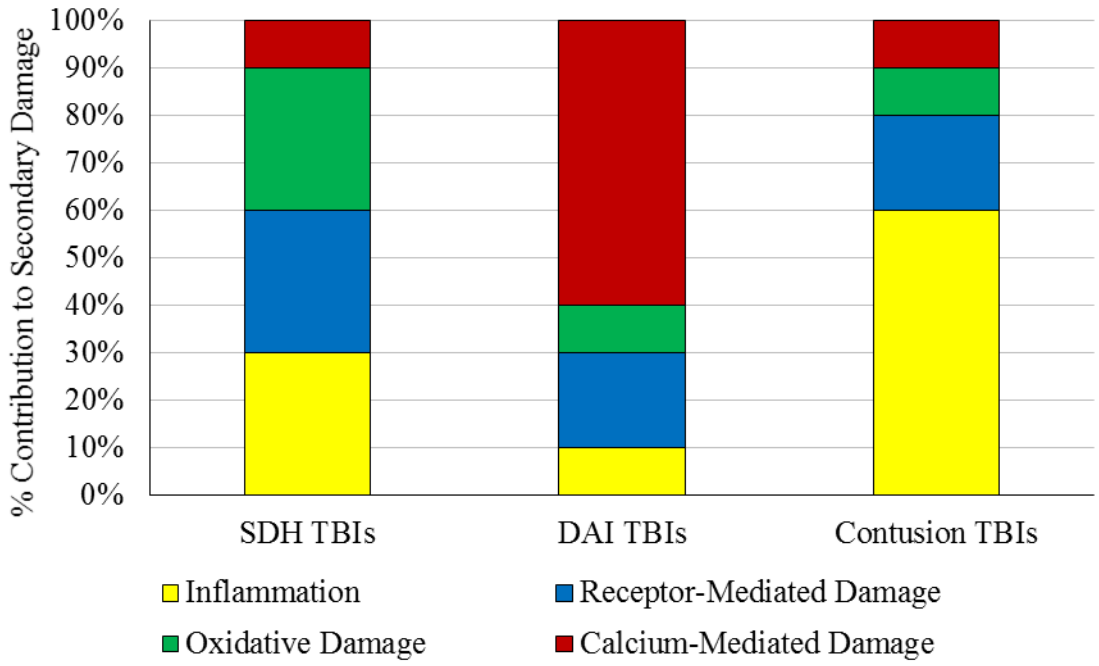

Figure 4.2: Contribution of different sources to TBI secondary damage

The amount of contribution of different type of secondary damage depends on the type of primary damage associated with a TBI [9].

4.1.2. Excitatory Amino Acids and Secondary Damage

It is widely acknowledged that the excitatory amino acid (EAA) neurotransmitter glutamate plays a pivotal role in the secondary damage following a TBI. The initial trauma produced will lead to increased production of EAA neurotransmitters. This excessive glutamate will cause depolarization of the cell membrane in nearby neurons, leading to the breakdown of ion channels that will consequently release more glutamate into the extracellular fluid (ECF) and lead to the depolarization of additional neurons. This will result in a phenomenon known as spreading depolarization, which damages the ability of neurons to propagate an action potential and leads to neuronal swelling and dendritic distortion [14]. Glutamate is also highly cytotoxic and can directly result in neurotoxicity when it overcomes the ability of transporters that would normally maintain safe levels in the ECF [15]. Excessive levels of glutamate will also open the gates of Ca^{2+} ion channels, leading to an influx of calcium ions that results in apoptosis [16, 17]. Additionally, excess levels of glutamate will result in mitochondrial dysfunction, which will produce the RNOS superoxide and lead to oxidative stress.

This pathophysiological pathway is collectively referred to as excitotoxicity due to the fact it is associated with excitatory neurotransmitters. Glutamate is not the only EAA that has proven to be highly deleterious in regards to secondary damage following a TBI [18, 19]. A simplified schematic of the mechanisms of EAA-driven damage in a neuron cell following TBI are shown in Figure 4.3. There has been a large degree of interest in being able to monitor these compounds *in vivo* using microdialysis sampling to assist medical professionals in determining the timing of secondary damage following a severe TBI.

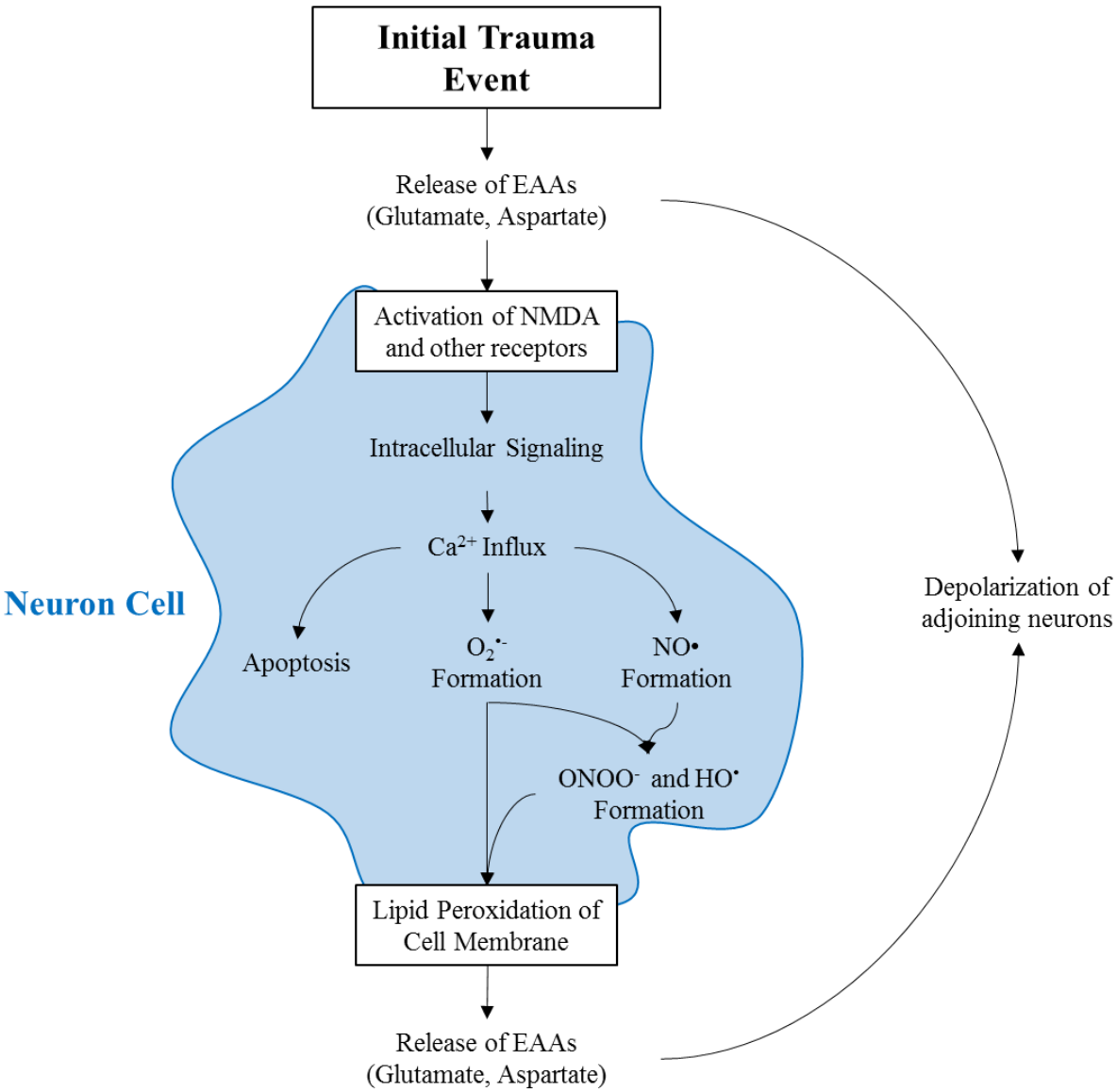

Figure 4.3: EAA-driven secondary damage following a TBI

4.1.3. Limitations of Biosensors for EAA Detection

Using biosensors for the detection of glutamate is by no means novel and has previously been previously reviewed [20]. Biosensors possess a biorecognition element that can generate electroactive species from glutamate to allow amperometric detection. Two enzymes used for this purpose are glutamate oxidase [21] and glutamate dehydrogenase [22]. In the former's case, the enzyme catalyzes a one-step redox reaction to consume O_2 and produce H_2O_2, either of which can then be directly detected on the electrode. These biosensors demonstrate excellent spatial resolution (10 – 20 µm) [20], but their design does not allow for the detection of multiple analytes simultaneously. Measuring the concentration of multiple amino acids in the brain would therefore require multiple sensors, complicating the overall system. Although electrochemical sensors for glutamate have been studied the most extensively, a biosensor for aspartate that uses aspartate aminotransferase as the biorecognition agent has also been reported in the literature [23].

4.1.4. Microdialysis Sampling

Microdialysis (MD) is a diffusion-based technique that allows for continuous sampling of an *in vivo* environment. A MD probe with a semi-permeable membrane is surgically implanted in the tissue of choice. A solution matching the *in vivo* environment, known as the perfusate, is flowed through the probe at low flow rates. Any analyte below the molecular weight cut-off (MWCO) of the semi-permeable membrane will diffuse across it and be collected in the final solution, which is referred to as the dialysate, as shown in Figure 4.4 [24]. This provides a continuous sampling technique that is clean of macromolecules (such as proteins) that might otherwise complicate analysis. The extraction efficiency of the analytes is directly dependent on the flow rate of the perfusate (with lower flow rates resulting in higher concentrations), as shown in Figure 4.5.

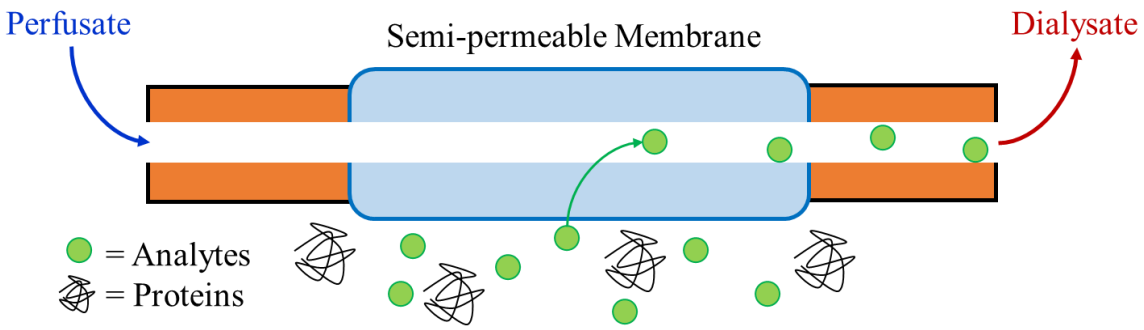

Figure 4.4: Schematic of a linear microdialysis probe

In this design, a semi-permeable membrane (PAN) attaches two lengths of polyimide tubing. Analytes below the molecular weight cut-off (MWCO) of PAN can diffuse across the membrane to be collected in the dialysate. The length of the membrane can be modified depending on the tissue site of interest and surgical requirements.

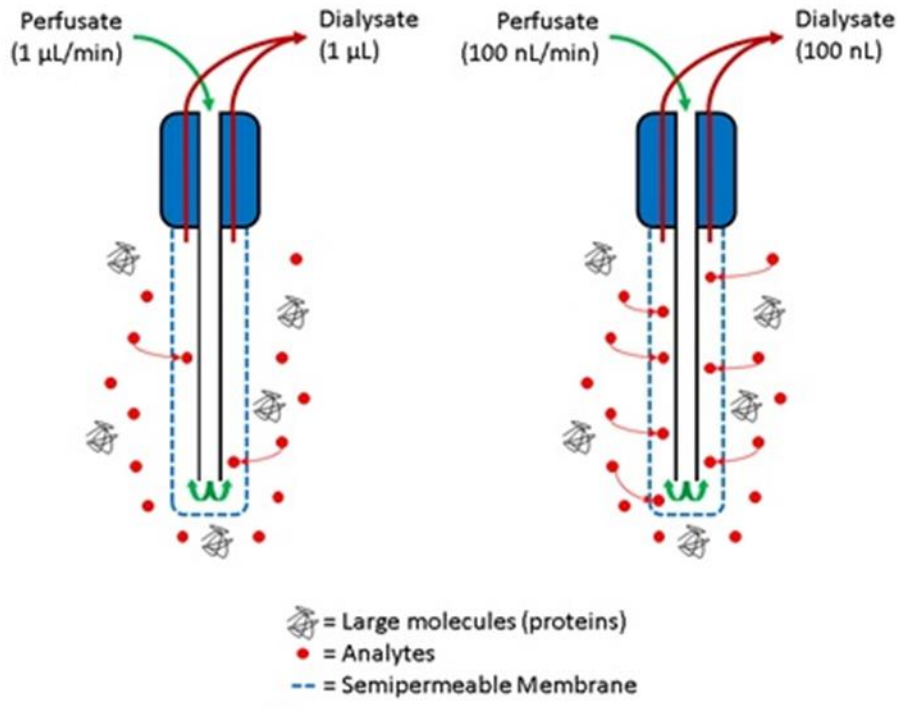

Figure 4.5: Dependency of MD extraction efficiency on flow rate

The extraction efficiency of analytes through a microdialysis probe is directly dependent on the flow rate of the perfusate, which impacts the sample volume collected. For the setup on the left, the perfusate is at a flow rate of 1 µL/min, which allows for a large volume of sample to be collected; however, a lower amount of analyte will diffuses across the membrane. For the setup on the right, higher concentrations of analyte are collected, but in a much smaller sample volume over the same time period due to the lower flow rate (100 nL/min).

Techniques that require larger sample volumes will either impact the extraction efficiency or temporal resolution of MD sampling. The extraction efficiency (EE) of an analyte across the membrane can be determined by Equation 5 [25, 26]:

$$EE = \frac{C_p - C_d}{C_p - C_s} \qquad (5)$$

Here, C_s is the concentration in the sample (brain ECF), C_p is the concentration in the perfusate, and C_d is the concentration in the final dialysate. In experiments where the analyte is not incorporated in the perfusate, the C_p value is zero, while the goal is to determine C_s. This simplifies the equation and allows for the experimental determination of the overall relative recovery (RR) of the analyte, as shown in Equation 6 [25]:

$$RR = \frac{C_d}{C_s} \times 100 \qquad (6)$$

As previously mentioned, MD sampling is often used to monitor the health of patients following a severe TBI in a medical setting [8]. Since these patients already require a section of their skull to be removed to relieve intracranial pressure, a MD probe can be surgically implanted in the brain tissue during the operation.

4.1.5. Monitoring Biomarkers of TBI with Microdialysis

The limitations of EAA biosensors has led to the development of several other methods to detect small molecules indicative of brain health and damage. Research by Martin Boutelle and colleagues has been instrumental in this field and they have used a wide range of equipment to monitor human patients after undergoing a decompressive craniectomy. They have incorporated strip electrodes to measure electrical activity and track spreading depolarizations [27], as well as developing microfluidic chambers that allow the detection of glucose, lactate, and potassium ions within a microdialysis sample using microelectrodes [28, 29]. These are all important markers of brain health that provide medical personnel with important information about the patient. In

combination with monitoring blood flow, they were able to combine this information in order to measure a chemical signature of spreading depolarizations *in vivo* [29]. However, their work has not yet focused on the detection of EAAs using these techniques.

Microchip electrophoresis (ME) was previously discussed in Chapter 1 and has been used extensively for the detection of amino acids, usually with fluorescence detection. Some examples of common fluorescent reagents used for this purpose were shown in Table 1.2. Some of the earliest studies using ME for the detection of amino acids reported separations that occurred within 15 seconds and boasted improved limits of detection due to sample stacking [30]. Additional studies using indirect fluorescence allowed for the separation of nineteen amino acids within two minutes [31]. Both of these studies were *in vitro* and were not focused towards working with biological sampling methods.

Microdialysis sampling (MD) coupled to microchip electrophoresis has recently grown as a subject of interest for analyses such as this, combining the continuous sampling of MD with the fast separations and small solvent requirements of ME, as has recently been reviewed in the literature [32]. The small sample size necessitated by the concentration-driven diffusion of the analytes in MD sampling is not a limitation for ME, which injects much smaller sample volumes than techniques like liquid chromatography [32]. Companies such as CMA Microdialysis produce standardized MD probes, syringe pumps, tubing, and other equipment for use by researchers and medical professionals.

Robert Kennedy published work using OPA and NDA derivatization (see Table 1.2 and Figure 1.5), along with various MD-ME designs, in order to track the change of glutamate and aspartate *in vivo* following the introduction of a glutamate transport inhibitor [33, 34]. Additional studies by our group led to the development of a MD-ME system that allowed continuous, *in vivo*

monitoring with microdialysis sampling using NDA [35]. The design of the microchip geometry was further improved to improve the on-line derivatization reaction and achieve better limits of detection [36].

4.2. Methods

4.2.1. Materials and Reagents

Sodium cyanide (NaCN), acetone, isopropyl alcohol, polyethylene tubing (I.D. 0.39 mm, O.D. 1.09 mm) and parafilm were all purchased from Fisher (Waltham, MA). SU-8 photoresist and developer were purchased from Microchem Corp (Flanders, MA). Sodium chloride (NaCl), potassium chloride (KCl), calcium chloride ($CaCl_2$), magnesium chloride ($MgCl_2$), sodium phosphate dibasic anhydrous (Na_2HPO_4), sodium phosphate monobasic ($Na_2H_2PO_4$), glutamate, aspartate, and *L*-cysteic acid were purchased from Sigma-Aldrich (St. Lous, MO). Silicone wafers (100-mm thickness) were obtained from University Wafer (Boston, MA). Sylgard^{TM} Silicone Elastomer Base and Curing Agent were both purchased from Dow Corning (Auburn, MI). A syringe pump designed for microdialysis (Model CMA 100) and appropriately sized syringes were obtained from CMA Microdialysis (Holliston, MA). Various port connecters with low dead volumes were obtained from Labsmith (Livermore, CA).

4.2.2. Fabrication of PDMS-Glass Microfluidic Devices

Microfluidic devices constructed using polymeric substrates have grown popular due to their shorter fabrication times compared to the all-glass devices described in Chapter 3, which makes them better suited for prototyping or other studies were rapid throughput is necessary. Polydimethylsiloxane (PDMS) is by far the most common polymer used due to its elastomeric properties, optical transparency, and low cost [37]. Combining the benefits of fabricating microchannels in PDMS with the rigidity and reproducibility of a glass substrate has led to the use

of hybrid devices using both materials [38]. This fabrication process still requires a clean room facility and the specialized equipment listed in Chapter 3 for glass-glass microchip fabrication, along with a Cee 200CBX Spin Coater (Brewer Science, Rolla, MO).

A schematic showing the fabrication microfluidic channels in PDMS is shown in Figure 4.6. Briefly, a silicon wafer is spin-coated with negative photoresist (such as SU-8) at the desired thickness. A photomask with the desired channel geometries is aligned on the wafer and exposed to UV light. This will cause the photoresist to polymerize. Unexposed photoresist can be removed with developer, at which point the wafer is baked to harden the remaining microfeatures. This silicon wafer can now be used to create multiple PDMS devices by pouring on elastomer and curing agent and allowing it to cure for at least two hours. After curing the PDMS can be peeled off of the master when needed and can be reversibly or irreversibly bound to another substrate to create the complete device. When coupling with MD, which includes a pressure-driven flow, it is necessary to irreversibly bind the PDMS to avoid delamination [32]. This is done by oxidizing the PDMS surface with a handheld plasma oxidizer and firmly pressing it to the substrate [37, 39]. This fabrication process is explained in further detail in Appendix 2.

4.2.3. NDA/CN Derivatization and Internal Standard Selection

The NDA/CN derivatization reaction was previously discussed in Chapters 1 and 3. Naphthalene-2,3-dicarboxaldehyde (NDA) is a fluorgenic reagent designed for derivatizing primary amines, such as EAAs, to form highly-fluorescent CBI derivatives, as shown in Figure 1.5 [40].

Due to the fact this will be an online device, it was desired that the derivatization reaction would also occur on-line, as has previously been accomplished [36]. In order to guarantee that the

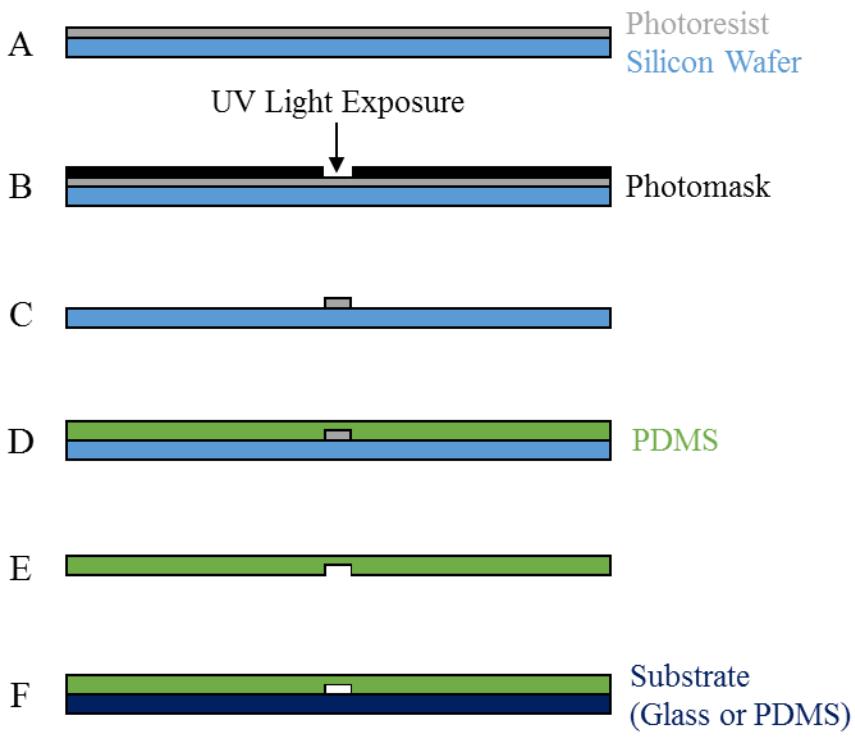

Figure 4.6: Schematic of polymer-glass microfluidic device construction

(A) Spin coat a substrate, such as a silicon wafer, with negative photoresist; (B) Align photomask on coated substrate and expose to UV light; (C) Remove photomask and soak in developer to remove non-polymerized photoresist to create the master, then confirm channel dimensions with profilometer; (D) Pour PDMS and elastomer at desired ratio on master, then cure for at least two hours; (E) Peel off PDMS with microchannels intact; (F) Reversibly or irreversibly bond PDMS to desired substrate to form complete device.

reaction was proceeding, an internal standard was incorporated into the derivatization reaction. L-cysteic acid has long been used as an internal standard for amino acid analysis [41] and has been previously shown to have no role in the biochemistry of NMDA-receptors [42]. It is structurally similar to the EAAs of interest (as shown in Figure 4.7), which should result in similar separation efficiencies and quantum yield, yet was not detected in brain microdialysis samples using an analytical method with a LOD of 356 pM [43]. Its low endogenous concentrations and similarity to the analytes of interest makes it a suitable internal standard for this study.

NDA was prepared at a concentration of 5 mM in ACN. NaCN was prepared at a concentration of 20 mM in BGE. L-cysteic acid was then prepared in the NaCN solution at a concentration of 75 µM in the NaCN solution. When combined in a 1:1:1 flow rate with NDA and the MD flow, this should result in a final derivatized concentration of 25 µM for L-cysteic acid.

4.2.4. Linear MD Probe Fabrication

Although the eventual goal of this system is to use intracranial microdialysis probes, these probe designs result in higher backpressures. For this reason, a linear microdialysis probe was fabricated and used for these *in vitro* studies, as was shown in Figure 4.4. Polyacrylonitrile (PAN) membrane with a MWCO of 20 kDa from Hospal (Lakewood, CA) was used as the semi-permeable membrane. This membrane had an outer dimension (OD) of 350 µm and an inner dimension (ID) of 260 µm. The membrane was attached with UV glue to two lengths of polyimide tubing (160 µm OD, 120 µm ID). The probe window was 10 mm long.

Since MD sampling is based on diffusion, the perfusate solution needs to mimic the extracellular fluid as closely as possible. Artificial cerebrospinal fluid (aCSF) has been developed in order to simulate the environment within the brain. The composition of aCSF used in these

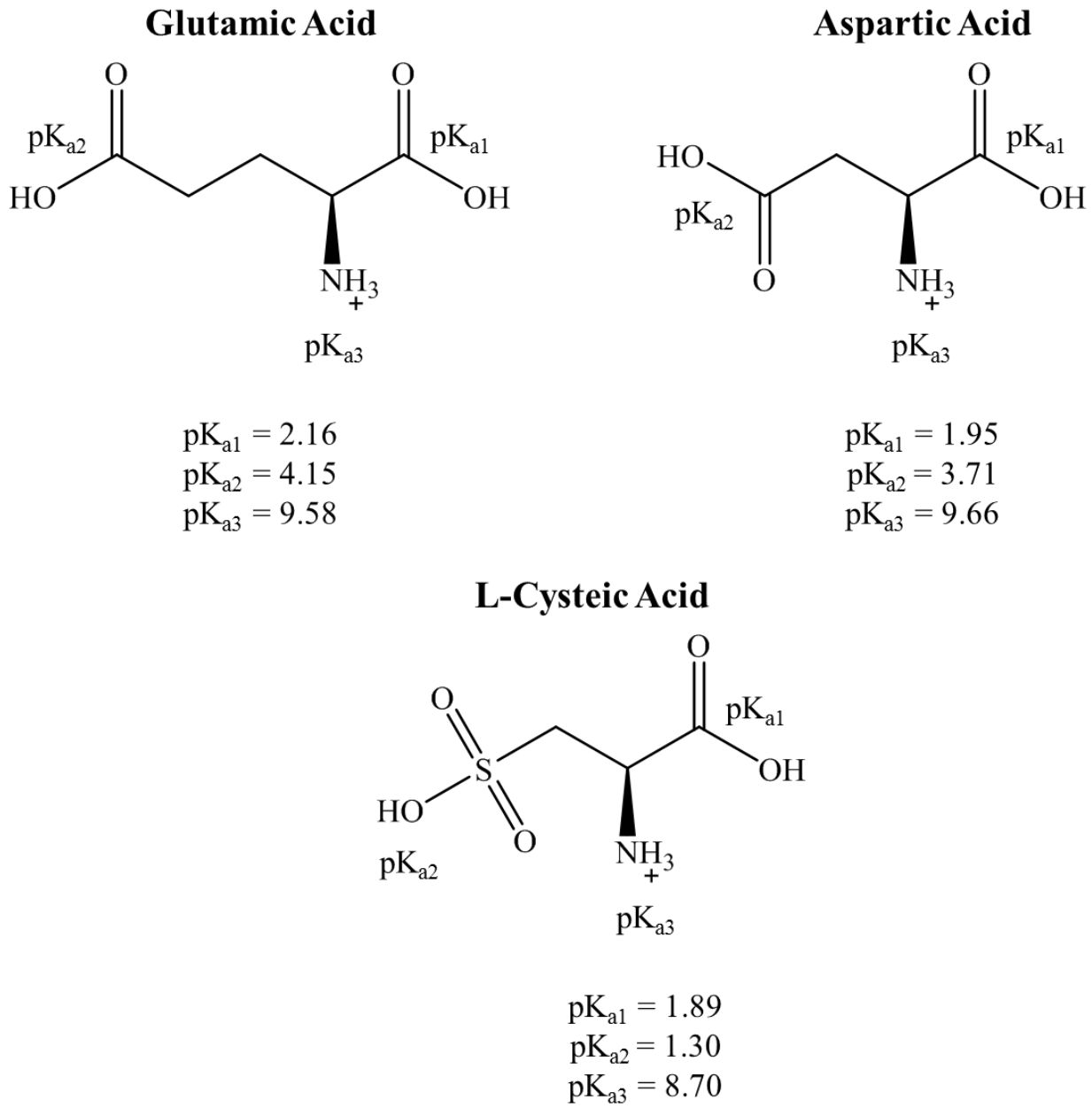

Figure 4.7: Chemical structures of glutamic acid, aspartic acid, and cysteic acid

At physiological pH (7.4), glutamic acid and aspartic acid are have a net charge of -1 and function as EAA neurotransmitters. The similarities in their size/structure (i.e. hydrodynamic radius) and charge states makes L-cysteic acid a good internal standard candidate [41].

studies was 125 mM NaCl, 2.7 mM KCl, 1.2 mM $CaCl_2$, 1 mM $MgCl_2$, 2.3 mM Na_2HPO_4, and 0.45 mM $Na_2H_2PO_4$, prepared in H_2O.

4.2.5. Microchip Electrophoresis with Laser Excitation Source

These experiments were performed using a double-T microchip design with a 15-cm separation channel. This particular design has a wider inlet channel to accommodate the pressure-driven flow coming from the MD probe and syringe pump. This channel was connected to the MD tubing via a steel pin pushed through the PDMS to reach the inlet. Prior to use the microchip was conditioned with 0.1 M NaOH and deionized H_2O before being filled with BGE via the application of a negative pressure using a vacuum system. After piercing the PDMS with the steel pin, BGE was also pushed through the inlet with a syringe to fully fill the inlet channel and guarantee that no de-lamination occurred.

The setup of the high voltage power supplies, benchtop laser system, and data acquisition were previously described in Chapter 3. The BGE and voltages applied for the separation were experimentally determined and are discussed later. An electrokinetic injection was accomplished by floating the separation voltage for 0.5 s to produce a sample plug, as previously shown in Figure 1.9.

4.3. Discussion

4.3.1. Online MD-ME System Design

The syringe pump was set up with three syringes connected with polyethylene tubing. The first syringe contained the NDA solution, while the second contained the NaCN solution with the internal standard. These two syringes were connected directly to a low-volume mixing tee by 5 cm of tubing. The third syringe contained the perfusate, which was aCSF. This flowed straight into

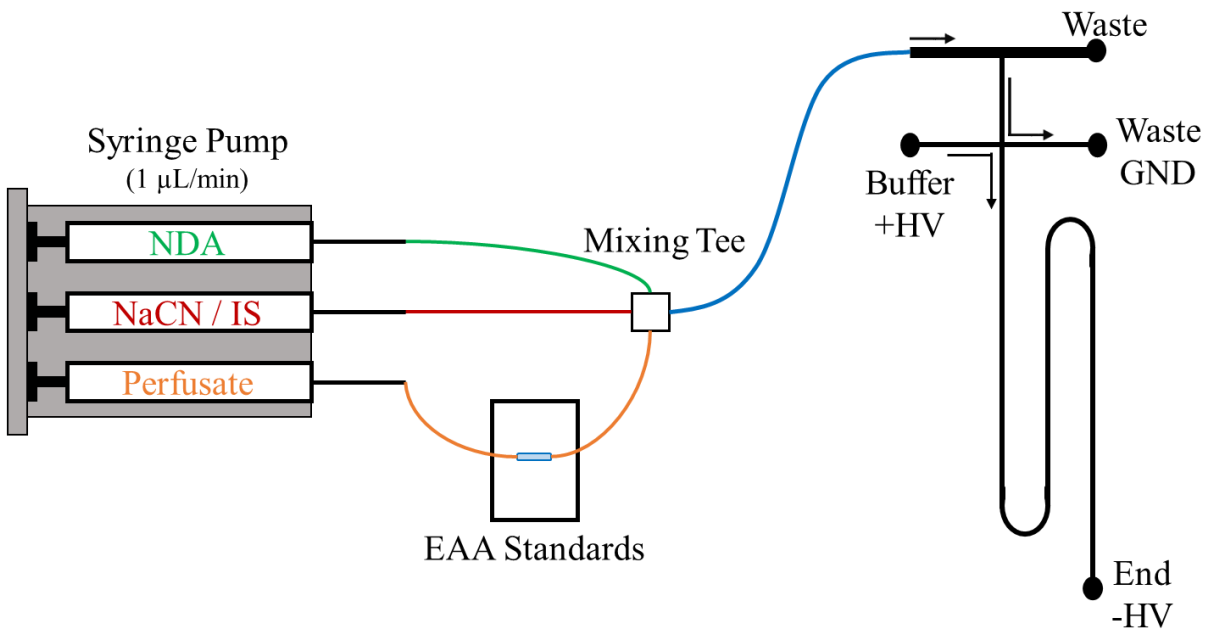

Figure 4.8: Schematic of total MD-ME analysis device

the fabricated linear MD probe with PAN membrane before being connected to the same mixing tee. The output from the mixing tee was then connected to the MD inlet on the PDMS-glass hybrid microchip, as shown in Figure 4.8.

4.3.2. ME Separation of EAAs with Offline Derivatization

The ME separation conditions were optimized using an *in vitro* setup in which a mix of the EAAs and internal standard were derivatized off-line, then placed in a syringe and flowed through the microdialysis inlet on the microfluidic device. In order to guarantee full derivatization, this reaction was allowed to proceed for 45 minutes in the dark before the CBI products were placed in the syringe. This eliminated any issues stemming from the incomplete reaction that would lower the signal response and complicate the analysis. As borate buffers have been extensively used for EAA analysis in the past [35, 36, 44, 45], it was decided that such a buffer would be well-suited for this system.

BGE was prepared by making boric acid ($pK_a = 9.24$) solutions at three concentrations (20, 50, and 80 mM) and adjusting the pH to 9.2 using 0.1 M NaOH in order to generate a buffer. As electrophoretic separations are also highly dependent on the applied voltages and corresponding field strengths (as discussed in Chapter 1), high- and low-field strength conditions were examined. The results of these experiments are shown in Figure 4.9. It was determined that a BGE of 50 mM borate (at pH 9.2) and a field strength of 224 V/cm provided ample resolution between the two EAAs of interest and the internal standard.

4.3.3. EAA Separation with MD Sampling and On-line Derivatization

After optimizing the separation conditions, two of the syringes were filled with the derivatization solutions as previously described. Fluid from the third syringe flowed through the

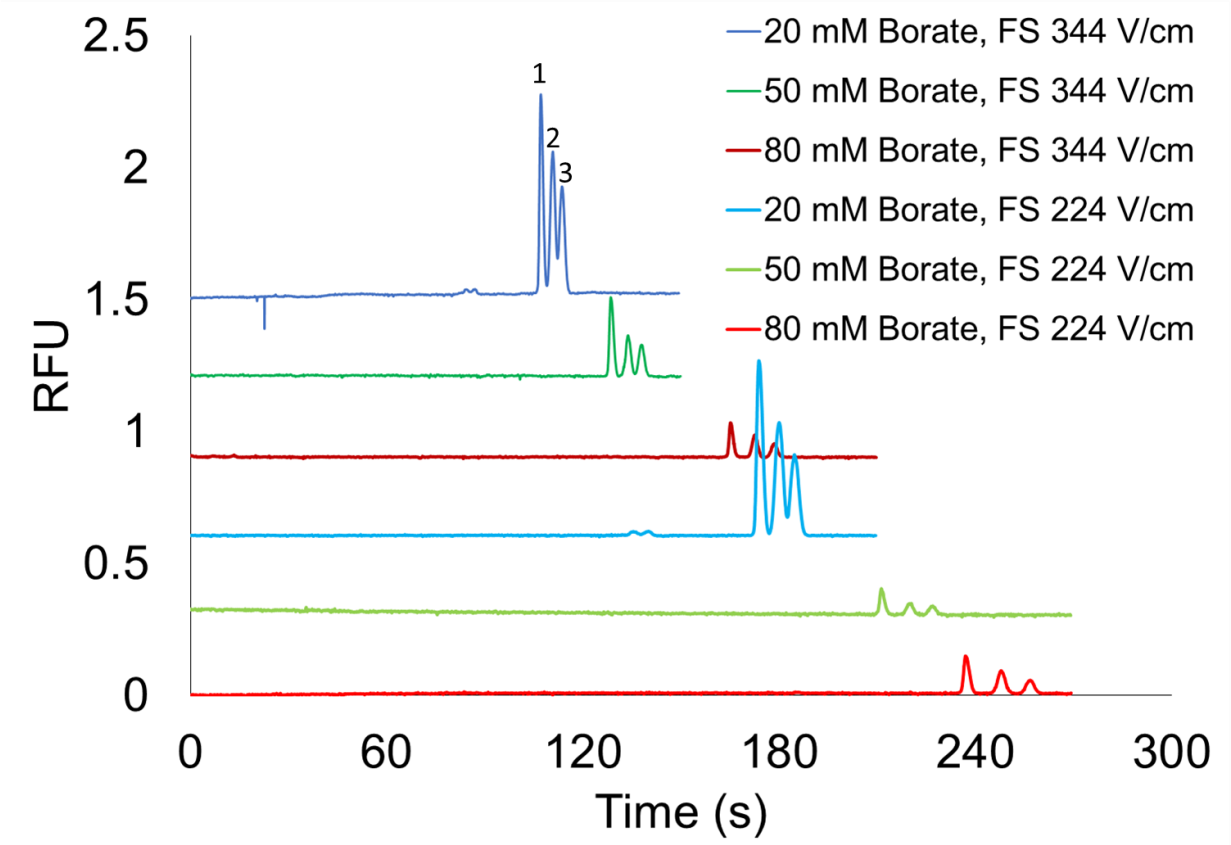

Figure 4.9: Optimization of MD-ME separation using offline derivatization

The final conditions were a BGE consisting of 50 mM borate (pH 9.2) and a field strength of 344 V/cm. (1) glutamate; (2) aspartate; (3) L-cysteic acid. This was the fastest separation in which all three of the analytes were fully resolved.

linear MD probe, which was placed in a solution containing glutamate and aspartate at a concentration of 200 µM in aCSF. The syringe pump was used to push solutions at 1 µL/min through each syringe. The length of tubing where the derivatization occurred (at a combined flow rate of 3 µL/min) was 10 cm long (internal volume of approximately 16 µL), resulting in a derivatization time of approximately five minutes before reaching the inlet channel. The overall lag time from the MD probe suspended in the EAA solution to the inlet was approximately 12 minutes (including the derivatization time), although this could be lowered by increasing the flow rate of the syringe pump.

The on-line derivatization system was run for over 30 minutes, over which time the background current remained stable. Although no peak for the EAAs was originally present, the internal standard was clearly visible from the first injection at a time of 86 s, suggesting that the derivatization reaction was proceeding correctly. Over the course of the experiment, small peaks that co-migrated with glutamate and aspartate developed within individual injections (as shown in Figure 4.10). Unfortunately, they were never detected above the LOD of the system, with a signal-to-noise ratio (S/N) of approximately 2.

This suggests that the on-line derivatization setup is viable, but further optimization would be necessary before it could be used *in vivo*. This is especially true because the *in vivo* concentrations of EAAs in the brain are much lower than in this i*n vitro* experiment (as low as 0.28 µM for basal glutamate) [46].

It was hypothesized that the difference in the height of the internal standard peak compared to that of the analytes was due to their diffusion across the MD membrane. Previous work has found that the polymer used to fabricate a MD probe can have large effects on the diffusion of

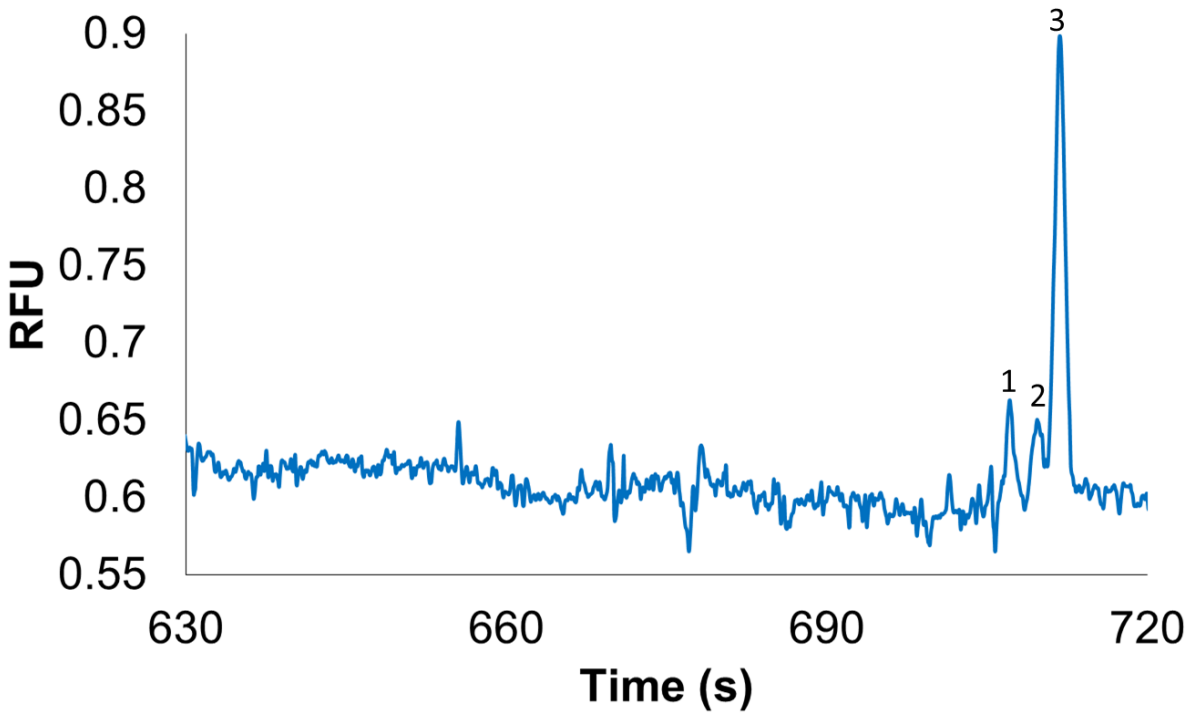

Figure 4.10: Final separation on MD-ME system with on-line derivatization

Although glutamate (1) and aspartate (3) peaks are present in the correct migration order before the internal standard peak (3), they are below the LOD of the system, with an S/N of approximately 2.

analytes across it (beyond its MWCO value) [47]. The extraction efficiency and relative recovery of these EAAs across the PAN membrane was not experimentally determined, but it is possible that other commercially-available membrane materials such as poly(ether) sulfone, polycarbonate, or cuprophan could provide for better analyte recovery. When moving to *in vivo* experiments, the biofouling of the membrane from tissue effects will also need to be considered and evaluated [48].

4.4. Conclusion

A microdialysis-microchip electrophoresis system with on-line derivatization was developed and optimized for the sepration and detection of excitatory amino acids following a traumatic brain injury. The EAAs were derivatized via the NDA/CN reaction. L-cysteic acid functioned as an internal standard and guaranteed that there were no mechanical issues in the overall system. There was a lag time of approximately 12 minutes between the MD probe and the electrokinetic injection onto the ME system, which included the on-line derivatization reaction. Although the presence of a reproducible internal standard peak demonstrated that the overall system was functional *in vitro*, it did not possess sufficient LODs for *in vivo* analysis due to the chosen MD membrane material.

4.5. References

1. C. R. Summers, B. Ivins and K. A. Schwab. Traumatic brain injury in the United States: an epidemiologic overview. *Mt. Sinai J. Med.,* **2009,** *76* (2), 105-110.

2. E. Zaloshnja, T. Miller, J. A. Langlois and A. W. Selassie. Prevalence of long-term disability from traumatic brain injury in the civilian population of the United States, 2005. *J. Head Trauma Rehabil.,* **2008,** *23* (6), 394-400.

3. M. W. Greve and B. J. Zink. Pathophysiology of traumatic brain injury. *Mt. Sinai J. Med.,* **2009,** *76* (2), 97-104.

4. J. D. Cassidy, L. J. Carroll, P. M. Peloso, J. Borg, H. von Holst, L. Holm, J. Kraus, V. G. Coronado and W. H. O. C. C. T. F. o. M. T. B. Injury. Incidence, risk factors and prevention of mild traumatic brain injury: results of the WHO Collaborating Centre Task Force on Mild Traumatic Brain Injury. *J. Rehabil. Med.,* **2004,** (43 Suppl), 28-60.

5. G. Teasdale and B. Jennett. Assessment of coma and impaired consciousness. A practical scale. *Lancet,* **1974,** *2* (7872), 81-84.

6. B. Singh, M. H. Murad, L. J. Prokop, P. J. Erwin, Z. Wang, S. K. Mommer, S. S. Mascarenhas and A. K. Parsaik. Meta-analysis of Glasgow coma scale and simplified motor score in predicting traumatic brain injury outcomes. *Brain Inj.,* **2013,** *27* (3), 293-300.

7. J. Sahuquillo and F. Arikan. Decompressive craniectomy for the treatment of refractory high intracranial pressure in traumatic brain injury. *Cochrane Database Syst. Rev.,* **2006,** (1), CD003983.

8. E. P. Thelin, K. L. Carpenter, P. J. Hutchinson and A. Helmy. Microdialysis Monitoring in Clinical Traumatic Brain Injury and Its Role in Neuroprotective Drug Development. *AAPS J.,* **2017,** *19* (2), 367-376.

9. A. I. Maas, N. Stocchetti and R. Bullock. Moderate and severe traumatic brain injury in adults. *Lancet Neurol.,* **2008,** *7* (8), 728-741.

10. B. J. Zink. Traumatic brain injury outcome: Concepts for emergency care. *Ann. Emergency Med.,* **2001,** *37* (3), 318-332.

11. M. C. Morganti-Kossmann, M. Rancan, P. F. Stahel and T. Kossmann. Inflammatory response in acute traumatic brain injury: a double-edged sword. *Curr. Opin. Crit. Care,* **2002,** *8* (2), 101-105.

12. S. Toulmond and N. J. Rothwell. Interleukin-1 receptor antagonist inhibits neuronal damage caused by fluid percussion injury in the rat. *Brain Res.,* **1995,** *671* (2), 261-266.

13. A. Lewen, P. Matz and P. H. Chan. Free radical pathways in CNS injury. *J. Neurotrauma,* **2000,** *17* (10), 871-890.

14. J. P. Dreier. The role of spreading depression, spreading depolarization and spreading ischemia in neurological disease. *Nat. Med.,* **2011,** *17* (4), 439-447.

15. N. C. Danbolt. Glutamate uptake. *Prog. Neurobiol.,* **2001,** *65* (1), 1-105.

16. M. Arundine and M. Tymianski. Molecular mechanisms of calcium-dependent neurodegeneration in excitotoxicity. *Cell Calcium,* **2003,** *34* (4-5), 325-337.

17. R. Sattler and M. Tymianski. Molecular mechanisms of calcium-dependent excitotoxicity. *J. Mol. Med. (Berl.),* **2000,** *78* (1), 3-13.

18. T. P. Obrenovitch and J. Urenjak. Is high extracellular glutamate the key to excitotoxicity in traumatic brain injury? *J. Neurotrauma,* **1997,** *14* (10), 677-698.

19. K. D. Sims and M. B. Robinson. Expression patterns and regulation of glutamate transporters in the developing and adult nervous system. *Crit. Rev. Neurobiol.,* **1999,** *13* (2), 169-197.

20. S. Qin, M. van der Zeyden, W. H. Oldenziel, T. I. F. H. Cremers and B. H. C. Westerink. Microsensors for in vivo Measurement of Glutamate in Brain Tissue. *Sensors,* **2008,** *8* (11), 6860-6884.

21. O. Soldatkin, A. Nazarova, N. Krisanova, C. A. Borsmall u, D. Kucherenko, I. Kucherenko, N. Pozdnyakova, A. Soldatkin and T. Borisova. Monitoring of the velocity of high-affinity glutamate uptake by isolated brain nerve terminals using amperometric glutamate biosensor. *Talanta,* **2015,** *135*, 67-74.

22. M. Zhang and L. Mao. Enzyme-based amperometric biosensors for continuous and on-line monitoring of cerebral extracellular microdialysate. *Front. Biosci.,* **2005,** *10,* 345-352.

23. G. Palleschi, M. G. Lavagnini, D. Compagnone, P. Bertocchi and D. Moscone. Flow Monitoring of Glutamate and Aspartate in Foods and Pharmaceutical Products with Immobilized Bienzyme Electrochemical-Cells. *Electroanalysis,* **1992,** *4* (9), 851-857.

24. W. F. Elmquist and R. J. Sawchuk. Application of microdialysis in pharmacokinetic studies. *Pharm. Res.,* **1997,** *14* (3), 267-288.

25. K. C. Chen, M. Hoistad, J. Kehr, K. Fuxe and C. Nicholson. Theory relating in vitro and in vivo microdialysis with one or two probes. *J. Neurochem.,* **2002,** *81* (1), 108-121.

26. J. A. Stenken, C. E. Lunte, M. Z. Southard and L. Stahle. Factors that influence microdialysis recovery. Comparison of experimental and theoretical microdialysis recoveries in rat liver. *J. Pharm. Sci.,* **1997,** *86* (8), 958-966.

27. K. I. Papadimitriou, C. Wang, M. L. Rogers, S. A. N. Gowers, C. L. Leong, M. G. Boutelle and E. M. Drakakis. High-Performance Bioinstrumentation for Real-Time Neuroelectrochemical Traumatic Brain Injury Monitoring. *Front. Hum. Neurosci.,* **2016,** *10*.

28. M. Rogers, C. Leong, X. Z. Niu, A. de Mello, K. H. Parker and M. G. Boutelle. Optimisation of a microfluidic analysis chamber for the placement of microelectrodes. *PCCP,* **2011,** *13* (12), 5298-5303.

29. M. L. Rogers, D. Feuerstein, C. L. Leong, M. Takagaki, X. Z. Niu, R. Graf and M. G. Boutelle. Continuous Online Microdialysis Using Microfluidic Sensors: Dynamic Neurometabolic Changes during Spreading Depolarization. *ACS Chem. Neurosci.,* **2013,** *4* (5), 799-807.

30. S. C. Jacobson and J. M. Ramsey. Microchip Electrophoresis with Sample Stacking. *Electrophoresis,* **1995,** *16* (4), 481-486.

31. N. J. Munro, Z. L. Huang, D. N. Finegold and J. P. Landers. Indirect fluorescence detection of amino acids on electrophoretic microchips. *Anal. Chem.,* **2000,** *72* (13), 2765-2773.

32. R. A. Saylor and S. M. Lunte. A review of microdialysis coupled to microchip electrophoresis for monitoring biological events. *J. Chromatogr. A,* **2015,** *1382,* 48-64.

33. Z. D. Sandlin, M. S. Shou, J. G. Shackman and R. T. Kennedy. Microfluidic electrophoresis chip coupled to microdialysis for in vivo monitoring of amino acid neurotransmitters. *Anal. Chem.,* **2005,** *77* (23), 7702-7708.

34. M. Wang, G. T. Roman, M. L. Perry and R. T. Kennedy. Microfluidic Chip for High Efficiency Electrophoretic Analysis of Segmented Flow from a Microdialysis Probe and in Vivo Chemical Monitoring. *Anal. Chem.,* **2009,** *81* (21), 9072-9078.

35. P. Nandi, D. P. Desai and S. M. Lunte. Development of a PDMS-based microchip electrophoresis device for continuous online in vivo monitoring of microdialysis samples. *Electrophoresis,* **2010,** *31* (8), 1414-1422.

36. P. Nandi, D. E. Scott, D. Desai and S. M. Lunte. Development and optimization of an integrated PDMS based-microdialysis microchip electrophoresis device with on-chip

derivatization for continuous monitoring of primary amines. *Electrophoresis,* **2013,** *34* (6), 895-902.

37. D. C. Duffy, J. C. McDonald, O. J. A. Schueller and G. M. Whitesides. Rapid prototyping of microfluidic systems in poly(dimethylsiloxane). *Anal. Chem.,* **1998,** *70* (23), 4974-4984.

38. B. H. Huynh, B. A. Fogarty, P. Nandi and S. M. Lunte. A microchip electrophoresis device with on-line microdialysis sampling and on-chip sample derivatization by naphthalene 2,3-dicarboxaldehyde/2-mercaptoethanol for amino acid and peptide analysis. *J. Pharm. Biomed. Anal.,* **2006,** *42* (5), 529-534.

39. W. K. T. Coltro, S. M. Lunte and E. Carrilho. Comparison of the analytical performance of electrophoresis microchannels fabricated in PDMS, glass, and polyester-toner. *Electrophoresis,* **2008,** *29* (24), 4928-4937.

40. P. S. De Montigny, John F.; Givens, Richard S.; Carlson, Robert G.; Srinivasachar, Kasturi; Sternson, Larry A.; Higuchi, Takeru. Naphthalene-2,3-dicarboxyaldehyde/cyanide ion: a rationally designed fluorogenic reagent for primary amines. *Anal. Chem.,* **1987,** *59* (8), 1096-1101.

41. A. Wainer and J. S. King. Use of Cysteic Acid as an Internal Standard in Amino Acid Analysis. *J. Chromatogr.,* **1965,** *20* (1), 143-&.

42. D. K. Patneau and M. L. Mayer. Structure-activity relationships for amino acid transmitter candidates acting at N-methyl-D-aspartate and quisqualate receptors. *J. Neurosci.,* **1990,** *10* (7), 2385-2399.

43. O. Orwar, M. Sandberg, I. Jacobson, M. Sundahl and S. Folestad. Photochemical Characterization and Optimization of Argon Ion Laser-Induced Fluorescence Detection of O-Phthalaldehyde Beta-Mercaptoethanol-Labeled Amino-Acids and Gamma-Glutamyl Peptides in

Liquid-Chromatography - Ultratrace Analysis with Neurobiological Samples. *Anal. Chem.,* **1994,** *66* (24), 4471-4482.

44. Z. D. Sandlin, M. Shou, J. G. Shackman and R. T. Kennedy. Microfluidic electrophoresis chip coupled to microdialysis for in vivo monitoring of amino acid neurotransmitters. *Anal. Chem.,* **2005,** *77* (23), 7702-7708.

45. M. Wang, G. T. Roman, M. L. Perry and R. T. Kennedy. Microfluidic chip for high efficiency electrophoretic analysis of segmented flow from a microdialysis probe and in vivo chemical monitoring. *Anal. Chem.,* **2009,** *81* (21), 9072-9078.

46. M. Shiraishi, Y. Kamiyama, P. C. Huttemeier and H. Benveniste. Extracellular glutamate and dopamine measured by microdialysis in the rat striatum during blockade of synaptic transmission in anesthetized and awake rats. *Brain Res.,* **1997,** *759* (2), 221-227.

47. K. L. Snyder, C. E. Nathan, A. Yee and J. A. Stenken. Diffusion and calibration properties of microdialysis sampling membranes in biological media. *Analyst*, **2001,** *126* (8), 1261-1268.

48. N. Wisniewski, B. Klitzman, B. Miller and W. M. Reichert. Decreased analyte transport through implanted membranes: Differentiation of biofouling from tissue effects. *J. Biomed. Mater. Res.,* **2001,** *57* (4), 513-521.

Chapter 5:

Conclusions and Future Directions

5.1. Conclusions

In this thesis, the development of analytical methods to fluorescently derivatize and detect small molecule biomarkers that are of pivotal information to epilepsy, the immune response, and traumatic brain injury was described.

A liquid chromatography-fluorescence method was developed that allowed for the detection of three reactive aldehyde biomarkers of lipid peroxidation: 4-hydroxynonenal, malondaldehyde, and acrolein. Previous research has shown that secondary damage following an epileptic seizure can lead to oxidative damage, which should be reflected by a change in concentration of these compounds. This method had sufficient limits of detection (6.1 nM for HNE, 192 nM for MDA, and 2.6 µM for acrolein) to measure all three analytes at endogenous levels in rat urine samples after derivatization with DNSH and pre-concentration using solid phase extraction. When combined with an animal model of epilepsy, acrolein demonstrated a statistically significant increase in the first 12-hour period following the seizure, while 4-HNE had no noticeable change. These aldehydes also displayed a previously unreported circadian cycling according to the light/dark cycle of the animal.

A microchip electrophoresis-fluorescence method was developed in order to detect carnosine in macrophages, the primary cells activated during the immune response. This method yielded a LOD of 65 nM and was linear over three orders of magnitude at physiologically relevant concentrations (50 nM – 50 µM). Native cell lysate was derivatized using the NDA/CN reaction to detect the endogenous level of carnosine, which was found to be 0.079 ± 0.02 nmol per 10^6 cells. The native presence of carnosine in macrophage cells supports its role as an antioxidant. The

uptake of carnosine into macrophages was also examined under normal and pro-oxidative conditions by stimulating the cells with LPS and INF-γ. There was a 2.83 ± 0.29 increase in uptake for the stimulated cells, suggesting that they will actively take up this dipeptide in order to mitigate the damage caused by pro-oxidative inflammation.

A second microchip electrophoresis-fluorescence system was developed to measure excitatory amino acids involved in neuronal damage in traumatic brain injury. The system was designed for used in a medical setting with minimal delay between sampling and analysis. Microdialysis sampling was coupled with on-line derivatization with a lag time of 12 minutes between the microdialysis probe and sample injection. L-cysteic acid was incorporated as an internal standard to guarantee the NDA/CN reaction was functioning and that no issues developed throughout the entire system. Although the overall system functioned for several sequential runs, a lack of response for the EAAs suggests that further optimization of the probe membrane and analyte recovery is necessary before this can be used as a monitoring tool.

5.2. Future Directions

5.2.1. Reactive Aldehyde Biomarkers of Lipid Peroxidation

Although a method was developed to detect reactive aldehydes in urine samples, being able to measure their concentrations in the brain with better temporal resolution would provide more relevant information to develop new therapies for epilepsy. Although brain microdialysis sampling has been used to study various biomarkers of epilepsy, the only reactive aldehyde to receive a strenuous examination using this sampling technique *in vivo* is MDA [1]. Using a similar animal model but studying more biomarkers of lipid peroxidation could provide a better understanding of the exact biomechanisms responsible for damage following an epileptic seizure.

Another benefit of microdialysis sampling when it comes to *in vivo* epilepsy experiments is that it can be used to dose a specific region of the brain with the convulsing agent, producing local seizures [2]. A series of experiments investigating the output of reactive aldehyde species following local seizures could reveal if there is any change in the response depending on the associated region of the brain. Differences in neurochemical concentrations following epileptic-like seizures have been previously reported [3], which was later linked to differences in brain region activity. This suggests that a similar study would prove necessary regarding reactive aldehyde species.

5.2.2. Antioxidant Properties of Carnosine in Macrophages

The exact role of carnosine in the antioxidant defense system has yet to be elucidated, despite the fact it is endogenously present in murine macrophage cells. One way to further explore this would be a more thorough examination of inducible nitric oxide synthase activity in these cells. This enzyme converts arginine to citrulline in order to produce nitric oxide. This means that the ratio of these two amino acids can be used as an indication of iNOS activity [4]. Since they will also be derivatized by the NDA/CN reaction, changing the separation conditions in order to measure them in addition to carnosine could prove information on whether its antioxidant properties come from interfering with the production of $NO^{\bullet}$ by iNOS. Some initial experiments have been done in this direction, with the peaks corresponding to citrulline and arginine identified and their relative signal response evaluated, as shown in Figure 5.1. In the native macrophage lysate, the signal response for citrulline and arginine was nearly equal. However, under pro-inflammatory conditions, it appears as if there is a larger signal response from citrulline than arginine, which corresponds with a higher degree of iNOS activity. Further studies need to be conducted in order to quantitate the difference in the cirtrulline to arginine ratio.

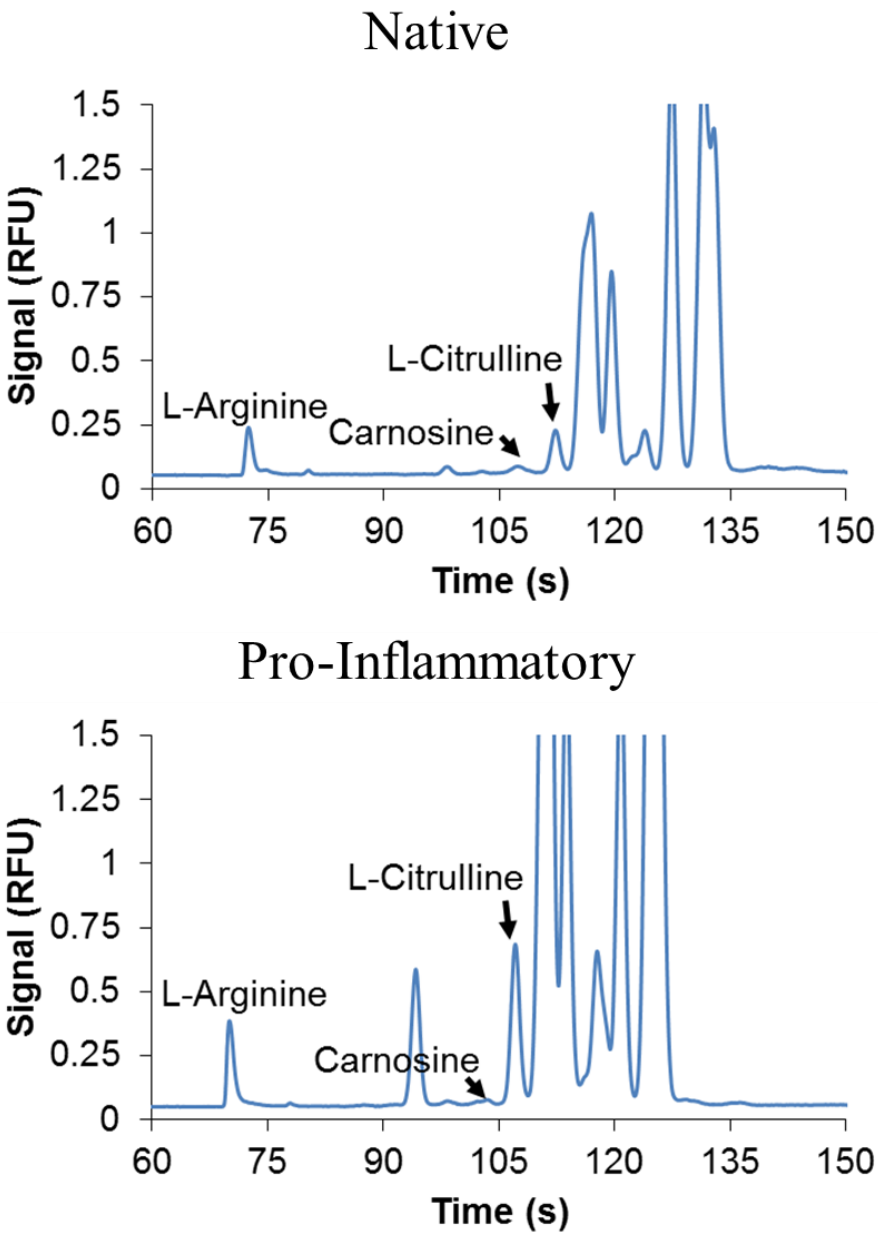

Figure 5.1: Separation showing differences in iNOS activity for activated macrophages

Under native conditions, the ratio of the citrulline to arginine signal response is nearly equal; under pro-inflammatory (i.e. activated) conditions, there appears to be a high amount of citrulline compared to arginine, which would correspond to a larger amount of iNOS activity.

It has long been known that histidine is one of the amino acids with the strongest antioxidant properties [5]. Since this is one of the constituent amino acids of carnosine, it is possible that the antioxidant activity of the dipeptide is simply due to its degradation, resulting in an increased intracellular concentration of histidine. Since the pK_a of histidine's amine moiety is 9.17, it has an overall net charge of approximately -1/2 at the pH of this study's BGE, which resulted in it co-migrating with the neutral amino acids. Changing the buffer conditions to a different pH (such as using phosphate buffer, which has a pK_a of 7.2), would allow for it to be more easily separated with electrophoresis and measured following the uptake of carnosine into macrophage cells.

The amount of damage done to the cell membrane could also influence carnosine permeability. There are several fluorescent dyes that can indicate cell health following M1 activation that would be able to identify if this is the cause of increased uptake.

5.2.3. Excitatory Amino Acids Related to Traumatic Brain Injury

Although these experiments used a benchtop laser system, work has been done in the development of a mobile fluorescence detection platform that couples with microchip devices [6]. This portable system uses a light-emitting diode as an excitation source and reported limits of detection near the physiological ranges of glutamate and aspartate in the extracellular spaces of the brain (1.3 and 1.2 μM, respectively). Combining this portable system with a wholly on-line separation would allow for the overall method to be used in a medical setting.

The current method also used off-chip derivatization, while previous research has been conducted using mixing geometries on-chip in order to increase the reaction rate and reduce any complications from excessive tubing [7]. Although this device was successful, it still struggled to achieve full derivatization using the NDA/CN reaction, which takes upwards of thirty minutes to

reach completion without ample agitation. The degree of mixing can be further improved by optimizing the design of the mixing channels, such as a double helix design that was recently discussed in the literature [8]. In order to maximize the throughput of prototyping new microchannel geometries, it would be preferable to switch to a substrate that could be prepared faster than glass, while providing more reproducible results than PDMS. One such option is cyclic olefin copolymer, which has been extensively used for microchip electrophoresis devices and can be bonded at room temperature [9].

Although a wide range of animal models for TBI exist [10], there has been extensive work done on creating *in vitro* models that limit the number of animals that are exposed to these models, which are violent by necessity. Three-dimensional cell cultures have shown promising results in this regard, with brain-like matrixes already under development that have demonstrated lifelike reactions and damage following a blunt force trauma [11].

5.3. References

1. J. C. Cooley and C. E. Lunte. Detection of malondialdehyde in vivo using microdialysis sampling with CE-fluorescence. *Electrophoresis,* **2011,** *32* (21), 2994-2999.

2. E. W. Crick, I. Osorio, N. C. Bhavaraju, T. H. Linz and C. E. Lunte. An investigation into the pharmacokinetics of 3-mercaptopropionic acid and development of a steady-state chemical seizure model using in vivo microdialysis and electrophysiological monitoring. *Epilepsy Res.,* **2007,** *74* (2-3), 116-125.

3. A. P. Mayer, I. Osorio and C. E. Lunte. Microperfusion of 3-MPA into the brain augments GABA. *Epilepsy Behav.,* **2013,** *29* (3), 478-484.

4. R. Pannu and I. Singh. Pharmacological strategies for the regulation of inducible nitric oxide synthase: neurodegenerative versus neuroprotective mechanisms. *Neurochem. Int.,* **2006,** *49* (2), 170-182.

5. R. Marcuse. Antioxidative effect of amino-acids. *Nature,* **1960,** *186,* 886-887.

6. N. J. Oborny, E. E. M. Costa, L. Suntornsuk, F. C. Abreu and S. M. Lunte. Evaluation of a Portable Microchip Electrophoresis Fluorescence Detection System for the Analysis of Amino Acid Neurotransmitters in Brain Dialysis Samples. *Anal. Sci.,* **2016,** *32* (1), 35-40.

7. P. Nandi, D. E. Scott, D. Desai and S. M. Lunte. Development and optimization of an integrated PDMS based-microdialysis microchip electrophoresis device with on-chip derivatization for continuous monitoring of primary amines. *Electrophoresis,* **2013,** *34* (6), 895-902.

8. X. L. Peng, L. Zhao, J. X. Guo, S. H. Yang, H. Ding, X. Y. Wang and Q. S. Pu. Double-helix micro-channels on microfluidic chips for enhanced continuous on-chip derivatization followed by electrophoretic separation. *Biosens. Bioelectron.,* **2015,** *72,* 376-382.

9. V. Sunkara, D. K. Park, H. Hwang, R. Chantiwas, S. A. Soper and Y. K. Cho. Simple room temperature bonding of thermoplastics and poly(dimethylsiloxane). *Lab Chip,* **2011,** *11* (5), 962-965.

10. S. X. Li, B. W. Wang, D. Liu, G. L. He, H. Wang, Y. J. Duan, J. J. Xing, H. Y. Zhou and Y. W. Zhou. Advance in animal models of traumatic brain injury. *Fa Yi Xue Za Zhi,* **2011,** *27* (4), 286-289, 294.

11. M. D. Tang-Schomer, J. D. White, L. W. Tien, L. I. Schmitt, T. M. Valentin, D. J. Graziano, A. M. Hopkins, F. G. Omenetto, P. G. Haydon and D. L. Kaplan. Bioengineered functional brain-like cortical tissue. *Proc. Natl. Acad. Sci. U. S. A.,* **2014,** *111* (38), 13811-13816.

Appendix 1:

Quick Reference to Glass-Glass ME Device Construction

This appendix will provide step-by-step instructions on the fabrication of glass-glass microchip electrophoresis (ME) devices, along with some notes gathered from personal experience that might not be reported in the literature.

Photolithography

1. Pre-bake glass substrate, photoresist side up, on a hotplate at 100 ºC for 2 minutes.

   Note: The prebake time will vary according to the photoresist type and thickness. Consult the photoresist documentation for more information.

2. Allow glass to cool to room temperature before proceeding.
3. Place photomask on glass substrate such that the printed side of the photomask is in contact with the photoresist. Apply a vacuum to ensure minimal distance between mask and photoresist.
4. While maintaining a vacuum, expose the photoresist to UV through the photomask. Duration of exposure will depend on resist type, thickness, and UV intensity.
5. Place exposed glass substrate in developer to remove exposed area.
6. Wash with water and dry gently with compressed nitrogen or air.
7. Place on hotplate at 100 ºC for 10 minutes to fully evaporate developer.

Chrome Removal

8. Place wafer in a Pyrex™ dish of chrome etchant.
9. Agitate gently until chrome regions are clear (wait 45+ seconds after the chrome appears to be gone).

10. Rinse with water and dry using compressed nitrogen or air.

    Note: Chrome and photoresist must be removed from glass before a glass cutter will be effective. If making multiple devices simultaneously, it is important to include these cut lines in the photomask design. Additionally, chrome-coated glass will appear transparent before all chrome has been removed. However, a thin layer of chrome that remains will prevent glass-glass bonding. For this reason, allow the glass substrate to remain in the chrome etchant for 45 seconds *after* it appears that the chrome has been removed. Additional etching beyond this period will begin to undercut features.

Glass Cutting and Drilling

11. Using a glass cutter, cut glass along exposed paths between individual devices.

    Note: Extreme care should be taken not to scratch the surface of the photoresist. If this is a problem, the glass cutting and drilling steps can be performed after the HF wet etching.

12. Once separated, place individual ME devices in approximately 1 cm of water with a sacrificial layer under the chip to allow the drill to pass through without being damaged.

13. Slowly drill glass, applying constant pressure. It may be necessary to use gradually increasing drill bit sizes.

    Note: More ME devices are destroyed in this step than any other. Using new diamond-coated bits can help prevent glass breakage. When choosing drill bit sizes, two things to consider are whether or not MD access ports will be glued into place over the holes and evaporation during operation. If the holes drilled in the glass to

create sample and buffer wells are too small, these solutions will evaporate rapidly during operation. As this evaporation proceeds, ionic strength will change. This in turn will cause additional current draw and, consequently, alter migration times. If MD access ports are to be placed over the holes, the holes must of course be smaller than the ports themselves.

HF Wet Etching

14. Place glass with photoresist/chrome side up in HF etchant and agitate for duration of etching process. Etching time will depend on desired depth as well as glass type.
15. Remove from HF etchant, rinse with a solution of calcium acetate to deactivate the HF etchant. Following this, rinse with water and dry using compressed nitrogen or air.
16. Measure channel depth using a profilometer. If the desired depth has not been achieved, calculate the etch rate and place the device back in the HF for the necessary amount of time.

    Note: Due to the extreme toxicity of HF, the best practice is to minimize the number of times the device is taken in and out of the HF etchant if at all possible. When handling the substrate, the HF remaining on the device should first be deactivated by rinsing with a slurry of calcium acetate in water, followed by rinsing with water.

Removal of Remaining Photoresist and Chrome

17. Remove all remaining photoresist by rinsing with acetone.
18. Rinse with water and dry with compressed nitrogen or air.

19. Place the glass substrate in chrome etchant, agitating gently, until all remaining chrome has been removed (wait 45+ seconds after the chrome appears to be gone).

    Note: The removal of all photoresist and chrome is necessary to facilitate a glass-glass bond.

Bonding Glass-Glass ME Devices

20. Cut blank glass to the necessary size.

    Note: To avoid breakage due to differences in thermal expansion, blanks should be of the same glass type as the etched device.

21. Clean both glass pieces using Alconox™ mixed to the manufacturer's specifications.

22. Rinse both sides well with deionized water (DI) water

23. Incubate the glass surfaces to be bonded using a solution of 0.5% (w/v) calcium acetate, approximately 30 mM, and 0.5% (w/v) Alconox™ in DI water for no less than 30 seconds.

24. Rinse thoroughly with DI water.

25. Under running DI water, bring glass pieces together from bottom to top.

    Note: Force out any remaining bubbles but allow a layer of water to remain.

26. Place the device in an oven for 1 hour at 60 ºC.

    Note: Do NOT force all water from between the layers. The evaporation from the oven will help force the glass together.

27. At the 1-hour mark, inspect the device for Newton rings indicating incomplete bonding of the surfaces. If found, separate using a razor blade and repeat steps 21–26.

28. Place binding clips around the device to apply additional pressure. Increase the temperature to 105 ºC for 2 hours.

29. Inspect device. If Newton rings have formed, separate using a razor blade and repeat steps 21–28.

30. If no Newton rings are found, execute the following program, slowly increasing the oven temperature to 630 ºC and holding before cooling gradually to room temperature. Steps shown in Table 1.

31. If the ME device is meant to be used online (MD-ME), access ports must be glued to the chip to allow the flow from the syringe pump to enter the device. Polyethelene tubing connecting the syringe pump can be connected directly to ports glued to the surface of the device. To glue ports in place, a strong UV source such as the ELC-450 (Electrolite Corp, Bethel, CT) should be used. UV glue (Fisher Scientific, Waltham MA) should be applied carefully to the ports while holding them in place.

    Note: Should glue enter the channels, flush with water and methanol until the glue has been cleared. Avoid UV exposure during this period if possible.

Appendix 2:

Quick Reference to PDMS-Glass ME Device Construction

This appendix will provide step-by-step instructions on the fabrication of PDMS-glass microchip electrophoresis (ME) devices, along with some notes gathered from personal experience that might not be reported in the literature.

Silicon Master Spin-Coating

1. Use nitrogen flow to clean surface of silicon wafer.
2. Center silicon wafer on spin coater platform.
3. Pipette 4 mL of SU-8 10 photoresist onto the exact center of wafer and spin coat at 2000 rpm until fully coated.

    Note: The amount of SU-8 10 photoresist used directly influences its thickness and, subsequently, the final depth of the microfeatures. The values stated in these steps are for a final thickness of 15 µm with SU-8 10. Values associated with other thicknesses and photoresists should be calculated based on manufacturers' specifications.

4. Prebake silicon wafer at 65 ºC for 2 minutes on hotplate, then increase temperature to 95 ºC for 5 minutes.

    Note: To avoid breaking the silicon wafer, it is better to start the hotplate at room temperature and gradually ramp up to each specified temperature before heating it for the desired length of time. This should be done in any step requiring heating the silicon wafer.

Silicon Master Photomask Alignment and UV Exposure

5. Align negative photomask on top of wafer on photolithography platform; use vacuum to hold substrate and mask in place.

    Note: When using a printed photomask, make sure that the printed side is facing down (flush with the substrate). This will prevent any diffusion of light across the width of the transparency and avoid unwanted enlargement of the features. Make sure the silicon wafer has cooled to room temperature before aligning the photomask.

6. Expose to UV light for 16 seconds.

    Note: Full UV exposure of SU-8 is dependent on the substrate thickness and light source intensity. In this case, a flood-source with output intensity of 21 mW/cm^2 is used.

Silicon Master Post-Exposure Processing and Profiling

7. Post bake silicon wafer at 65 ºC for 1 minute on hotplate, then increase temperature to 95 ºC for 2 minutes.
8. Place developed wafer in SU-8 developer; gently swirl for 2 minutes to remove un-developed photoresist.
9. Remove master from developer; wash with isopropyl alcohol and dry with nitrogen flow.

    Note: Acetone will cause developed SU-8 to dissolve. Only isopropyl alcohol should be used for cleaning silicon masters using this photoresist.

10. Hardback at 200 ºC for 2 hours.
11. Use a profilometer to confirm the dimensions of the microfeatures on the master.

PDMS Curing

12. Measure 12 grams total of a 9:1 ratio of Sylgard™ 184 elastomer (10.4 g) and curing agent (1.6 g) into a small cup; mix thoroughly.

    Note: This amount of polymer was chosen because the surface tension will be sufficient to hold the mixture on the master's surface. Greater amounts can be used, but a mold will be necessary to hold the polymer on the wafer's surface. Using 12 g will result in a final thickness of approximately 1.2 mm.

    Note: Different ratios of elastomer to curing agent can be used in order to modify the elasticity of the PDMS. In general, the more curing agent used, the less elastic is the final polymeric substrate.

13. Place cup inside vacuum desiccator and remove all gas bubbles via repeated application of vacuum, being careful not to spill polymer over the edges of the container.

14. Pour mixture onto master and allow it to settle to a uniform thickness; place in oven and heat at 70 ºC for at least two hours.

    Note: Make sure that the master is level once it is placed in the oven. If it is placed at an angle, the PDMS will cure unevenly and potentially be unusable.

15. Use a razor blade to scrape the PDMS off of the edges of the master, then slowly peel off the polymer layer, being careful not to stretch or rip the substrate.

16. Either bond immediately (the next two sections detail the process for reversible and irreversible bonding) or place the PDMS on a piece of Parafilm™, channel-side down; fold Parafilm™ over the top of PDMS to fully seal it.

Note: If protected from air exposure, PDMS can safely be sealed within Parafilm™ for up to one week. If cracks are visible in the microchannels when examined using a microscope, the polymer has dried out and should not be used.

Reversible Bonding to Glass

17. Use a PDMS hole puncher to remove PDMS at reservoirs and create wells, using a Kimwipe to clean the puncher surface between each use.

    Note: This step is not needed if wells have been drilled in the glass substrate.

18. Wipe down the glass substrate with a Kimwipe soaked in 50% isopropyl alcohol (IPA), then dry with lint-free paper and nitrogen flow.

19. Peel Parafilm™ off PDMS

    Note: If bonding in a cleanroom facility, there should be no dust or other detritus on the substrate surface. A piece of clear tape can be used to remove any particulates on both glass and PDMS if necessary.

20. Slowly place PDMS on glass substrate, channels facing inwards; run fingers over the PDMS to force out any air bubbles that form between the layers.

21. Examine device using a microscope to guarantee the microfeatures are preserved and no clogs are present.

    Note: If there is particulate in the channels or improper sealing, the PDMS can be peeled off the glass and re-applied after using tape to clean both substrate surfaces.

Irreversible Bonding to Glass

22. Use a PDMS hole puncher to remove PDMS at reservoirs and create wells, using a Kimwipe to clean the puncher surface between each use.

    Note: This step is not needed if wells have been drilled in the glass substrate.

23. Wipe down the glass substrate with a Kimwipe soaked in 50% IPA, then dry with lint-free paper and nitrogen flow.

24. Peel Parafilm™ off PDMS.

    Note: If bonding in a cleanroom facility, there should be no dust or other detritus on the substrate surface. A piece of clear tape can be used to remove any particulates on both glass and PDMS if necessary.

25. Run a handheld plasma oxidizer (BD-20AC, Electro-Technic Products, Chicago IL) over the surface with the electrode a centimeter above the polymer surface, spending around 30 seconds on each piece of PDMS

    Note: A conventional plasma oxidizer (Harrick Scientific, Ithaca NY) can also be used. It is not recommended to oxidize PDMS for more than 2 minutes, as this can result in degradation of the surface and potential damage to any microfeatures or improper bonding.

26. Firmly press the substrates together, taking care to avoid touching the oxidized surface; run fingers over the PDMS to force out any air bubbles that form between the layers

27. Apply pressure with fingertips around the edges of the microchip until sealed, usually within one or two minutes.

    Note: Applying pressure directly over the channels can result in forcing them closed and ruining the device.

28. Examine device using a microscope to guarantee that the microfeatures are preserved and no clogs are present.

    Note: If there is particulate in the channels or improper sealing, the PDMS must be removed by scraping it off with a razor blade. The glass substrate should be washed

with IPA and acetone to clean away any residual PDMS before attempting a second bonding.